UNIVERSITAT DE BARCELONA

Shedding light on the temporal organisation of tissue physiology

Valentina Maria Zinna

Barcelona 2021

Shedding light on the temporal organisation of tissue physiology

A Doctoral Thesis Submitted in Fulfilment of the Requirements
for the Title of Ph.D. at the Universitat de Barcelona

presented by

Valentina Maria Zinna

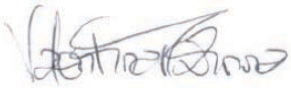

Supervisors

Dr. Salvador Aznar-Benitah

Dr. Patrick-Simon Welz

Tutor: Prof. Albert Tauler Girona

Universitat de Barcelona
Facultat de Farmàcia
Programa de Doctorat en Biomedicina

Institute for Research in Biomedicine
IRB Barcelona

This project has received funding from the European Union's Horizon 2020 research and innovation programme under the Marie Skłodowska-Curie grant agreement No. 713673.

This project has received the support of a fellowship from "la Caixa" Foundation (ID 100010434). The fellowship code is LCF/BQ/IN17/11620018.

We are born to this World for a certain period,
which we can fill with joy, work, ambitions, sorrow, love, hate,
or just nothing,
and share these with other people.
But then it comes time when we have to resign.
This is the Law of Nature.
Sooner or later we are sucked back into this big Recycling Machine
and become parts and energy of new molecular complexes
and even new individuals (...)

Jure Piškur, 1960-2014

Acknowledgments

I would like to thank Salva for welcoming me in his Circadian Team and for giving me the opportunity to carry out my PhD project on this topic of tremendous interest to me. I truly want to thank him for his enormous support throughout this experience and in the final “transitioning” steps of it, for his constant scientific enthusiasm, for his positive (and fun!) attitude towards life and work, for the nice relationship we have built over these years, for everything he has taught me during this exciting path.

I would like to thank Patrick for welcoming me in his project, for sharing with me his knowledge and experience, and for helping me throughout the PhD. I believe we have learnt a great deal from each other, especially thanks to the ridiculous work schedules we endured together, from crazily early time points to up to 30 continuous hours of circadian experiments (which definitely contributed to disrupt our own rhythms!).

I want to thank every single member of SAB lab for contributing to build the person and professional I very proudly am today. Particularly, I want to thank two extremely important people to me: Tom and Carmelo. Although they arrived to the lab when I had already started this adventure, they both quickly became invaluable colleagues and friends to me. I think of them as skilled scientists, incredibly supportive colleagues, and, outside the lab, as extraordinary people, true friends, and companions of life.

I am really thankful for having been part of this lab, also because of people like: Andres with his endless knowledge, best chocolate mousse skills in the whole world, and love for cats (which I very much share!); Paloma with her silly jokes and cheerful attitude, with whom I shared a few of the craziest lab nights (with Michi definitely bringing her significant contribution to the crazy part of them!); Miguel with his kind character, great taste for music (and flamenco!) and positive karma around him. I would also like to thank Guio and Alex for all the science I learnt from them and for their advises, and then Uxue (alias *Polpetta*), Diana, Gloria, Inés, Monica, Claudia, Julia, for contributing to these great years of PhD. And of course all the SAB “alumni” with whom I shared lots of memorable moments and stayed good friends with, such as Valentina (*mia figlia*), Magdi (for all our “hamaca” moments), Marion and Michi.

A special thanks goes to the collaborators of my project and all the people linked to them. In particular, I want to thank Pura Muñoz for being a fantastic TAC committee member, always ready to help and immensely supportive throughout this experience. From her lab, I would like to thank Mireia and Arun for all the joint lab meetings together, inspiring discussions, and, well, *paellas* by the beach! I would like to

spiritually thank prematurely departed Paolo Sassone-Corsi for his great ideas and inputs, and all the people in his laboratory that I got the chance to work with and get inspired from, such as Paul, Carolina, as well as Kevin and Jacob that I even met personally and got to know the great people they are beyond a computer screen. I take this chance to thank the other TAC members for the great support and input to this project, namely Albert Tauler, and Manuel Serrano, who also welcomed me in his laboratory for my 1st year lab rotation and never stopped encouraging me throughout my path. Additionally, I really want to further thank everyone who has significantly contributed to this PhD project, such as all the people from the animal facility, the microscopy and the histopathology facilities, and the list could go on indefinitely.

Yet there are still so many more people from IRB that I would like to personally thank one by one. Starting from Leyre who has truly been the best supporter and adviser that any PhD student could ever wish for. Her smiles and *cariño* will always warm my heart. I would like to thank Clara for always being there for me and for giving me the fantastic chance to be part of the ENABLE scientific organising committee, which represented one of the most enriching experiences of my PhD, and through which I got to meet wonderful people from all around Europe. The ENABLE journey has provided me with a wealth of skills that I could not have achieved otherwise, besides having brought me closer to amazing people who then became true friends to me, such as Nevenka. I really want to thank Tiago who has introduced me to the amazing PRISMA community and has nicely supported my Events Officer activity at YEBN, which has further represented such an enriching, turning-point experience in my scientific life. In this regard, I am grateful to all the YEBN Executive Board members for being such a great team, and the people in my events team for their commitment. Finally, from IRB I also want thank Alba, Muriel, Natalia, for always having shown me their kindest side.

But all this would not have been possible without the precious support from “la Caixa” INPhINIT Fellowship Program and all the people contributing to it and who have invaluably supported me in this endeavour. A big thanks goes to Gisela for her willingness to help with literally every single issue that has ever arisen, and for her great competence and personality. I also want to thank Diana, Paola, Emilia, as well as all the Caixa fellows that have gone through this “rollercoaster” experience with me. Being trained as a “la Caixa” fellow has been a true honour for me, and altogether the most amazing and constructive experience of all. And among the Caixa fellows, I would like to thank a true companion of so many steps in my life: Lucia has walked right next to me throughout our Master studies in Dresden, has witnessed and shared with me

very difficult and very happy moments, and has persisted by my side as “la Caixa” mate, PhD mate, flatmate, and, most importantly, friend.

In this line, there is a great deal of people who make my life in Barcelona just happy, and for which I am enormously grateful. Starting from my angels Marta and Dafni (and Magdi), whose friendship is priceless to me. I deeply love them and feel immensely lucky to be part of their lives. I would like to thank Anna and Giovanna for their constant support and demonstrations of affection, for all the fun and “*disagio*” times at home, for being my only *Reinas*. I want to truly thank Silvia and Marco, who were the very first to welcome me to my new life in Barcelona, who have never left my side ever since, and who are true examples of life and love to me. And obviously I would like to thank *mis chiquillas* Yolanda, Elisa and Sandra, for all the moments of *“Flamenco y Amistad”* that they have gifted me. We could not have more different personalities and lives, yet we could not be more aligned and attached to each other. Finally, a huge thank you goes to Joan, Mar, Xenia, Gianmarco and the whole Italian crew, especially Simona, Marcello, Francesco and Fonzie, for being part of my life in Barcelona and for enriching it every single day.

I want to take this chance to further thank all those people who always stayed by my side, despite still living elsewhere. I would like to thank the Dresdeners, such as Shady, Felix, Sandra, Olga, Ioanna, David, and all the other *Kommilitones.* A very special place in my heart will always be reserved to my old mentor and friend Andy. I want to thank all my Berliner friends, especially João, Ana, Neşe, Andrea, and of course Kami who has always been by my side ever since the times in Pavia. They are among the best people I know and have represented such a source of strength for me, in particular during my time in Germany. Beyond any doubt, the biggest thanks of all goes to the real pillars of my life, to the friends who helped me grow the awareness of my capabilities and that have constantly made me feel loved and respected: Ketty, Mimma, Cri, Jack and Elsa.

Finally, I want to thank my parents and brother, who, despite the immense difficulties that we had to go through, always stood up to life stronger than ever. To them, I most certainly owe the perseverance and stubbornness to accomplish my objectives. It is people like them who will always make me feel tremendously homesick during every single take-off next to that beloved mountain of Cinisi. Because after all: *“Io sono nato in Sicilia e lì l'uomo nasce isola nell'isola e rimane tale fino alla morte, anche vivendo lontano dall'aspra terra natìa circondata dal mare immenso e geloso”* (Luigi Pirandello).

Table of Contents

List of Figures

Abstract

Circadian rhythms regulate tissue physiology throughout the day in response to environmental cues. The primary entraining cue for the mammalian circadian clock is light, which is perceived by the retina and transmitted to the suprachiasmatic nucleus (SCN) in the hypothalamus. The SCN establishes behavioural rhythms and coordinates neuronal and hormonal rhythmic signals to be sent to the different peripheral tissues, where the tissue-intrinsic circadian clockwork organises tissue physiology according to the time of the day.

The transcription factor BMAL1 is the master circadian regulator, which lies at the core of interdependent positive and negative feedback loops that establish cell-autonomous 24h rhythms of transcription and translation. Understanding the mechanisms of clock synchronisation is highly relevant, as alterations of clock function shorten the life span, cause ageing-related pathologies, and predispose to a number of diseases. However, it remains unclear whether communication between the different clocks is necessary when responding to environmental signals.

The main aim of this project was to understand whether the circadian clocks of different tissues respond independently to environmental signals or whether inter-tissue communication is required to achieve a synchronised rhythmic physiology. To test whether circadian functions are tissue-autonomous, or rather derive from systemic tissue communication, we developed a novel murine model: The *Bmal1-stopFL* mouse. This mouse model enables reconstitution of *Bmal1* expression, from its endogenous locus, exclusively in Cre recombinase-expressing cells, thus enabling the circadian clock to be activated in specific tissue/cell types. Hence, we crossed *Bmal1-stopFL* mice with mice expressing Cre recombinase under the regulation of different promoters in a tissue specific manner, and by doing so, we obtained mice having *Bmal1* expression reconstituted only in the epidermis (RE mice), only in the liver (Liver-RE mice), only in the SCN (SCN-RE mice), or in both the SCN and the epidermis (RERE mice).

By using these mice, we uncover that a tissue-specific functional clock suffices to maintain local rhythmicity of the core circadian machinery. Strikingly, the observed tissue-autonomous oscillations seemed to occur without any rhythmic feeding or drinking behaviour, metabolic cycles or daily locomotor activity rhythms. Importantly, we demonstrate that local epidermal oscillations are mediated by the sympathetic nervous system in response to light signalling. In addition, we find that tissue-specific

BMAL1 suffices to sustain tissue homeostasis in otherwise arrhythmic and prematurely-ageing animals. Remarkably, we further reveal that communication between the SCN and the epidermal clock is sufficient for maintaining robust core clock rhythms, and for establishing a significant portion of the overall WT circadian transcriptional output.

Altogether, these results provide a better understanding of the mechanisms underlying circadian regulation of tissue functioning. In addition, our work allows distinguishing for the first time which parts of the daily functions of the epidermis (and other tissues) depend solely on its local clock, and which ones depend on the communication of the tissue with the SCN. The acquired knowledge can be used in the future to prevent the physiological consequences of clock desynchronisation that regularly occurs in our modern lifestyle.

Resumen

Los ritmos circadianos regulan la fisiología de los tejidos a lo largo del día en respuesta a señales ambientales llamadas *Zeitgebers*, es decir "dadores de tiempo". El principal *Zeitgeber* que modula el reloj circadiano de los mamíferos es la luz que es percibida por la retina y transmitida al núcleo supraquiasmático (SCN) en el hipotálamo. El SCN establece ritmos de comportamiento (sueño, vigilia, hora de la comida, etc) y coordina señales rítmicas neuronales y hormonales que envía a los diferentes tejidos periféricos. El reloj circadiano intrínseco de cada tejido organiza su fisiología tisular según la hora del día que recibe del SCN.

El factor de transcripción BMAL1 es el principal regulador circadiano que impulsa las oscilaciones transcripcionales de varios genes controlados por el reloj para establecer un ritmo de 24h. Comprender los mecanismos de sincronización del reloj es muy relevante, ya que las alteraciones de la función del reloj acortan la vida, causan patologías relacionadas con el envejecimiento y predisponen a muchas enfermedades. Sin embargo, no está claro si la los diferentes relojes periféricos, además de comunicarse con el SCN en el cerebro, necesitan comunicarse entre sí para lograr una fisiología rítmica sincronizada.

El objetivo principal de este proyecto era comprender si los relojes circadianos de diferentes tejidos responden de manera independiente a las señales ambientales o si se requiere comunicación entre tejidos para lograr una fisiología rítmica sincronizada. Para probar esto, utilizamos un nuevo ratón generado en nuestro laboratorio: el ratón *Bmal1-stopFL*. Este ratón permite la expresión del gen del reloj central *Bmal1* desde su locus endógeno exclusivamente en células que expresan la recombinasa Cre. Por lo tanto, cruzamos ratones *Bmal1-stopFL* con ratones que expresan recombinasa Cre bajo la regulación de diferentes promotores, y al hacerlo obtuvimos ratones con expresión de *Bmal1* reconstituida solo en la epidermis (ratones RE), solo en el hígado (ratones Liver-RE), solo en el SCN (ratones SCN-RE), o tanto en el SCN como en la epidermis (ratones RERE).

Mediante el uso de estos ratones, descubrimos que BMAL1 específicamente en la epidermis o en el hígado es suficiente para mantener el ritmo local de la maquinaria de su reloj. Sorprendentemente, las oscilaciones de los tejidos impulsadas por la luz parecían ocurrir sin la necesidad de una alimentación rítmica, de ciclos metabólicos circadianos, o de una actividad locomotora rítmica. Es importante destacar que parte de las oscilaciones locales en los tejidos periféricos estaban mediadas por el sistema nervioso simpático en respuesta a las señales luminosas. Además, descubrimos que

la expresión de BMAL1 específica en la epidermis era suficiente para mantener la homeostasis tisular en animales que presentaban una arritmia general (es decir, en todos los demás tejidos del animal) y que por lo tanto presentan un envejecimiento prematuro. Además, nuestro trabajo nos ha permitido por primera vez entender qué parte de las funciones diarias de la piel (y de otros tejidos) dependen únicamente de su reloj local, y cuáles dependen de la comunicación del tejido con el SCN.

En conjunto, nuestros resultados abren el camino para empezar a comprender mejor los mecanismos subyacentes a la regulación circadiana del funcionamiento de los tejidos y las consecuencias fisiológicas derivadas de su desincronización. Estos datos nos están permitiendo identificar porqué la desincronización del reloj contribuye al envejecimiento y formas de posiblemente mantener su correcto funcionamiento en base a nuestro estilo de vida moderno.

Abbreviations

6-OHDA	6-hydroxydopamine
ACTH	Adrenocorticotropin
Alfp	Albumin-α-fetoprotein
AMPK	AMP-activated protein kinase
Arntl	Aryl hydrocarbon receptor nuclear translocator like
ATAC-seq	Assay for Transposase-Accessible Chromatin using sequencing
AVP	Arginine Vasopressin
BMAL1	Brain and Muscle ARNT-Like 1
BMP	Bone Morphogenetic Protein
cAMP	cyclic Adenosine Monophosphate
CCG	Clock-Controlled Gene
cDNA	complementary DNA
CK1	Casein Kinase 1
CLOCK	Circadian Locomotor Output Cycles Kaput
CRE	cAMP-Response Element
CREB	cAMP-Response-Element-Binding protein
Cry	Cryptochrome
CT	Circadian Time
DAB	3-3′-diaminobenzidine
DBP	albumin D-element-Binding Protein
DD	24h Darkness
DEG	Differentially Expressed Gene
DNA	Deoxyribonucleic Acid
DOR	Differentially Opened Region
E-box	Enhancer box
ECM	Extracellular Matrix
FBXL3	F-Box And Leucine Rich Repeat Protein 3
FDR	False Discovery Rate
GABA	Gamma-Aminobutyric Acid
GC	Glucocorticoid
GO	Gene Ontology
H/E	Haematoxylin/Eosin
HAT	Histone Acetyltransferase
HDAC	Histone Deacetylase

HF	Hair Follicle
HPA	Hypothalamic-Pituitary-Adrenal
IFE	Interfollicular Epidermis
ipRGCs	intrinsically photoreceptive Retinal Ganglion Cells
K	Keratin
LD	12h Light /12h Dark
Liver-RE	*Bmal1* Reconstituted in the liver
mRNA	messenger Ribonucleic Acid
mTOR	mammalian Target Of Rapamycin
NAD	Nicotinamide Adenine Dinucleotide
NAMPT	Nicotinamide Phosphoribosyltransferase
NPAS2	Neuronal PAS Domain Protein 2
NR1D1/2	Nuclear Receptor Subfamily 1 Group D Member 1/2
PBS	Phosphate Buffered Saline
Per	Period
PGC-1α	PPARγ Coactivator-1α
PPAR	Peroxisome Proliferator-Activated Receptor
PVN	Paraventricular Nucleus
qPCR	quantitative real-time Polymerase Chain Reaction
RE	*Bmal1* Reconstituted in the epidermis
RERE	*Bmal1* Reconstituted in epidermis and SCN
REV-ERB	Reverse-Erythroblastosis Virus
RHT	Retino-Hypothalamic Tract
RNA	Ribonucleic Acid
ROI	Region Of Interest
ROR	RAR-related Orphan Receptor
RORE	Retinoid Orphan Receptor Element
ROS	Reactive Oxygen Species
RT	Room Temperature
SCN	Suprachiasmatic Nuclei
SCN-RE	*Bmal1* Reconstituted in the SCN
SD	Standard Deviation
SEM	Standard Error of the Mean
SIRT1	Sirtuin 1
Syt10	Synaptotagmin10

TGF	Transforming Growth Factor
TSS	Transcription Start Site
TTFL	Transcriptional Translational Feedback Loop
UTR	Untranslated Region
UV	Ultraviolet
VIP	Vasoactive Intestinal Polypeptide
WNT	wingless/int
ZT	*Zeitgeber* Time

1. Introduction

1.1 Circadian biology

1.1.1 The "origins" of circadian rhythms

Life on Earth has evolved while adapting to the rotation of our planet around its own axis that takes place during the 24 hours of a day[1]. In order to anticipate the daily environmental changes given by this rotation, most species have evolved endogenous molecular oscillators that generate the so-called "circadian" rhythms in behaviour, metabolism and physiology[2]. The term *circadian* (from Latin circa="about" and diem="day") means "about a day"; thereby, all those functions that organisms carry out on a daily basis are under circadian control[3].

The very first studies about circadian rhythms started with observations made on the movements of leaves in plants[4]. In 1729, the French astronomer Jean Jacques d'Ortous de Mairan noticed that, when placed under conditions of constant darkness, mimosa plants continued opening and closing their leaves according to the correct time of the day. This movement continued for several days, thus implying the existence of an endogenous timing system[4]. Later in the 1930s, the German plant physiologist Erwin Bünning observed that bean plants, placed under constant light conditions, moved their leaves with a period of 24.4 hours (rather than 24 hours). He saw that this rhythm was inherited, thereby confirming that an endogenous clock is present in plants and can be synchronised by environmental cues, such as light[4]. In 1960, Colin Pittendrigh comprehensively laid down the main principles of diurnal rhythms in living beings, and speculated about the existence of a light-dependent central oscillator that aligns peripheral clocks[5]. Finally, towards the end of the 1960s, Benzer and Konopka performed mutagenesis studies and discovered that genes on the X chromosome control the rhythmic behaviour of the fruit fly *Drosophila melanogaster*[6].

The first clock gene *period (per)* was only uncovered in 1984, thanks to the collaborative effort of Jeffrey Hall, Michael Rosbash, and Michael Young. They cloned and characterised PER structure[7–10]. After identifying this first clock gene, Hall and Rosbash found that the levels of PER protein and of *per* mRNA were oscillating in a circadian manner in *Drosophila* brain, with *per* mRNA peaking earlier than PER protein[11,12]. Soon after, the first transcriptional-translational feedback loop (TTFL) model was proposed, and it derived from: Firstly, the discovery of PER being a transcription factor that shuttles between nucleus and cytoplasm[13]; and secondly, the finding that PER overexpression decreases its own mRNA levels[14]. In the 90s, Young's

group discovered the second clock gene in the fruit fly, called *timeless (tim)*, whose expression was found to be in phase with *per*[15,16]. Moreover, it was shown that TIM protein binds PER, in order to promote its entry into the nucleus, where it inhibits the expression of its own gene in a negative feedback mechanism[17]. Later, it was found that *Per1-3* and *Cry1-2* are the mammalian homologs of *Per* and *Tim,* respectively[18,19]. Subsequently, the group of Takahashi discovered the positive regulators of *Per* transcriptional oscillations in mouse: Circadian Locomotor Output Cycles Kaput (CLOCK), and Brain and Muscle ARNT-Like 1 (BMAL1), also called Aryl Hydrocarbon Receptor Nuclear Translocator-Like (ARNTL)[20–23]. Soon after, Hall and Rosbash found the orthologs of these positive transcription factors in *Drosophila*, i.e. CLOCK and CYCLE, further consolidating the TTFL model, whereby the clock auto-regulates itself[24,25].

Although the main core clock proteins may differ from species to species, the feedback loop model, that was elaborated thanks to the early studies carried out in *Drosophila,* is still nowadays considered the canonical mechanism through which circadian biology works[26,27]. Circadian clocks are conserved in nearly all forms of life, highlighting the extraordinary importance of a timing system that regulates physiology while anticipating the daily external changes.

1.1.2 Organisation of the circadian clock

1.1.2.1 Molecular core clock architecture and auxiliary loops

In mammals, virtually every cell contains a circadian oscillator, which drives molecular processes and physiological functions specific to a given tissue, in accordance to the appropriate time of the day[28]. Central and peripheral clocks share the same molecular circadian machinery. The positive arm of the TTFL model is characterised by two transcription factors, BMAL1 and CLOCK (or its paralog Neuronal PAS Domain Protein 2 [NPAS2]) (Figure 1). They dimerize and bind to enhancer box (E-box) regulatory sequences in the genome, in order to control the downstream expression of thousands of clock-controlled genes (CCGs)[23,29] (Figure 1). Among the target genes are the negative regulators of the TTF loop, which are three *period* (*Per1-3*) and two *cryptochrome* (*Cry1-2*) genes (Figure 1). Upon accumulation and dimerisation in the cytoplasm, PER and CRY proteins translocate into the nucleus, where they inhibit the transcriptional activity of BMAL1 and CLOCK (Figure 1). By doing so, they also suppress their own gene expression, thereby closing the core TTF loop[29,30]. Subsequently, *Per* and *Cry* mRNA levels decrease and their respective proteins are degraded via ubiquitin-dependent pathways (Figure 1). Hence, BMAL1 and CLOCK levels are high again to carry out their transcriptional activity, and the self-sustained feedback loop starts all over again. In order to give the right pace to the core clock activity and maintain a 24 hours periodicity, further proteins intervene in the main TTF loop. Two members of the casein kinase 1 family, CK1δ and CK1ε, phosphorylate PER, thereby contributing to its degradation (Figure 1), whereas the phosphatases PP1 and PP5 counteract this activity[31–33]. On the other hand, CRY is phosphorylated and subsequently degraded via F-Box And Leucine Rich Repeat Protein 3 (FBXL3)-mediated ubiquitination[34–36] (Figure 1). A third component that plays an important role in the rate of TTFL timing and in clock proteins stability is the AMP-activated protein kinase (AMPK), which regulates the phosphorylation of CRY1 and the activity of CK1[37,38] (Figure 1).

A second auxiliary feedback loop that is driven by BMAL1 activity comprises Reverse-erythroblastosis virus ([REV-ERBα/β], also known as Nuclear Receptor Subfamily 1 Group D Member 1/2 [NR1D1/2]), as well as RAR-related Orphan Receptor (RORα-γ) (Figure 1). Their main function is to either repress (REV-ERBα/β) or activate (RORα-γ) *Bmal1* expression, while competing for Retinoid Orphan Receptor Elements (ROREs) in the *Bmal1* promoter[39] (Figure 1). A further CCG and critical regulator of *Bmal1* expression is Peroxisome Proliferator-Activated Receptor alpha (PPARα), whose

activity takes place through binding to PPAR response sequences in the *Bmal1* promoter[40].

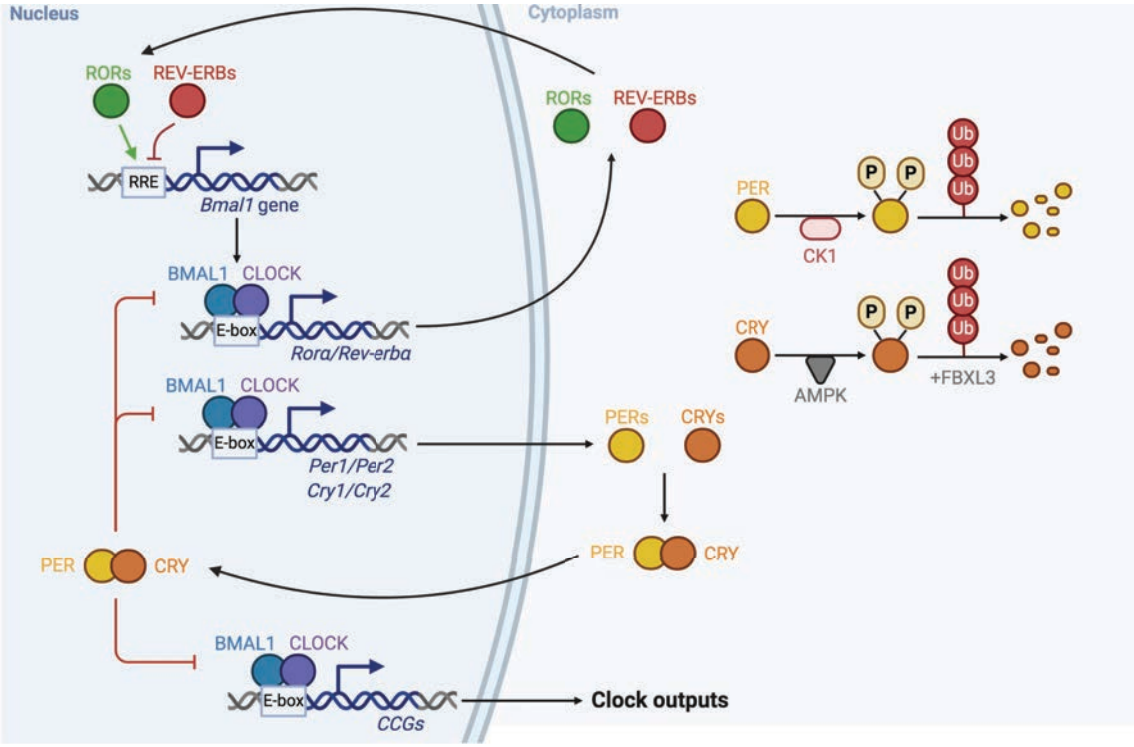

Figure 1. Model of the mammalian molecular circadian clock

Simplified schematic of the feedback loops that characterise the circadian architecture. REV-ERBα represses *Bmal1* expression and RORα activates it, while competing for Retinoid Receptor Elements (RRE) in the *Bmal1* promoter. The main positive arm of the transcriptional-translational feedback loop (TTFL) model is represented by BMAL1 and CLOCK. This heterodimer binds to E-box regulatory sequences of thousands of clock-controlled genes (CCGs), in order to modulate the various clock outputs. Among the target genes are the negative regulators PERs and CRYs. Upon accumulation and dimerization in the cytoplasm, PER and CRY proteins translocate into the nucleus, where they inhibit the transcriptional activity of BMAL1 and CLOCK. PER and CRY proteins are then degraded via ubiquitin-dependent pathways and the feedback loop starts again. Specifically, CK1 phosphorylates PER, thereby contributing to its degradation, while CRY is phosphorylated by AMPK and subsequently degraded via FBXL3-mediated ubiquitination.

Finally, a third accessory feedback loop stabilising the transcriptional-translational core clock machinery is operated by: Positive regulators, such as albumin D-element-binding protein (DBP), Thyrotroph Embryonic Factor (TEF), and Hepatic Leukemia Factor (HLF); as well as the negative regulator Nuclear Factor Interleukin 3 (NFIL3 or E4BP4)[1]. These factors compete for D-boxes in the *Per* promoter and are crucial determinants of period length. In fact, overexpression of *Dbp* leads to a longer period, whereas the opposite holds true when *Nfil3* is overexpressed[41]. Two additional factors that negatively regulate circadian rhythms are *Dec1* and *Dec2*, whose E-box enhancers can be bound either by BMAL1:CLOCK to positively affect their activity, or by

PER1/2:CRY1/2 for negative regulation[42]. Therefore, the molecular architecture of the circadian oscillatory machinery is organised and controlled by a plethora of positive and negative regulators that together form cooperative, interlocked feedback loops.

1.1.2.2 Clock regulatory dynamics

Post-transcriptional, post-translational and chromatin modifications tightly regulate the activity of all the factors involved in the clockwork, thereby adding further robustness to temporal control of gene expression. This additional layer of regulation is exemplified by the timing of phosphorylation on Serine 5 of the C-terminal domain of the enzyme RNA polymerase II (RNAPII-Ser5P). Serine 5 phosphorylation mediates RNAPII's recruitment to BMAL1:CLOCK-bound transcription start sites (TSS), thus favouring initiation of transcription[43].

Epigenetic modifications, such as H3K4me3, H3K9ac and H3K27ac, which all display a robustly circadian presence at TSSs, also favour the opening of the chromatin for RNAPII recruitment[43]. CLOCK itself possesses an intrinsic histone acetyltransferase (HAT) activity, and acetylates histone 3 on its lysine 9 (H3K9ac), as well as on its lysine 14 (H3K14ac), further supporting initiation of transcription[44,45]. The additional interaction of BMAL1:CLOCK with the HAT coactivators p300 and cyclic adenosine monophosphate (cAMP)-response-element-binding (CREB)-protein renders the chromatin overall more accessible[46,47]. On the other hand, this HAT's function is opposed by many histone deacetylases (HDACs), such as Sirtuin 1 (SIRT1), which also deacetylates BMAL1 and PER2[48]. The HDAC activity of SIRT1 is robustly circadian, besides being Nicotinamide Adenine Dinucleotide (NAD^+)-dependent[49]. NAD^+ and SIRT1 link metabolism and circadian rhythms[50].

Whole genome sequencing technologies have made it possible to deeply investigate the circadian transcriptome of specific tissues. In numbers, approximately 20-30% of oscillating transcripts come from circadian *de novo* transcription, whereas only up to 50% of rhythmic mRNAs translate into circadian proteins[43,51,52]. One of the most exhaustive systems biology approaches in recent years focussed on constructing a rhythmic transcriptional atlas from 12 murine organs by means of RNA-sequencing and DNA arrays[53]. Here, the authors provided a spatio-temporal multitude of genomic information with regards to not only the coding versus non-coding circadian transcriptomes, but also the physiological context of tissue-specific rhythmic processes. They showed that 43% of protein-coding genes are rhythmic in at least one organ, in line with the proportion of transcripts encoding for proteins in the liver[53,54]. Of all organs

examined in the study, liver appeared to be the richest in circadian genes, as opposed to the hypothalamus that had the fewest rhythmic transcripts[53]. Similarly, others reported that the hepatic transcriptome is robustly oscillating, in order to regulate liver-specific metabolic and other functions in time[55–57].

Interestingly, approximately 30% of conserved non-coding RNAs were found to be rhythmic within the atlas project, and their expression patterns were highly tissue-specific[53]. Accordingly, a few studies demonstrated that each organ displays a set of core rhythmic genes, characterised by little inter-tissue overlap[53,55,56]. Most of the analysed organs in the atlas project exhibited similar phase distributions, with a peak of circadian gene expression at dawn[53]. However, this pattern of distribution differed in lung and heart, further highlighting the great specificity of each tissue in a healthy organism[53,55]. Moreover, circadian genes displayed a greater variety of spliceforms and were consistently longer than non-rhythmic transcripts, like previously described for hepatic circadian genes[53,58]. Additionally, a significant proportion of the circadian transcriptome, including most of the core clock genes, was synchronised across organs. This means that in the context of a healthy life-style, i.e. in the absence of shift-work or jet lag conditions, peripheral organs are physiologically aligned to one another. In this regard, the timing of oscillation of the rhythmic genes follows their underlying specific function, i.e. their phase distributions reflect the peak and trough of activity of their products[53]. A number of further studies have reported the highly tissue-specific circadian transcriptome of several tissues, from skeletal muscle to liver and heart[55,56,59,60].

In addition to all the fine-tuned epigenetic and transcriptional mechanisms described so far, a vast number of further post-transcriptional/translational processes confer the right pace to the tissue-specific clock output. Some examples span from initial transcript processing and exit of mature mRNA from the nucleus, to alternative splicing, protein stabilisation and degradation. A detailed description of all the post-transcriptional/translational regulatory mechanisms goes beyond the purpose of this thesis, but it is excellently reported by a handful of studies and reviews[61–72]. Altogether, the percentage of transcriptional/translational output that oscillate in a circadian manner depends on the given tissue and is mostly non-overlapping between different tissues, underlying the high specificity of the temporal control of tissue physiology.

1.1.2.3 Central clock entrainment

The circadian clock is essentially a time-keeping machinery, which can be entrained by periodic environmental cues called *Zeitgebers* that means “time-givers” in German. *Entrainment* is the process by which biological clock systems are synchronised or aligned to the external time by *Zeitgebers*, such as the light schedule. In order to be defined circadian, biological processes should be endogenously “free-running”, temperature-compensated and entrainable[2,73,74]. Therefore, under stable environmental conditions (i.e. “free-running” conditions), such as constant darkness (DD), circadian rhythms persist[75]. At the same time, circadian rhythms compensate against changes in ambient temperature, in order to anticipate (and synchronise with) the solar time[76]. The photoperiod is the primary *Zeitgeber* entraining the cellular oscillator systems present in the various organisms, from bacteria to plants and animals[3]. In mammals, sleep-wake cycles are the most obvious behavioural circadian outcomes. In fact, cognitive mechanisms are upregulated during the day and downregulated during the night, while typical processes of the sleeping phase, like memory consolidation, are upregulated at night[77].

The widely accepted model for synchronisation of the mammalian circadian clocks is the “orchestra” model. Here, a pacemaker-like clock is the “director” of the orchestra, which coordinates the timing of the peripheral clocks that are the “musicians”[3]. Early studies in the 70s suggested the suprachiasmatic nucleus (SCN) of the anterior hypothalamus as the ”master” clock. The SCN is both necessary and sufficient for circadian behavioural rhythms. In fact, experiments of SCN lesions done in rodents resulted in a loss of circadian locomotor activity, feeding and drinking behaviours, as well as hormone release[78–80]. Moreover, grafting neonatal SCN tissue into rodents whose SCN was surgically removed, rescued their sleep-wake cycles[81]. Additionally, *in vivo* and *ex vivo* studies showed that SCN nuclei display spontaneous electrical firing in a circadian manner, reinforcing the hypothesis of the SCN being the central autonomous pacemaker[82]. Indeed, by using bioluminescent reporters, it was confirmed that SCN explants continue to oscillate in culture indefinitely, due to a strong intercellular coupling mediated by gap junctions; in contrast, cultured peripheral tissues lose oscillatory amplitude and phase coherence over time[83,84].

The murine SCN consists of around 20,000 neurons located above the optic chiasm, hereby the term “suprachiasmatic”[30]. Light is perceived by the photopigment melanopsin of intrinsically photoreceptive retinal ganglion cells (ipRGCs) in the retina[85]. This allows these cells to process short-waved photic information that is then synaptically transmitted to the SCN via axons of the retino-hypothalamic tract (RHT)

(Figure 2). Furthermore, ipRGCs convey light signals also coming from rods and cones of the retina[86]. The conversion of photic information into electro-chemical signal along the RHT is achieved by the depolarizing action of melanopsin, which causes the release of glutamate, substance P (SP), and pituitary adenylyl cyclase activating peptide (PACAP) from the RHT into the SCN. In order to first obtain a synchronised rhythmicity within neurons of the central clock, glutamate acts by enhancing the intracellular levels of Ca^{2+}. This leads the protein kinase A (PKA) to phosphorylate CREB. CREB protein induces the transcriptional oscillations of SCN neurons, by binding to cAMP response elements (CREs) in the promoters of target genes, such as *Per1-2*, thus initiating their transcription[87]. Another major source of glutamate to "feed" SCN neurons comes from the SCN astrocytes, which provide further robustness to the central circadian rhythms. In fact, the extracellular concentration of glutamate in the SCN is in phase with glial levels of Ca^{2+}, whose intracellular fluctuations are instead antiphasic compared to the ones found in SCN neurons[88].

Within the SCN, interneuron communication occurs via a number of neurotransmitters, like SP, vasoactive intestinal polypeptide (VIP), and gastrin-releasing peptide (GRP)[89–91]. At the same time, SCN neurons also communicate with the rest of the hypothalamus, as well as with extra-hypothalamic structures, mainly through gamma-aminobutyric acid (GABA), arginine vasopressin (AVP), and diffusible signals[92]. The SCN output is tuned according to not only the photic input, but also the cues coming from extra-SCN brain areas that integrate the retrograde signals coming from the periphery back to the central clock[87].

One of the major hypothalamic areas receiving SCN efferents is the subparaventricular zone (SPZ). SCN neurons act on receptors of the SPZ via the neuropeptide transforming growth factor (TGF)-α[93]. The main outcome of this TGFα-mediated activity is a suppression of the locomotor activity in nocturnal animals upon light stimulus, a phenomenon known in the circadian field as "light masking". Another peptide neurotransmitter critically involved in decreasing locomotor activity during the day is prokineticin 2 (PK2)[94]. One of the brain structures that is more densely composed of PK2 receptors is the paraventricular nucleus (PVN)[3]. Here, there is a high concentration of pre-autonomic and hormone-producing neurons, whose processed signalling is then relayed to the peripheral tissues[95].

Once the SCN is synchronised with the external solar time, it entrains the peripheral oscillators by aligning the phases of their circadian clocks to external solar time through rhythmic neuroendocrine cues, following a unidirectional type of entrainment[96]. However, reciprocal entrainment (or "bidirectional coupling") occurs at many different levels: a) within the molecular network of each cell, i.e. via the TTFL, which leads to molecular coupling; b) among cells of the same tissue, giving rise to cellular coupling; c) across organs of the same organism, in order to attain systemic coupling, and thus an overall rhythmic physiology[97].

1.1.2.4 Peripheral clock entrainment

The routes of central and peripheral clock entrainment have been subject of intense studies in recent years, which have pointed at autonomic innervation, temperature, humoral and behavioural/metabolic signals as major synchronising mechanisms[30] (Figure 2). On the one hand, hormonal cues allow the entrainment of the different peripheral clocks to the SCN phase (Figure 2); on the other hand, neuronal signals modulate the response of the peripheral tissues either directly or indirectly, by adjusting their sensitivity to hormones[95]. The rhythmic release of glucocorticoids (GCs) is a key circadian synchroniser (Figure 2), mediated by the interplay between the SCN, the autonomic nervous system, the pituitary gland and the adrenal clock, referred to as Hypothalamic-Pituitary-Adrenal (HPA) axis[98]. Upon AVP-mediated SCN signalling, PVN neurons generate corticoliberin (CRH) that leads the pituitary to free adrenocorticotropin (ACTH) into the blood. From here, ACTH reaches the adrenal cortex, thereby causing the rhythmic release of GCs, such as corticosterone in rodents (equivalent of cortisol in humans). GCs harbour the ability to suppress production of CRH and ACTH, thus closing the HPA axis-mediated loop[99]. The latter directly controls the circadian behaviour of mammals, as ACTH levels display robust circadian rhythms peaking at the onset of the locomotor activity phase, which is in the morning for humans and in the evening for nocturnal mammals like rodents[100,101]. Moreover, GC rhythms reset the phase of essentially all cellular oscillators throughout the body, since GC receptors are nearly ubiquitous, though absent in the neurons of the SCN[102].

GC-response elements are present in the promoter of several core clock genes, thereby GCs also modulate the transcription of many CCGs[103–105]. This explains why GC agonists, such as dexamethasone, display clock-resetting capabilities on different peripheral tissue types, both *in vitro* and *in vivo*[102,104,105]. Moreover, adrenalectomised mice have been shown to re-entrain faster to the photoperiod, pointing to a central role

of GCs in the re-alignment of the clock network under jet lag conditions[106]. In this regard, hydrocortisone administered to humans in the late afternoon leads to phase shifts of clock gene expression in peripheral oscillators, like blood mononuclear cells[107].

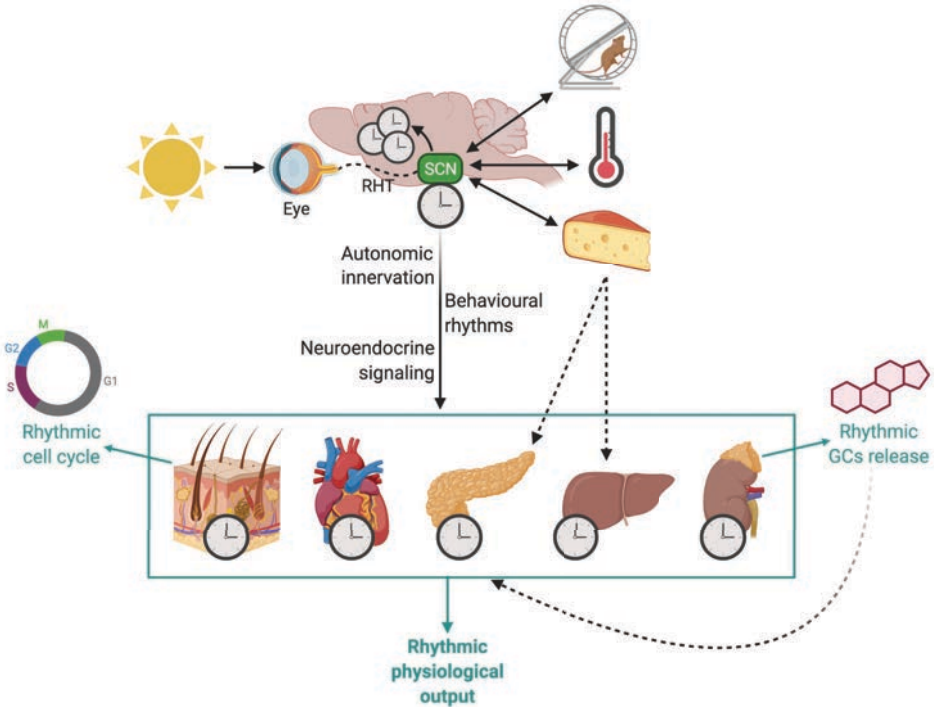

Figure 2. Mechanisms of circadian clock entrainment

Simplified schematic of central and peripheral clock entrainment in mammals. The SCN is considered the central clock, which receives retinal innervation via the retinohypothalamic tract (RHT), in order to be synchronised to the external light/dark cycle. Further *Zeitgeber* signals, such as food, temperature and physical activity, can entrain the central or the peripheral clocks. In turn, the SCN clock projects to various local circadian clocks that modulate behavioural (e.g., feeding rhythms and sleep–wake cycles), but also autonomic and neuroendocrine rhythmic signals. These systemic cues synchronise the molecular clocks of the different peripheral tissues, in order to regulate tissue-autonomous physiological functions, such as metabolism in the liver, blood pressure in the heart, cell cycle in the skin (as depicted), and rhythmic glucocorticoids (GCs) release by the adrenal gland (as depicted). GCs are themselves peripheral circadian synchronisers.

Another neuro-hormone that is involved in clock entrainment and output is melatonin, which is rhythmically produced by the pineal gland upon sympathetic signals coming from the SCN. Concentration of melatonin reaches the peak at night, thereby being in phase with GCs levels in rodents, and in anti-phase with GCs in humans. Its rhythmic release not only strictly regulates sleep-wake cycles, but also a number of peripheral functions, such as insulin secretion from the pancreas, and glucose homeostasis[108].

In addition to the humoral signalling pathways, the SCN communicates to peripheral organs, such as liver, white adipose tissue, ovary, heart, etc. (besides adrenal gland), through pre-sympathetic and pre-parasympathetic neurons situated in the PVN[109–113] (Figure 2). The contribution of two main neuronal pathways indicates that, upon light stimulus, the SCN harbours the ability to modulate the functions of peripheral tissues simultaneously but in different neuroendocrine ways. A number of studies reported the key involvement of the autonomic nervous system in the circadian control of physiological functions of different peripheral tissues, such as kidney, liver, and hematopoietic stem cells[114–116]. In this context, the SCN relays light signalling to peripheral oscillators, like the submaxillary salivary gland and the liver, via autonomic innervation, in order to regulate the local clockwork[116–118]. Accordingly, supplementation of epinephrine/norepinephrine is able to stimulate the local circadian machinery in murine liver and submandibular glands[117,119]. Furthermore, the rhythmic egress and homing fluctuations of hematopoietic stem cells are modulated by the sympathetic nervous system, along with other key functions of the bone marrow[120–122]. Hence, the autonomic nervous system plays a crucial role in the entrainment of several peripheral cellular and tissue clocks.

1.1.2.5 Peripheral clock (de)synchronisation

Despite light being considered the strongest *Zeitgeber* for entraining the central pacemaker, peripheral clocks receive the synchronising influence of further *Zeitgebers*, such as temperature changes and food intake (Figure 2). The endogenous temperature of internal organs, like the liver, is significantly different than the one of more exposed tissues, like the skin. Therefore, these temperature fluctuations can shift their phase and affect the respective physiological rhythms accordingly[3]. On the other hand, the SCN-driven circadian oscillations are by definition temperature-compensated. However, the SCN is able to influence body temperature in a circadian manner as one of the many clock outputs, thereby inducing a phase resetting on the peripheral oscillators[123]. There is strong evidence suggesting that Heat-Shock Factor 1 (HSF1) acts as a potent synchroniser of peripheral rhythms. Its activity has been shown to be circadian, with a peak at the beginning of the behaviourally active and feeding phases, which are accompanied by an increase in body temperature[124].

A potent *Zeitgeber* able to entrain many peripheral oscillators is the timing of food intake. In experiments of daytime restricted feeding, metabolic organs of rodents, like liver and pancreas, were re-entrained to the feeding rhythms[125,126]. In contrast, SCN and lung stayed synchronised to the external Light-Dark (LD) schedule[125,126]. Studies were also carried out with SCN-lesioned animals, where time-restricted feeding was able to restore overall behavioural rhythms, as well as the circadian expression of clock genes in peripheral organs like the liver[80,127,128]. Therefore, peripheral organs can be synchronised not only by SCN-mediated signals, but also by metabolic signals. The SCN may also indirectly co-opt these pathways through its regulation of food intake and locomotor activity (Figure 2). Among the main contributors to the downstream activation of rhythmic metabolic cascades are nuclear receptors, such as PPARs, RORs and REV-ERBs[30,40]. For example, PPARγ coactivator-1α (PGC-1α) conveys nutrient information, especially after fasting, to the clock machinery[129]. It does so by promoting the expression of BMAL1 and REV-ERBα. Moreover, PGC-1α interacts with SIRT1, thereby controlling glucose homeostasis in liver[130]. The HDAC activity of SIRT1 is NAD^+-dependent and robustly circadian[49]. When *de novo* NAD^+ biosynthesis is not possible, NAD^+ has to be provided through the salvage pathway. The rate-limiting enzyme of the salvage pathway is Nicotinamide Phosphoribosyltransferase (NAMPT), which is a BMAL1:CLOCK target gene, and is therefore under circadian control as well. NAMPT makes it possible for nicotinamide to be transformed into rhythmically available NAD^+, hereby feeding back the HDAC activity of SIRT1 on BMAL1. Together, NAD^+ and SIRT1 link the cells metabolic status to the activity of the circadian clock[50].

Another connection existing between clock and metabolism is represented by AMPK, which plays a crucial role in energy homeostasis as it responds to the nutritional status of cells, but it also controls CRY1 stability[37,38] (Figure 1). This connection, among other factors, makes it possible for the feeding schedule to reset the phase of the liver clock. In a "*Zeitgeber* desynchrony" experiment to study the contribution of conflicting schedules of light versus food on clock re-alignment, mice displayed intermediate behaviours between the two regimes[131]. While peripheral tissue clocks, like liver and adipose tissue, seemed to primarily adjust to the feeding schedule, SCN, adrenal clock, as well as locomotor activity were influenced by both *Zeitgebers*[131].

Among the metabolic hormones modulating clock function is leptin. Leptin deficiency has been shown to affect circadian rhythms of adipose tissue and liver, whilst not affecting SCN rhythms[132]. Conversely, leptin administration partially rescues peripheral clock disruption[132], and recovers photic entrainment of the SCN as a result[133]. Further, ghrelin has been implicated to signal peripheral nutritional state to the central clock

system, via its interaction with ghrelin receptors expressed in hypothalamic regions[134]. Another central hormone connecting metabolism to circadian rhythms is insulin, which has been demonstrated to exert potent phase-resetting functions on peripheral tissues, like the liver, both *in vitro* and *in vivo*[135,136]. Furthermore, GCs also play a role in conveying diet information into rhythmic metabolism. In fact, GCs act at the beginning of the feeding phase, by rhythmically binding to GC receptors that are situated within regulatory sequences of genes involved in amino acid, carbohydrate and lipid metabolic processes[137]. The GC-mediated clock output may differ depending on the target tissue. For instance, at their peak serum concentration, GCs boost the release of glucose from the liver and of fatty acids from the adipose tissue, in order to face the energy requirements of the active phase[138,139].

1.1.3 Chronobiology and health

Chronobiology influences nearly all the fundamental aspects of mammalian physiology, from sleep/wake and feeding/fasting cycles, to blood pressure and hormone secretion. Recently, circadian rhythmicity and inter-tissue temporal alignment have been defined as key hallmarks of health[140]. Conversely, the invention of the light bulb, along with the optimisation of modern means of transportation, have made it possible for humans to work longer hours or at night, easily travel across multiple time zones, acquire sedentary habits, and access food at any time of the day. This chronic circadian disruption predisposes, in the long-term, to a higher risk of developing cancer, cardiovascular and neurodegenerative diseases, as well as metabolic and mood disorders[141–145]. A plethora of human studies have reported a strong correlation between long-term shift working and several pathological conditions[146–150]. Long-term chronodisruption is also responsible for the onset of many other diseases whose molecular mechanisms are not directly connected to the circadian system, yet their symptoms manifest in a circadian fashion, such as allergies, respiratory problems and epileptic episodes[151,152].

The phenomenon of jet lag is one of the primary disruptors of physiological circadian rhythms. Causes of jet lag include excess or untimely light exposure, shift work or travel across time zones, all of which are hallmarks of modern lifestyles. This state leads to desynchronisation within the clock network of the body, which in turn causes misalignment with external time. Clock network desynchronisation occurs because of the circadian misalignment between the SCN and peripheral organs, which slowly re-

adjust to a new light schedule upon SCN-derived signalling[153,154]. In mammals, this internal temporal desynchronisation that uncouples central and peripheral timekeepers can ultimately lead to a number of mental and physical impairments, such as decreased appetite, vigilance, cognitive and coordination skills[155,156]. In this regard, experiments of chronic exposure to jet lag in rodents observe deregulation of innate immunity associated with increased inflammation[157], premature cellular ageing caused by telomere shortening[158], and the onset of pathologies, such as obesity, diabetes, and cancer[159–161]. Moreover, when mice were continuously subjected to an 8h advance or delay in the light schedule, they developed non-alcoholic fatty liver, which subsequently gave rise to steatohepatitis and fibrosis, and ultimately led to hepatocellular carcinoma[162]. Notably, aged mice exposed to a chronic 6h advance in the light regimen have a higher mortality rate[163]. Altogether, a regular light schedule ensures correct circadian alignment and overall organismal health.

It is crucial to use the current knowledge of chronobiology in order to boost the field of chronotherapy, and develop timed treatments according to the specific pathologic conditions. Chronotherapy aims at timing drug administration based on the diurnal expression levels of the specific target, or related pathway, in order to maximise the impact of the treatment while minimising potential side effects. Most notably, in the context of cancer therapy, it has been shown that chemotherapy's efficacy and tolerability can follow a circadian pattern[164]. Chronomedicine further offers the possibility to make diagnoses and interventions based on the different patient chronotypes (morningness, eveningness), aside of parameters like gender and age[165].

1.1.4 Chronobiology and ageing

A general weakening of the circadian output rhythms is known to occur during physiological ageing. Notably, in humans, disruption of sleep-wake cycles, accompanied by a phase-shift and a decreased amplitude of daily rhythms, like body temperature and hormonal fluctuations, frequently occur with age[166,167]. Similar changes in amplitude and phase of rhythmic functions, such as locomotor activity and feeding and drinking behaviours, have been observed in a number of mammalian ageing studies[168].

Growing evidence indicates that the SCN clock itself is afflicted by the ageing process through a range of mechanisms. A solid proof of this was given by transplantation studies of fetal SCN tissue into aged animals, which was sufficient to restore behavioural and hormonal rhythms in hamsters and rats, respectively[169,170]. A major reason accounting for the deterioration of the central clock is given by a weaker light signalling coming through the eye and reaching the SCN, likely caused by age-associated retinal degeneration, as well as impaired light perception by the SCN itself[171–173]. Additionally, a reduction of the number of ipRGCs has been reported in older mice[174]. This results in loss of proper light entrainment of the central pacemaker needed to synchronise with the external environment. Accordingly, SCN neurons have been seen to display a diminished amplitude of electrical rhythms over time, both *in vitro*[175] and *in vivo*[176]. Moreover, the impairment of intercellular communication, as one of the main features of the process of ageing[177], further affects the activity of the central clockwork. GABA, VIP and AVP expression levels and relative signallings are strongly reduced in aged animals, thereby leading to the loss of phase coherence and intercellular coupling among SCN neurons[175,178,179]. As a consequence, the resulting aged central clock is not capable of sustaining synchronous rhythms to be sent to the different peripheral oscillators[167].

Numerous studies have focussed on possible age-related changes to the core molecular clock machinery[167,180]. In most studies, the gene expression oscillatory patterns of peripheral tissue clocks remained unchanged over time, suggesting an underlying robustness of the timing system against potential age-related perturbations (as recently reviewed[167,181,182]). Further evidence of this phenomenon has recently been provided by two systems biology approaches undertaken on aged mice, which demonstrated that liver, epidermal and skeletal muscle stem cell clocks maintain a robust core rhythmic machinery[183,184]. Nevertheless, the resulting circadian transcriptome was significantly reprogrammed, and newly oscillating transcripts arose. Epidermal and muscle stem cells reprogrammed their daily rhythms towards a more stress-related signature characterised by inflammation, DNA damage and impaired autophagy[183]. On the other hand, Sato and colleagues found that the circadian reprogramming in liver affected processes such as NAD^+ metabolism and protein acetylation, further highlighting the importance of NAD^+/SIRT1-mediated deacetylating activity in the process of ageing[184]. Strikingly, when mice were fed a calorie restricted diet, the aged circadian signature resembled that of young mice[183,184].

SIRT1 has been demonstrated to possess anti-ageing properties thanks to its negative influence on the mammalian target of rapamycin (mTOR), and its related signalling

pathway, via AMPK action[185]. mTOR signalling pathway has been shown to be under circadian control in a BMAL1-dependent manner[186]. mTOR signals high nutrient and energy states, and favours anabolism, which in the long-term accelerates ageing[187]. In contrast, AMPK and SIRT1 sense low cellular energy levels, thus promoting catabolism and extending the life span. These anti-ageing effects are recapitulated in dietary restriction and mTOR inhibition experiments[187]. Furthermore, SIRT1-mediated activation of PGC-1α boosts mitochondrial biogenesis and antioxidant defenses, thereby counteracting the mitochondrial decay and the reactive oxygen species (ROS)-mediated detrimental effects that arise during ageing[188]. Finally, SIRT1 also downregulates inflammatory signalling pathways with its HDAC activity, hence tempering the pro-inflammatory environment that consistently develops with ageing. Such environment is referred to as “inflammageing”, and hinders proper intercellular communication[189,190]. Since SIRT1 requires NAD^+ to exert its pleiotropic activity, but NAD^+ decreases over time, a widely implemented experimental strategy has been to sustain NAD^+ levels during ageing[191,192]. These experiments have led to an overall improvement of many age-related conditions, accompanied by a prolonged life span[191–195]. These are only a few of the examples that reinforce the powerful functional connection between epigenetics, metabolism and the clock.

Further supporting a role for the decay of circadian processes in physiological ageing, targeted disruption of the circadian clockwork activity drives an accelerated ageing phenotype. For example, full-body *Bmal1*$^{-/-}$ or *Clock*$^{-/-}$ mice have a shorter life span compared to their WT counterparts[196,197]. Additionally, they experience age-related conditions, such as eye pathologies. However, *Bmal1*$^{-/-}$ mice undergo a far more severe premature ageing, which include significant weight loss, arthropathy, osteoporosis, as well as impaired hair growth and increased epidermal differentiation[196,198]. At the behavioural level, full-body *Bmal1*$^{-/-}$ mice fail to display robust locomotor rhythms that are instead completely lost in conditions of DD[198]. Lack of BMAL1 is also associated with established hallmarks of ageing, such as dysfunctional mitochondrial bioenergetics and dampened ROS homeostasis[199–201]. Overall, a robust physiological clockwork is essential for a healthy ageing process.

1.1.5 Mouse models in the circadian field

To better understand the underlying mechanisms of circadian rhythms, and the physiological consequences derived from clock dysfunction, great efforts have been dedicated to the development of suitable murine models that allow nuanced manipulation of circadian biology. For instance, *Cry1/Cry2*-double-deficient mice remain nocturnally active under LD conditions, but become arrhythmic when placed in DD[202,203]. Moreover, they exhibit a significantly increased bone mass[204]. *Per2* mutant mice display reduced angiogenesis, due to the inability of endothelial progenitor cells to proliferate and form vessels, accompanied by a high cellular senescence[205]. Furthermore, *Per2* mutations cause hyperinsulinemia, hyperglycemia, loss of GCs rhythms, and diet-associated obesity[206,207]. Intriguingly, *Cry1*$^{-/-}$ and *Cry2*$^{-/-}$ mice have a normal life expectancy[208], while no reports on the life span of *Per1*$^{-/-}$ or *Per2*$^{-/-}$ mice are available to date. A missense mutation in the *Clock* gene (*Clock-Δ19*) was the first genetic connection described in mice between circadian rhythms and metabolism[209]. *Clock* mutant mice remain rhythmic under LD conditions, but are largely arrhythmic in DD. They further display weaker behavioural rhythms associated with arrhythmic gene expression in peripheral organs, like liver, pancreas and muscle. Therefore, they develop diabetes, obesity and a metabolic syndrome of hypoinsulinaemia, hyperglycemia and hyperlipidemia[144,209,210]. Conversely, *Clock*-KO mice show robust behavioural rhythms even in DD, as CLOCK function is partially redundant with its paralog NPAS2[211]. Hence, the complete loss of rhythmic behaviour is only seen in mice that are KO for both genes[212].

Bmal1 is the sole core clock gene indispensable for circadian tissue function in mammals. Indeed, full-body *Bmal1*-KO results in reduced overall locomotor activity and loss of behavioural rhythmicity in DD[198,213]. Moreover, *Bmal1*-KO mice present a significantly shorter life span, accompanied by a number of ageing-related pathologies, such as arthropathy, osteoporosis, decreased weight gain and impaired hair growth[196,198,214]. To deepen the knowledge on the role of *Bmal1* in specific tissues, conditional *Bmal1*-KO mouse models have been generated. For example, endothelium-specific *Bmal1* deficiency alters vascular function by lowering the blood pressure during the active phase and boosting the heart rate throughout the day[215]. Liver-specific deletion of *Bmal1* leads to arrhythmic expression of key regulatory genes, which therefore disrupts glucose homeostasis[216]. Finally, loss of *Bmal1* in epidermal stem cells affects overall tissue homeostasis and causes a premature epidermal ageing-like phenotype, further underlining the physiological importance of *Bmal1* at the tissue level[217].

A further central mouse model in the circadian field, which has greatly expanded the current understanding of circadian entrainment, is the SCN-specific *Bmal1*-KO mouse[218]. Here, the authors used the Cre-loxP system to remove *Bmal1* mainly from the SCN, thanks to the generation of a Synaptotagmin10 (Syt10)-Cre driver line. Syt10-Cre activity mostly concentrates in the SCN cells, in the testis, and in very few other neural areas, like the olfactory bulbs[218]. This SCN-specific *Bmal1*-KO mouse displays altered locomotor activity and arrhythmic gene expression in the SCN[218]. Surprisingly, peripheral tissues, such as adrenal gland, kidney, liver and heart, exhibit clock transcriptional rhythmicity in LD. When subjected to a new light regime, the peripheral clocks of SCN-clock deficient mice re-adjusted faster than in WT mice[218]. Furthermore, when these mice were exposed to DD conditions for two days, peripheral rhythmicity was impaired. A major difference between this transgenic model and the surgical approach adopted in the past is that SCN lesion procedures often disrupted further neural structures and/or connections in the brain. In this regard, SCN injury experiments led to whole organismal arrhythmia both at the behavioural and transcriptional levels[57,78,81,117,219–222], which is a quite different outcome compared to the one obtained by specifically deleting *Bmal1* from the SCN neurons[218]. Based on their results, Husse and colleagues proposed a light-driven non-canonical pathway that goes through the SCN, albeit being independent of the SCN clock, in order to synchronise the peripheral clocks[223]. However, the precise molecular mechanisms behind peripheral clock entrainment are yet to be determined.

With the aim to investigate the contribution of the local clockwork on tissue physiology, additional mouse models have been developed that allow for tissue-specific rescue of BMAL1 in a *Bmal1*-KO murine background[80,224]. McDearmon *et al.* used a transgenic murine model of hemagglutinin (HA)-tagged *Bmal1*, whose conditional expression was triggered by the tetracycline transactivator system, in either the brain or the muscle of full-body *Bmal1*-KO mouse. Brain-rescued mice displayed circadian locomotor activity but lower overall activity levels, whereas muscle-rescued animals were arrhythmic in their behaviour though maintaining high activity levels[224]. However, this group did not report any evidence regarding the transcriptional output of these animals. Conversely, Sinturel *et al.* reconstituted *Bmal1* expression from the endogenous *Bmal1* locus in the liver of full-body *Bmal1*-KO mice, which led to behavioural arrhythmia but cyclic clock gene expression in liver[80]. Altogether, circadian *in vivo* models are essential to boost the current understanding about systemic and tissue-specific mammalian rhythmic physiology.

1.2 The skin tissue

Mammalian skin is a multi-layered organ that functions as a barrier, in order to protect the organism from external challenges. It is characterised by the epidermis, underlying dermis, and subcutaneous fat layer (Figure 3). The subcutaneous adipose tissue provides thermoregulation and structurally sustains the skin[225]. The dermis supports and nourishes the epidermis, and is crucially involved in wound healing[225]. The epidermis is the outermost part of the skin and is composed of a multi-layered epithelium, the interfollicular epidermis (IFE) and all the associated specialised structures, namely hair follicles (HFs), sweat and sebaceous glands[226] (Figure 3). HFs are elaborate mini-organs that span the entire width of the skin (Figure 3). They are in the order of millions throughout the mammalian body, and their main function is to provide a suitable seasonal coat for thermoregulation, protection and touch sense. The glands are essential for lubrication of hair and skin. The sweat glands provide thermoregulation and aid movements, whereas the sebaceous glands secrete a lipid-based fluid to protect the epidermis and hair[227]. From inner to outer, the different layers (or strata) of the skin epithelium are: stratum basal, spinous (or squamous), granulosum (or granular), and stratum corneum (Figure 3). The latter is essentially composed of anucleate dead cells, which constantly shed from the body.

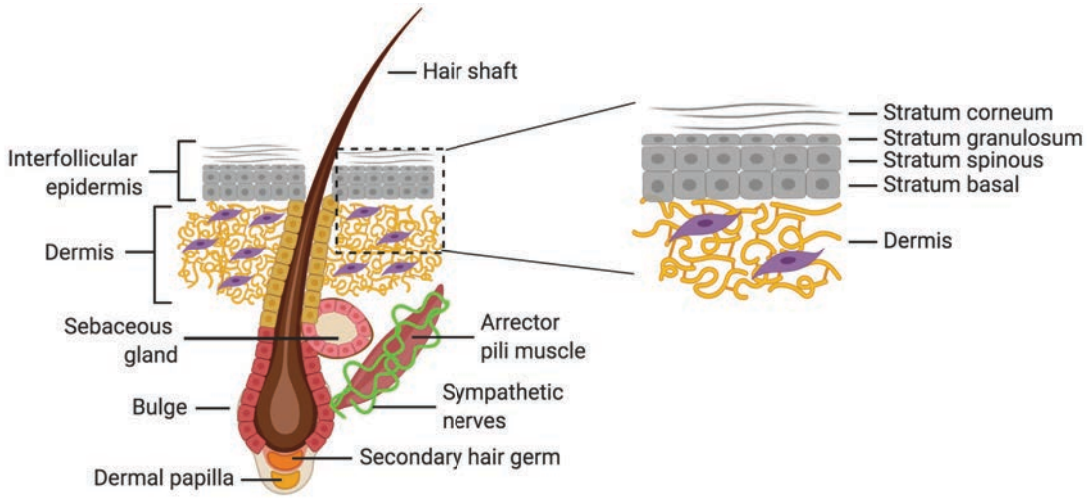

Figure 3. The skin complex architecture

Simplified schematic of the skin tissue. Hair follicles are scattered throughout the epidermal tissue and emerge from the skin through the hair shaft. In this schematic, a hair follicle in resting (telogen) phase is depicted, with the dermal papilla situated below the secondary hair germ. The bulge structure hosts self-renewing stem cells that ensure epidermal turnover. The interfollicular epidermis is flanked by hair follicles and is characterised by many layers, from the corneum to the basal one (grey cell layers). The underlying dermal tissue is rich in fibroblasts (purple cells) and collagen (yellow structure), and provides support to the adjacent epidermis. The sebaceous gland is one of the main accessory structures that contribute to the protective function of the skin, while the arrector pili muscle allows contraction of the hair, thanks to the sympathetic innervation (green structure).

The epidermis is characterised by a high cellular turnover, whereby cells of the basal layer proliferate upwards into the suprabasal part. Here, they terminally differentiate, eventually lose their nucleus, and finally shed from the uppermost cornified layer[228]. Differentiating/dying cells moving towards the skin's surface contribute to form the hard external layer characterised by cross-linked lipid/protein complexes that ultimately function as a defensive barrier.

The most abundant cellular component of the epidermis are the keratinocytes, followed by melanocytes, Merkel and Langerhans cells. Melanocytes are melanin-producing cells, which in mouse skin are situated within the HFs, whereas in human skin they localise to the IFE. Melanin is the pigment responsible for skin colour (including hair pigmentation), and is taken up by keratinocytes to protect against UV radiation[229]. Merkel cells are mechanoreceptor cells that are located in the epidermal basal layer in structures called "touch domes", where they enable touch sensation[230]. Langerhans cells are dendritic cells that are ubiquitous in the epidermis, but are mostly present in the squamous layer, and function as antigen-presenting cells in cases of skin infections[231].

The epidermis is separated from the collagen- and fibroblast-rich dermis by a basement membrane, as to allow communication between these two skin compartments[232] (Figure 3). Specifically, the dermis is extremely important for proper epidermal development, and plays a critical role in the formation of HFs[233]. Moreover, the arrector pili muscle situated in the dermis attaches the HFs to the IFE (Figure 3). This connection is crucial for piloerection, which is mediated by the sympathetic nervous system and ensures proper thermoregulation as one of the main functions of the skin[234] (Figure 3). However, it has been suggested that this functional triad of epidermis, muscle and nerves might play further physiological roles within the skin tissue[235].

The keratinocytes of the basal epidermal layer, as well as the cells localised to the protruding bulge region of the lower HF, are mostly stem and progenitor cells, which synthesise structural proteins, such as Keratin (K)14 and K5[236]. Upon differentiation, K10 and K1 become the major markers expressed by these cells[237]. Emphasising their importance for integrity of the skin barrier, mutations affecting these keratins lead to serious skin diseases. For instance, epidermolysis bullosa simplex is triggered by mutations in K14, causing frailty of the epidermal stem cells layer[238,239]. Moreover, epidermolytic hyperkeratosis is a disorder of K10 and leads to instability of the terminally differentiated skin barrier[240]. Indeed, the keratins structural network is

essential for maintaining skin integrity and protection against external challenges. Further structural proteins that also interact with keratins are loricrin, involucrin and filaggrin, whose concentration is proportionally related to the differentiation status of the epidermis[241–243].

The skin tissue can transition from a resting to a tissue-regenerating phase during the hair cycle. Starting from approximately 18 days after birth, murine HFs continuously undergo cycles of cell proliferation-induced growth, apoptosis-driven regression (or destruction), and relative resting (or quiescence), termed anagen, catagen, and telogen phases, respectively[244]. During the resting phase, HFs receive the inhibitory signals coming from the lower dermis and the subcutaneous adipose tissue[245], particularly the Bone Morphogenetic Protein (BMP). This state lasts until BMP activity is suppressed, leading to a state called “competent telogen”[246,247]. The HF responsive region to anagen-promoting signals is the hair germ: a structure situated below the bulge that forms after the first postnatal destructive HF phase. Anagen entry occurs when BMP levels reach their trough, while wingless/int (WNT)-activating signals are at peak and nuclear β-catenin is stabilised[248,249]. The HF regenerative phase is fueled by bulge stem cells that are supported by melanocyte stem cells, which in turn receive TGFβ signals produced by HF stem cells to maintain them in a quiescent state[250]. At the onset of the anagen phase, WNT signalling coming from both bulge and melanocyte stem cells favours their proliferation, as well as pigment production[229]. This is accompanied by dermal fibroblast proliferation and extracellular matrix (ECM) remodeling[251], in order for the HF to expand downwards within the dermis and fully regenerate. The earliest HF morphogenesis takes place within two weeks from birth, which is then followed by two synchronised HF complete cycles. Later, especially during ageing, HF cycles happen asynchronously, with each HF following its own rhythm[252]. The robust regulation of HF regeneration emphasises the importance of a spatio-temporal organisation of tissue function in skin.

1.2.1 The skin clock in homeostasis

Circadian rhythms temporally coordinate peripheral tissue function. Particularly, ECM-rich tissues, such as skin, arteries and lungs, undergo substantial physiological fluctuations in a daily fashion[253]. In recent years, skin has become a valuable model for circadian studies[254], due to its well-characterised structure and predictable HF cycles. The daily rotation of the earth renders several natural phenomena, such as UV radiation and temperature fluctuations, circadian. Hence, organisms have employed their circadian clocks, including the one in the skin, in order to face the diurnal environmental challenges, and guarantee proper tissue homeostasis[227].

The first evidence of circadian mitotic activity of murine keratinocytes dates back to 1948, when Bullough sampled ear epidermis around the clock at two-hour intervals and studied peak and trough of mitosis[255]. However, circadian expression of clock genes in both human and mouse skin was first formally demonstrated 20 years ago[256–258]. Functional proof of an intrinsic circadian clockwork in the skin was provided instead by Tanioka and colleagues[259]. By analysing the circadian expression profiles of core clock genes and CCGs in epidermal samples of mice kept under DD conditions, they found that rhythmic oscillations were maintained in WT mice, but were lost in SCN-ablated or *Cry1/Cry2* double-KO mice[259]. Further, mutations in *Bmal1* and *Clock* genes were found to delay HF cycling and anagen entry because of a lack of synchronous mitotic activity mediated by the core clock genes[260]. Subsequently, Janich and colleagues characterised the role of the time-keeping system in coordinating epidermal stem cell function, as well as the consequences of its disruption[217]. They found that *Bmal1* controls the circadian expression of regulatory genes, such as key components of the WNT and BMP signalling pathways required for fine-tuning the balance between stem cell quiescence and activation[217].

One of the main mechanisms through which the circadian clock modulates tissue physiology is via the cell cycle. This connection is mediated by WEE1 kinase that is a fundamental regulator of the CYCLIN B1/CDC2 (cell division control protein 2, also known as cyclin-dependent kinase 1 [CDK1]) complex, which gates entry to the mitosis[261]. Its activity follows a circadian pattern, as BMAL1 and CLOCK are able to rhythmically bind to the E-box sequences present in its promoter region[261]. Moreover, the CYCLIN B1/CDC2 complex phosphorylates SIRT1, thereby regulating its HDAC function that is important for cell cycle progression[262]. In this regard, it has been suggested that temporal cell cycle gating in the skin evolved as a mean to protect the tissue, by avoiding the overlap between DNA replication and genotoxic factors, like UV radiation and ROS production[181,263,264]. A further regulator of temporal cell cycle

progression is p21 that is a cyclin-dependent kinase inhibitor. By binding to regulatory sequences on its promoter, p21 activity is positively or negatively modulated by RORs or REV-ERBα, respectively[265]. Therefore, this represents an additional layer of circadian control of cell cycle that BMAL1 executes indirectly. In fact, *Bmal1* deficiency leads to an increased *p21* expression in murine skin[260].

In addition to the cell cycle, DNA repair is also under circadian control in order to make it coincide with the highest frequency of DNA damage and ensure overall epidermal homeostasis. This circadian regulation of DNA damage repair is lost in *Bmal1*-KO mice[198]. Notably, the expression of the nucleotide excision repair (NER) factor Xeroderma Pigmentosum group A (XPA) oscillates in a circadian fashion and troughs at night when the cell cycle S-phase peaks[266]. This anti-phasic relation is linked to the fact that DNA lesions induced by UV radiation, ROS, and other genotoxic products are corrected by the protracted process of NER, which could delay DNA replication, leading to genomic instability[227,267].

With the aim to study the circadian regulation on epidermal cell proliferation, Geyfman *et al.* performed circadian transcriptomic studies of the different HF growth phases[268]. Cells in telogen and anagen were found to have very distinct circadian signatures, with only the core clock genes being common between the two conditions[268]. They showed that the resting stage is largely characterised by cell cycle and metabolic processes, whose genes are antiphasic to each other, peaking in the evening and in the morning, respectively. Moreover, epidermal stem cells of clock-deficient mice failed to exhibit regular rhythmic cycles of proliferation and differentiation, underlying a defective cell cycle coordination[217,268,269]. Indeed, radio-protective effects, including hair loss prevention, were seen in mice exposed to γ-radiation during the evening versus the morning when there is the lowest HF mitotic activity[269]. Nevertheless, these effects largely disappeared when *Cry1/Cry2* double-KO mice were subjected to the same experimental conditions. Altogether, these radio-protective effects were seen to be mediated by circadian synchronisation of the HF cell cycle and DNA repair mechanisms, further supporting the importance of the skin clock machinery in diverse homeostatic processes[269]. These observations have obvious implications for the daily susceptibility of skin to UV radiation[270], whose DNA-damaging effects are among the main causes of skin cancer and ageing.

1.2.2 The skin clock in regeneration

Tissue regenerative processes are strictly regulated physiological mechanisms occurring in healthy individuals. The skin is the most exposed tissue to external damage and thus undergoes repeated rounds of tissue damage and repair in a lifetime. Wound healing is a spatio-temporal fine-tuned process[271]. The very first step of this regenerative program is the inflammatory phase, which consists of the formation of a fibrin clot (eschar) that stops blood loss, while allowing for recruitment of innate immune cells, fibroblasts and epidermal cells[272,273]. A key second phase of tissue repair is the proliferative stage and wound re-epithelialization. The latter is mainly represented by keratinocyte, fibroblast and endothelial cell proliferation, followed by actin-mediated cell migration towards the injury site[274,275].

During skin wound repair, a major role is played by the resident tissue stem cells. In this context, lineage fidelity and spatial restrictions are downregulated, in order to allow epidermal stem cells to differently contribute to wound healing[276–281]. Lineage tracing studies have demonstrated the ability of HF and IFE stem cells to be quickly recruited to the injury site in order to repair it. After the wounding process is over, these cells often migrated back to their site of origin, suggesting a rather temporary plasticity and an underlying long-lasting lineage and positional memory[282]. Finally, the last step of the wound healing program is the remodeling and resolution stage. This phase mainly affects the collagen-rich dermis, with fibroblasts playing a central role in synthesising new ECM and closing the lesion, ultimately restoring skin architecture and integrity[271,273,280].

The whole wound repair process has been demonstrated to exhibit a rhythmic pattern, along with the striking observations that the time of the day at which damage occurs matters for the overall injury resolution. In *in vitro* wounding assays of synchronised skin fibroblasts, the best healing response was triggered when *Per2* expression was peaking at the moment of wound induction[283]. Accordingly, synchronised human keratinocytes underwent a better healing response *in vitro* when lesioned at *Bmal1* trough. On the same line, human skin burns occurring at night have a slower healing rate than those happening during the day[283].

Alongside skin stem cell populations, fibroblasts also display robust circadian fluctuations in their contribution to wound healing. For instance, fibroblast recruitment to the injury site follows a circadian pattern. In this context, the cell-intrinsic fibroblast clock temporally organises the actin cytoskeletal dynamics that allow rhythmic cell motility[283]. Furthermore, *Cry*-deficient fibroblasts fail to drive rhythmic regulation of

actin[283]. Moreover, fibroblasts from NONO$^{-/-}$ mice have been shown to maintain their rhythmic oscillations, but display defective wound healing properties, with poor or no ECM production, a higher cell division rate and a reduction in cellular senescence[284]. NONO is a nuclear protein that has been found to partner with PER1[285]. In addition, NONO is able to directly bind to the promoter of yet another clock gene, namely REV-ERBα[286]. Indeed, when NONO expression was knocked down, dampened circadian rhythms were obtained in mammalian cells and in fruit flies[285]. The cell cycle inhibitor and senescence regulator p16^{Ink4a} is a direct target of NONO rhythmic transcriptional activity, indicating a possible explanation of why NONO deficiency leads to fibroblast hyperproliferation and lower senescence[284,287]. Impaired wounding healing ability has also been observed in *Per1/Per2* mutant mice and *Bmal1*-KO mice, further highlighting the central role of the circadian clock in this physiological process[284].

In a recent study, wound healing dynamics were extensively characterised in *Bmal1*-KO mice, revealing a slower wound closure than WT mice[288]. In this regard, a significantly lower number of proliferating cells was seen in the *Bmal1*-KO mice upon injury, likely due to the observed additional deregulation of phosphorylated SIRT1. As a result, the damaged skin from *Bmal1*-KO mice displayed higher levels of ROS production[288]. Therefore, when ROS accumulation was experimentally inhibited, a rescue in the healing delay of *Bmal1*-KO lesions was obtained[288]. These results suggest a functional connection between metabolism and the circadian clock as a central interplay in skin regenerative processes.

1.2.3 The skin clock in ageing

Skin ageing is the consequence of physiological cellular ageing, in part caused by the constant exposure to environmental challenges like UV radiation. As a result, the mammalian epidermal structure deteriorates extensively during ageing[289,290]. In humans, this manifests as adult epidermal stem cell exhaustion, leading to decreased regenerative potential[291,292]. In this regard, the pool of stem cells in the aged murine bulge stays unchanged[293,294], while their self-renewal capacity decreases during ageing[217,295].

A growing body of evidence suggests that ageing has profound effects on the identity of rhythmically expressed genes in both human and murine epidermal stem cells[183,296]. In particular, Solanas *et al.* demonstrated that the daily oscillating transcriptome is extensively reprogrammed towards a stress-like signature containing categories like DNA damage and inflammation[183]. Nevertheless, aged murine epidermal stem cells maintain a robust core clock machinery[183]. Notably, this study indicated that circadian models of premature ageing, such as full-body *Bmal1*-KO mice, cannot fully recapitulate the circadian transcriptional reprogramming observed during physiological ageing[183]. However, a disrupted clock machinery still results in premature cellular ageing. In fact, *Bmal1*-KO mice display lower epidermal self-renewal, impaired hair growth and increased epidermal differentiation[196,217]. Furthermore, deficiency of *Bmal1* specifically in $K14^+$ cells results in severe epidermal ageing, as highlighted by the increased expression of differentiation markers, such as loricrin and filaggrin, and by the development of a thicker layer of epidermal cornification[217]. Altogether, the circadian clock tightly regulates physiological skin ageing. Therefore, in recent years the circadian field has been given a major focus for understanding the molecular and physiological mechanisms of ageing.

2. Objectives

According to the accepted circadian model, the main *Zeitgeber,* i.e. light, synchronises the central pacemaker (SCN) with the external time. In turn, the SCN establishes behavioural rhythms and coordinates neuronal and hormonal rhythmic signals to be sent to the different peripheral tissues, where the tissue intrinsic circadian clockwork regulates physiological processes according to the time of the day[3].

In contrast to this hierarchical model of circadian clock regulation, it has been suggested that light can entrain peripheral oscillators in mice with no functional molecular clock in the SCN[218]. Hence, in addition to an SCN-dependent clock pathway, the existence of alternative pathways that synchronise peripheral tissue clocks in an SCN-independent manner has been proposed[223]. However, it remains unclear how, in the absence of a central pacemaker, peripheral tissues preserve transcriptional rhythmicity and synchrony upon light stimulus.

Therefore, the present PhD project aimed to address the following major questions:

1. Do tissue clocks require communication with each other to maintain a robust clock machinery?
2. How do peripheral tissues adapt their clockwork to the daily environmental changes?
3. Which clock interactions are key for driving epidermal circadian physiology?
4. Which mechanisms are responsible for peripheral clock entrainment to the external environment?
5. What are the minimal requirements for physiological circadian processes to occur in the skin?

3. Materials and Methods

3.1 Animal models

All mice were bred and maintained at the animal facilities of the Barcelona Science Park in strict accordance with the Spanish and European Union regulations. The Catalan Government approved all experimental protocols, in accordance with applicable legislation and the guidelines of the Institutional Animal Care and Use Committee (IACUC) of the Barcelona Science Park. Animal experiments were designed and conducted with consideration of the ARRIVE guidelines.

3.1.1 Generation and breeding strategy of the *Bmal1-stopFL* mice

Bmal1-stopFL mice were generated in the C57BL/6 background, adopting a conditional gene-trap approach. A stop cassette including a splice acceptor (SA), an mCherry reporter, a poly-A tail, and a neomycin resistance cassette delimited by Flippase Recognition Target (FRT) sites was flanked by loxP sites and inserted immediately after the first translated exon (i.e. exon 5) of the *Arntl* gene, which codes for BMAL1 protein (Figure 4A). The neomycin cassette was utilised for clonal selection and excised by Flippase (FLP)-mediated recombination after successful germ line transmission. Thus, the stop cassette prevents transcriptional read-through after exon 5 of the *Arntl* gene. Cre-mediated recombination allows removal of the loxP-flanked stop cassette, including the mCherry reporter, hence reconstituting the WT *Arntl* locus, leaving behind only one loxP site between exon 5 and exon 6 (Figure 4A). *K14-Cre*[297]*, Syt10-Cre*[298]*,* and *Alfp-Cre*[299] mice were backcrossed to the C57BL/6 background for at least ten generations. Mice that were heterozygous for *Bmal1-stopFL* and for the *K14-Cre* were crossed to generate the following experimental animals: WT: $Arntl^{wt/wt}$, $K14\text{-}Cre^{tg/wt}$; RE: $Arntl^{stopFL/stopFL}$, $K14\text{-}Cre^{tg/wt}$; KO: $Arntl^{stopFL/stopFL}$, $K14\text{-}Cre^{wt/wt}$. Mice that were heterozygous for *Bmal1-stopFL* and for the *Syt10-Cre* were crossed to generate the following experimental animals: WT: $Arntl^{wt/wt}$, $Syt10\text{-}Cre^{tg/wt}$; SCN-RE: $Arntl^{stopFL/stopFL}$, $Syt10\text{-}Cre^{tg/wt}$; KO: $Arntl^{stopFL/stopFL}$, $Syt10\text{-}Cre^{wt/wt}$. Mice that were heterozygous for *Bmal1-stopFL* and for the *Alfp-Cre* were crossed to generate the following experimental animals: WT: $Arntl^{wt/wt}$, $Alfp\text{-}Cre^{tg/wt}$; Liver-RE: $Arntl^{stopFL/stopFL}$, $Alfp\text{-}Cre^{tg/wt}$; KO: $Arntl^{stopFL/stopFL}$, $Alfp\text{-}Cre^{wt/wt}$. Mice that were heterozygous for *Bmal1-stopFL* and for the *K14-Cre/Syt10-Cre* were crossed to generate the following experimental animals: WT: $Arntl^{wt/wt}$, $K14\text{-}Cre^{tg/wt}$, $Syt10\text{-}Cre^{tg/wt}$; RERE: $Arntl^{stopFL/stopFL}$, $K14\text{-}Cre^{tg/wt}$, $Syt10\text{-}Cre^{tg/wt}$; KO: $Arntl^{stopFL/stopFL}$, $K14\text{-}Cre^{wt/wt}$, $Syt10\text{-}Cre^{wt/wt}$. Table 1 depicts the primers used for genotyping of the various mouse lines.

Table 1. Primers for genotyping

Primer	Sequence 5'-3'
stopFL-WT forward	CCCCCTACTCCTCTTCACCT
stopFL-WT reverse	TCAGCCAGAGTAGCCAGACA
stopFL-Tg reverse	GCCTGTCCCTCTCACCTTCT
K14-Cre-Tg forward	TTCCTCAGGAGTGTCTTCGC
K14-Cre-Tg reverse	GTCCATGTCCTTCCTGAAGC
K14-Cre-WT forward	CTAGGCCACAGAATTGAAAGATCT
K14-Cre-WT reverse	GTAGGTGGAAATTCTAGCATCATCC
Syt10-Cre forward	AGACCTGGCAGCAGCGTCCGTTGG
Syt10-Cre reverse	AAGATAAGCTCCAGCCAGGAAGTC
Syt10-Cre knock-in	GGCGAGGCAGGCCAGATCTCCTGTG
Alfp-Cre forward	TCCAGATGGCAAACATACGC
Alfp-Cre reverse	GTGTACGGTCAGTAAATTGGAC

3.2 Experimental setups and procedures

3.2.1 Transcriptomic circadian studies

For the transcriptomic experiments, four 8-week-old mice were used per genotype per time point. Specifically, females were used for the first 12h Light/ 12h Dark (LD) and 24h Darkness (DD) experiments that were carried out with RE and Liver-RE mice, as well as for the DD experiment with RERE mice, whereas males were used for the LD experiment with RERE mice. For the LD experiments, mice were kept under standard LD photoperiod for the whole time, until sacrifice. For the DD experiments, mice were transferred into constant darkness when they reached 7 weeks of age, and were kept in darkness for a total of 156h to 176h. The animals were sacrificed with CO_2, under red light illumination in the case of the DD experiments, in accordance with the local and national regulations. Mice were entirely shaved, and whole skin was collected and placed into ice-cold phosphate buffered saline (PBS). Liver collection was performed after skinning the mice, and liver samples were immediately snap frozen in TRIzol (Invitrogen) for later RNA extraction.

3.2.2 Time-shift experiment

For the time-shift experiment, four WT and four RE 8-week-old females were used per time point. Mice were maintained under standard LD photoperiod, and then underwent an inversion of this light cycle by advancing the light cycle by 12 hours (i.e. 24h of continuous light), similar to a “westward” traveling. Epidermis collection was performed in 4h intervals at twelve time points for the two consecutive days following the 12h shift, and for another seven time points corresponding to day 4 after the time-shift exposure.

3.2.3 Sympathectomy procedure

Chemical sympathectomy was performed on 6 weeks old female mice, by subcutaneous injections of 10mg/ml 6-hydroxydopamine (6-OHDA; Tocris) diluted in 0.1% ascorbic acid and protected from light. Specifically, mice were subjected to two rounds of injection under isoflurane anaesthesia. For the LD sympathectomy experiment, mice underwent the first round of injections on experimental day 0, where a total of 200µl of 10mg/ml 6-OHDA (or 0.1% ascorbic acid for the sham injections) was subcutaneously injected into the centre of four quadrants in the back of the mice on a X-shape basis. The substance was then spread through the back by massaging from the injection sites. On day 2, the subcutaneous injections were repeated, this time by administering 200µl of 10mg/ml 6-OHDA (or 0.1% ascorbic acid for the sham injections) on a cross-shape basis, and again massaging from the injection sites to spread the compound throughout the back. Mice were monitored every two days until they were sacrificed on day 14 for IFE collection.

For the DD sympathectomy experiment, the timing and procedure of the injections was the same as for the LD experiment. However, on day 7 mice were transferred into constant darkness, and were kept in darkness until they were sacrificed on day 14 for IFE collection.

3.2.4 Ageing studies

For the first ageing study carried out with RE mice, shaved back skin samples were harvested from 12 WT, 17 RE and 7 KO 30-week-old males. For the second ageing study that was performed with RERE mice, shaved back skin samples were harvested from 5 WT, 5 RE, 5 SCN-RE, 5 RERE, and 5 KO 26-week-old males and females. Skin samples were placed in 10% neutral buffered formalin for 3h at room temperature (RT), washed in PBS, and paraffin-embedded. All mice used in ageing studies were weighed once a week. For the aged epidermal transcriptomic studies 5 WT, 5 RE, 5 SCN-RE, 5 RERE, and 5 KO 26-week-old males and females were used for IFE collection.

3.2.5 Wounding assay

For the wound healing assay, 14 WT, 11 RE, 9 SCN-RE, 12 KO, and 7 RERE 8-week-old males, as well as 12 WT, 9 RE, 6 SCN-RE, 8 KO, and 5 RERE 15-week-old males were wounded and then monitored every two days for wound closure. For the histological analyses, two to six wounds were used from the respective genotypes. Wounding was done by performing two symmetrical 5mm biopsy punches on the lower back of the mice. To achieve this, mice were anesthetised using isoflurane and subsequently maintained under anaesthesia for the duration of the experiment. The area to be lesioned was then shaved and sterilised with 70% ethanol solution. Subsequently, buprenorphine (0.03mg/kg) was subcutaneously injected into the neck scruff to provide analgesia. The mouse was then flipped onto a side, and a sterile 5mm biopsy punch was used to make two symmetrical wounds through the skin in the lower part of the back. If necessary, the remaining skin was removed with tweezers, and measures of the lesions' longest sides were taken using digital calipers. Wounded mice were individually housed and warmed with red lamp illumination until recovery from anaesthesia. 24h after the procedure, buprenorphine injections were administered to provide continued post-surgical analgesia. The animals were then monitored every day and wounds were measured every second day until scar tissue establishment. For histological analyses, wounds, including immediately surrounding region, were excised, cut in half, fixed in 10% neutral buffered formalin at RT for 3h, and paraffin-embedded.

3.3 Isolation of epidermal cells

The whole mouse skin was used to isolate the IFE, as previously described[183,300]. First, the hypodermis was scraped off with a scalpel, and the skin samples were floated on 1mg/ml dispase (Sigma-Aldrich) dissolved in PBS at 37ºC for 45min. Dispase activity was inactivated with 15% chelated fetal bovine serum (GIBCO) diluted in EMEM medium without calcium (Lonza). To separate the IFE from the dermis, the former was scraped off with a scalpel, mechanically disaggregated, and then sequentially filtered through a 100µm and a 40µm cell strainer. Cell suspensions were centrifuged at 4ºC for 20min at 300g. Pellets of 1 million cells were lysed and then frozen in TRIzol (Invitrogen) at -80ºC for subsequent RNA extraction. The remaining cells were washed with ice-cold PBS and stored at -80ºC for later protein extraction.

For sequential collection of ear snip epidermis from the same individual mouse, small pieces of ear were taken every 4h at six consecutive time points around the clock, under red light illumination. The experimental mice, namely 3 WT, 3 RE and 2 KO

mice, were kept in DD for one week prior to sample collection. Ventral and dorsal halves of the ear snips were manually separated with forceps and floated on 1mg/ml dispase (Sigma-Aldrich) dissolved in PBS, at 37ºC for 40min. After incubation, the epidermal sheet was separated from the dermis and immediately stored in TRIzol (Invitrogen) at -80ºC for subsequent RNA extraction.

3.4 Behavioural analyses

3.4.1 Drinking behaviour analysis

As an indicator of rhythmic physiological activity, drinking behaviour of mice was measured. Mouse drinking activity was monitored using IntelliCage cages[301], which measure basal physiological activity in a social environment. Microchips were surgically inserted in the upper back of three females per genotype (ranging from 9 to 20 weeks of age), in order to track individual visits to the drinking bottle. Prior to the start of the experiment, the mice were adapted to the IntelliCage cages for one week. Subsequently, mice were monitored under standard LD conditions for the first week, followed by constant darkness for one week, and finally a normal LD photoperiod for a further week. The behaviour of each mouse was analysed separately for each week and is displayed as average visits per day during each 4h time bin.

3.4.2 Metabolic data analysis

Indirect calorimetry was carried out with negative flow Oxymax-CLAMS (Columbus Instruments) hardware system cages. Mice of 10 to 14 weeks of age were individually housed, and were allowed a 24h acclimation period to the metabolic cage. In all metabolic experiments, standard chow and water were available *ad libitum* and mice were kept under either LD or DD conditions. Measurements of VO_2, VCO_2, food intake, and energy expenditure were taken every 10min for two consecutive days. Respiratory exchange ratio ($RER=VCO_2/VO_2$) was calculated by the accompanying Oxymax software itself.

3.4.3 Locomotor activity analysis

Locomotor activity of singly housed 10 to 16 weeks old mice was measured using optical beam motion detection (Starr Life Sciences). The resulting data were then collected using Minimitter VitalView 5.0 data acquisition software and analysed using Clocklab (Actimetrics).

3.5 RNA extraction

Total RNA extraction was performed from liver or IFE by homogenization in TRIzol (Invitrogen). Upon RNA, DNA and protein layer separation with chloroform, epidermal cells and livers were lysed with RLT buffer (Qiagen) and RNA was precipitated with absolute ethanol. RNA was washed three times with RPE buffer (Qiagen) and pelleted using the Qiagen RNeasy mini columns. RNA was resuspended in RNase-free water and quantified using the NanoDrop system (Thermo Fisher).

3.6 Real-Time quantitative PCR

200ng of RNA extracted from either IFE or ear snips epidermis was converted into complementary DNA (cDNA) by reverse transcription, using the Applied Biosystems High Capacity cDNA Reverse Transcription Kit (Thermo Fisher). Gene expression levels were quantified by real-time quantitative PCR (qPCR), using TaqMan Gene Expression Master Mix (Thermo Fisher) on an Applied Biosystems QuantStudio 6 Flex (Thermo Fisher). The results were examined using the ΔΔCT method and are shown as changes of gene expression relative to the *B2m* and *Hprt1* housekeeping genes. The TaqMan probes used in this study are listed in Table 2.

Table 2. TaqMan probes

Gene	Probe
Arntl	Mm.PT.58.11121936
B2m	Mm.PT.39a.22214835
Dbp	Mm.PT.58.16911772
Hprt1	Mm.PT.39a.22214828
Nr1d1	Mm00520708_m1
Per2	Mm.PT.58.5594166
Per3	Mm00478120_m1
Th	Mm.PT.58.33106186

3.7 RNA-sequencing

Quality control and quantification of the extracted total RNA was performed using the Qubit RNA HS Assay (Life Technologies) and the RNA 6000 Nano Assay on a Bioanalyzer 2100 (Agilent), respectively. Starting from 500ng of total RNA, libraries were prepared with the TruSeqStranded mRNA LT Sample Prep Kit (Illumina, Rev.E, October 2013). The final libraries were then validated on an Agilent 2100 Bioanalyzer with the DNA 7500 assay (Agilent).

Libraries generated from the experiments with RE mice were sequenced on HiSeq2000 (Illumina, Inc) in paired-end mode with a read length of 2 x 50 bp using TruSeq SBS Kit v4. On average, 48 million paired-end reads were generated for each sample.

To sequence all other epidermal transcriptomes, libraries were sequenced on HiSeq2000 (Illumina, Inc) in single-end mode with a read length of 50 bp using TruSeq SBS Kit v4. On average, 20 million single-end reads were generated for each sample.

3.8 ATAC-sequencing

For assessing chromatin accessibility, three 8 weeks old females were used per genotype per time point. IFE was isolated and library preparation for ATAC (Assay for Transposase-Accessible Chromatin)-sequencing was performed as previously described[302]. Samples were sequenced on a HiSeq2500 sequencer (Illumina) using V4 chemistry, generating 50 bp paired-end reads.

3.9 Protein isolation and western blot

Cell pellets were lysed in standard Radioimmunoprecipitation Assay (RIPA) Buffer with cOmplete protease inhibitor cocktail (Roche), phosphatase inhibitor cocktail I (Abcam), nicotinamide and trichostatin A (both Sigma-Aldrich) and sonicated five times for 10s with 20% amplitude (Vibra Cell VCX750). Pierce BCA Protein Assay Kit (Thermo Fisher Scientific) was used to calculate the concentration of the isolated proteins, following the Microplate Procedure section of the provided protocol. Absorbance was then measured at 562nm on a multimode microplate reader.

Isolated proteins were diluted in RIPA buffer, to achieve a final concentration of 10µg (50µg for the detection of acetylated BMAL1). Subsequently, samples were mixed with a loading buffer (1:4) and a reducing reagent (1:20) and heated at 95°C for 5min. Next, proteins were immediately placed on ice, and further loaded on pre-cast 6–10%

polyacrylamide gels (Bio-Rad Laboratories) for separation. At this point, membranes were washed in ddH_2O and stained with Ponceaux Red dye for 5min, for visualisation of proteins. Sections of interest were cut and membranes were further washed in 200 mM Tris-HCl buffered saline pH7.5 with 1% Tween 20 (TBS-T) and subsequently blocked at RT with 5% BSA (NZYTech) for at least 1h. After washing in TBS-T, membranes were incubated with primary antibody at 4°C overnight. Table 3 shows the list of the primary antibodies used. Finally, membranes were incubated with HRP-conjugated secondary antibody (Dako) at RT for 1h, and blots were visualised with West Pico Plus kit and chemiluminescence films (Amersham Hyperfilms ECL, Cytiva).

Table 3. Primary antibodies used for western blot and immunohistochemistry

Antibody	Dilution	Company	Code
anti-BMAL1	1:1,000	Abcam	ab93806
anti-phosphorylated BMAL1 (Ser42)	1:1,000	Cell Signalling	13936
anti-acetylated BMAL1 (Lys538)	1:1,000	Merck Millipore	AB15396
anti-TUBULIN	1:5,000	Sigma-Aldrich	T7816
anti-ACTIN	1:5,000	Sigma-Aldrich	A5228
anti-pHH3	1:100	Abcam	ab47297
anti-Ki67	1:100	Abcam	ab15580
anti-CD31	1:100	Abcam	ab28364
anti-LORICRIN	1:500	Abcam	ab85679
anti-K14	1:1000	BioLegend	Poly9060
anti-TH	1:500	Sigma-Aldrich	AB152

3.10 Immunohistochemistry

1cm^2 of shaved back skin was collected immediately after sacrifice, and placed in 10% neutral buffered formalin at RT for 3h; the fixed skin samples were then washed in PBS and paraffin-embedded. Paraffin-embedded tissue sections of 3µm thickness were cut, air-dried and further dried at 60ºC overnight. Table 3 shows the list of antibodies used for the stainings. In the stainings for pHH3, Ki67 and CD31, antigen–antibody complexes were visualised with 3-3′-diaminobenzidine (DAB). Specificity of the staining was confirmed by staining with a rabbit IgG isotype control (ab27478, Abcam).

3.10.1 H/E staining

Haematoxylin/Eosin (H/E) staining was carried out using a CoverStainer (Dako - Agilent) and following standard procedures[303]. Subsequently, sections were de-waxed, and antigen retrieval was performed in a boiler filled with pH9 Tris-EDTA buffer for 20min. 10min incubation with Peroxidase-Blocking Solution (Dako REAL S2023) was carried out to quench endogenous peroxidase activity. R.T.U Animal Free Block and diluent (SP-50035, Vector) were utilised to block non-specific labelling for 30min. Primary antibody RFP Rabbit polyclonal IgG (1:100; Rockland, 600-401-379) was incubated at RT overnight. AffiniPure Goat Anti-Rabbit IgG (H+L) (1:200; Jackson ImmunoResearch Labs, 111-005-003) was incubated for 60min to amplify the signal. BrightVision Poly-HRP-Anti Goat IgG Biotin-free, Ready-to-use (ImmunoLogic, DPVG 55HRP) was used to detect the labelling. Antigen–antibody complexes were revealed with DAB (K3468, Dako), with the same time exposure in each sample (i.e. 30s). Sections were counterstained with Haematoxylin (Dako, S202084) and mounted with Mounting Medium, Toluene-Free (CS705, Dako) using a Dako CoverStainer. Specificity of staining was confirmed by secondary-only control.

3.10.2 Immunofluorescence staining

Antigen retrieval was performed on 3µm tissue sections with citrate (pH6) at 97ºC for 20min. Subsequently, sections were permeabilised with a 0.05% Triton X-100 in PBS solution for 20min, and blocked with 10% goat serum in PBS solution at RT for 1h. Primary antibody incubation was done at 4ºC overnight (with the exception of TH incubation that was done over two days at 4ºC). Table 3 shows the list of antibodies used. Three 15min washes were done with 3% BSA + 0.1% Tween20 in PBS with gentle agitation. Secondary antibody incubation was done at RT for 2h. Three 10min washes were done with 3% BSA + 0.1% Tween20 in PBS with gentle agitation. Nuclei were stained with DAPI (1:10,000; Invitrogen) at RT for 10min. The final washing step of the glass slides was done in PBS for 10min and was followed by mounting with Dako mounting medium.

3.10.2.1 Whole-mount staining

For the whole-mount staining, the murine back skin was waxed, in order to remove the maximum amount of hairs possible and avoid light scattering during imaging. The skin sample obtained upon dissection was fixed at RT in 4% Paraformaldehyde (PFA) in PBS for 2h. The fixed sample was then placed into a 24-well plate, and washed with gentle agitation in 0.5ml 0.3% Triton X-100 in PBS (PBST), changing the PBST every 30min for 6h. The plate was sealed with parafilm during the wash steps. Afterwards,

primary antibodies were diluted in PBST (approximately 200µl/sample), to a final concentration of 1:50 for anti-TH, and 1:100 for anti-K14. Primary antibody incubation was performed at RT for 24h with gentle agitation. Samples were then washed with gentle agitation in PBST, changing the PBST solution every 30min for 6h. Plate was sealed with parafilm during the wash steps. Afterwards, secondary antibodies were diluted in PBST, to a final concentration of 1:100. After secondary antibody incubation, nuclei staining was carried out for 3h at RT using 5µg/ml DAPI. Samples were once again washed with gentle agitation in PBST, changing the PBST solution every 30min for 6h, and were then transferred into 100% methanol for dehydration at 4ºC for 24h. Methanol was changed every 8h. Finally, skin samples were incubated at RT in a mix of 1ml of Benzyl Alcohol with 2ml of Benzyl Benzoate (BABB) until reaching transparency of the tissue (approximately 10min incubation).

3.11 Microscopy and image analysis

3.11.1 Image acquisition

Bright-field images were acquired using a NanoZoomer-2.0 HT C9600 digital scanner (Hamamatsu, Japan) equipped with a 20X objective. Images were visualised with a gamma correction set at 1.8 in the image control panel of the NDP.view 2 U12388-01 software (Hamamatsu, Photonics).

Fluorescence pictures were acquired using a Leica TCS SP5 confocal microscope at 1024x1024 pixel resolution. Fluorescence images were processed using the Fiji v2.0.0-rc-14/1.49 g software (ImageJ[304]).

3.11.2 Image analysis

In the ageing studies, thickness of the cornified layer was quantified with QuPath software[305], by measuring the maximum extension of the cornification between each pair of hair follicles in a skin section. One tissue section was evaluated per sample.

In the wound healing studies, selection of the lesioned skin area, i.e. region of interest (ROI), was done manually. The criterion to select the wounded areas was the presence of an altered dermis with or without existence of epidermis. In all cases, ROI always included epidermis and dermis, but excluded hair follicles, sebaceous glands, hypodermis and muscular layer when present. In all lesioned areas, the diametric extension of wounded tissue was measured in 2-3 different depths. In non-lesioned skin tissues, the maximum diametric extension of the wounded area was used to

determine each diametric of the ROI for the Ki67 and CD31 stainings. Tissue artefacts were excluded from the ROI (e.g. non-specific labelling or broken areas). One tissue section was evaluated per each sample. For the analyses, both epidermis and dermis were assessed independently. The dermis was subdivided into two parts (upper and lower). The changes detected in the epidermis and dermis (i.e. hyperplasia, hyperkeratosis, inflammation) were scored from 1 to 5 as follows: 1 – Minimal; 2 – Mild; 3 – Moderate; 4 – Marked; 5 – Severe.

Quantification of positive cells for the markers pHH3, Ki67 and CD31 was carried out with QuPath software[305]. The positive cell detection algorithm in which nuclei are segmented into DAB positive or negative (DAB negative pixels - haematoxylin) was used. Default stain vectors for haematoxylin/DAB staining were used.

3.12 Quantifications, statistics and GO analyses

3.12.1 ATAC-sequencing analysis

Adapter-trimming and quality correction were done on the raw ATAC-sequencing data (fastq files), using Trimmomatic (version 0.36)[306]. Paired-end reads were aligned to the mm10 genome (UCSC) using BowTie 2 Aligner (version 2.3.3.1)[307]. GenRich (version 0.6, available at https://github.com/jsh58/Genrich) was used to remove duplicate reads, reads mapping at mitochondrial genes or reads mapping at blacklist regions. Peak calling was done using GenRich that allows analysing all replicates together, generating a consensus peak set. Peaks were considered if present in at least two samples. Peaks with a False Discovery Rate (FDR) ≤ 0.05 were selected for further analysis. Additionally, differential peaks were determined using the DiffBind package (version 2.4.8)[308] in R (version 3.54.24) and those with an FDR ≤ 0.05 were selected for further analysis. The distribution of the differential opening regions within genomic features was assessed with HOMER's annotatePeaks.pl. (version 2015-03-22)[309].

3.12.2 RNA-sequencing analysis

Quality correction and removal of possible contaminations from the RNA-seq data were done using Trimmomatic (version 0.36)[306]. Paired-end or single-end reads were aligned to the reference genome (mm10) using TopHat (version 2.1.1)[310]. Upon alignment, the read count was carried out using the featureCounts (version 1.6.0)[311]. From the first LD experiment, three samples were removed from further analysis: 1 WT from ZT16 and 1 RE from ZT8 due to low quality reads, and 1 KO from ZT8 due to wrong genotype.

From the first DD experiment four samples were removed, all due to low quality reads: 1 WT from ZT20, 1 RE from ZT16, 1 RE from ZT20, and 1 KO from ZT20.

3.12.3 Identification of rhythmic genes

The Jonckheere-Terpstra-Kendall (JTK_CYCLE) algorithm[312] was used to identify circadian genes from the different sets of RNA-seq data. Count data were normalised with the RPKM normalisation, using the edgeR rpkm function (version 3.18.1). For all RNA-seq sets, a *p* value of ≤ 0.01 was considered significant. Expression levels for circadian genes in each time point were calculated as the average $\log_2$ RPKM of the biological replicates, with error bars of the replicates representing standard deviation (SD). Amplitude and phase estimations of circadian genes were generated by the JTK_CYCLE algorithm and plotted using the ggplot package in R. The R version used was 3.4.4. The heatmaps of circadian transcripts were generated by using the mean expression value of all replicates per genotype and time point, which was subsequently normalised by calculating the z-score of each gene (RPKM) per genotype and time point over all genotypes and time points. Oscillating genes were ordered according to their phase as defined by the JTK_CYCLE. The heatmaps were plotted using the pheatmap package in R. Venn diagrams were created with Oliveros, J.C. (2007-2015) Venny: An interactive tool for comparing lists with Venn's diagrams (https://bioinfogp.cnb.csic.es/tools/venny/index.html).

3.12.4 Gene Ontology

All GO analyses were performed using PANTHER Classification System (version 16.0). The GO terms belonging to “biological processes” were used for GO term comparison, and the q values were calculated by PANTHER.

3.12.5 Differential expression analysis

The differential expression analysis between the different genotypes was conducted with DESeq2[313]. Differentially expressed genes (DEGs) were defined as genes having an adjusted *p* value ≤ 0.05 and a Fold Change ≥ 1.2. The heatmaps display the z-score per gene (rows) of the RPKM for each genotype (columns). The heatmaps were created using the pheatmap package in R, except those in Figure 30E that were created with Python (version 3.6.1). Venn diagrams were created with Oliveros, J.C. (2007-2015) Venny: An interactive tool for comparing lists with Venn's diagrams (https://bioinfogp.cnb.csic.es/tools/venny/index.html).

3.12.6 Classification analysis

Classification analysis was carried out using "mixOmics" R package 6.1.3. Briefly, we adopted a supervised version of Partial Least Squares (PLS) regression[314], called sparse PLS-Discriminant Analysis (sPLS-DA)[315–317], because a Lasso penalisation[318] has been added to selected variables. The sPLS-DA approach fits a classifier multivariate model that assigns samples to known classes. This extended method denotes X a predictor dataset (expression dataset of all samples), and Y a categorical outcome response matrix that records the membership of each observation (genotypes). Specifically, X is the n*p sample data matrix, where n is the number of samples, and p is the number of variables (genes). In this supervised classification framework, we assume that the samples n are partitioned into K groups leading to replace the dataset for a dummy matrix Y, and the sparse extension aims to optimally maximise the discrimination between the K outcome classes in Y.

3.12.7 Statistics and data visualisation

Circadian genes were determined by the JTK_CYCLE algorithm[312], with a Bonferroni adjusted *p* value cut off of ≤ 0.01. Graphs of the core clock and cell cycle genes, of the survival and body weight, as well as of the various histological parameters of the skin, were generated with Prism 7 (version 7.0b). For each experiment, the number of biological replicates, the statistical test used, and the visual representation information (i.e. mean, error bar, etc.) can be found in the figure legend descriptions (or alternatively in the corresponding Materials and Methods section). Comparison of the survival curves was performed with Prism 7 (version 7.0b) using the log-rank (Mantel–Cox) test. Figures 1-3, 4A, 18A, 36, were created with BioRender.com.

4. Results

4.1 Peripheral clocks respond independently to light to maintain homeostasis

Valentina M. Zinna[1*], Patrick-Simon Welz[1*], Aikaterini Symeonidi[1], Carmelo Laudanna[1], Thomas Mortimer[1], Kevin B. Koronowski[2], Kenichiro Kinouchi[2], Jacob G. Smith[2], Inés Marín Guillén[1], Andrés Castellanos[1], Stephen Furrow[1], Ferrán Aragón[1], Neus Prats[1], Juan Martín Caballero[3], Paolo Sassone-Corsi[2], and Salvador Aznar Benitah[1,4]

[*] These authors contributed equally

Affiliations:

[1]Institute for Research in Biomedicine (IRB Barcelona), Barcelona Institute of Science and Technology, 08028 Barcelona, Spain

[2]Center for Epigenetics and Metabolism, University of California, Irvine, CA 92697, USA

[3]PCB-PRBB Animal Facilities, 08028 Barcelona, Spain

[4]ICREA, Catalan Institution for Research and Advanced Studies, 08010 Barcelona, Spain

4.1.1 A novel *Bmal1-stopFL* mouse model recapitulates the ageing phenotype of full-body *Bmal1*-KO mice

Within the present PhD project, we set out to understand how peripheral tissues adapt to daily environmental changes and whether communication between the circadian clocks in different tissues is necessary to achieve a synchronised rhythmicity. To address this question, we generated a novel mouse model that reconstitutes BMAL1 in selected tissues of an otherwise full-body *Bmal1*-KO mouse (Figure 4A), allowing us to dissect inter-tissue clock communication. To achieve this, we leveraged the Cre/loxP technology and generated a *Bmal1-stopFL* mouse with a stop cassette, flanked by loxP sites, inserted within the *Bmal1* locus (*Bmal1*$^{-/-}$) between exon 5 and 6 (Figure 4A). By crossing these *Bmal1-stopFL* mice with mice expressing Cre recombinase under a tissue-specific promoter, the stop cassette was excised giving tissue-specific reconstitution of clock activity (Figure 4A).

To determine whether the genetic strategy employed was effective, the expression of BMAL1 in various bodily tissues of the *Bmal1-stopFL* mouse was characterised. Importantly, western blot of small intestine, skin, liver, spleen and brain tissues showed an absence of BMAL1 (Figure 4B). Moreover, the *Bmal1-stopFL* mouse displayed all signs of premature ageing previously described for full-body *Bmal1*-KO mice[196], such as impaired weight gain, shorter lifespan, corneal degeneration and arthropathy (Figure 5A&B). As mentioned, the *Bmal1-stopFL* mouse allows for the expression of the core clock gene in the presence of Cre. Hence, by crossing these animals with mice bearing the Cre recombinase under the K14 promoter, we obtained mice expressing *Bmal1* exclusively in K14^{+} cells that are mainly epidermal cells, i.e. *Bmal1-stopFL/K14Cre* mice (Figure 4A). Of note, these mice express the Cre recombinase in the epidermis as early as between E13.5 and E14.5[297]. We refer to the *Bmal1-stopFL/K14Cre* mice as REconstituted (RE) mice, where the core clock gene is reconstituted in only one specific tissue of interest, in this case the epidermis[198] (Figure 4A). We demonstrated this by checking for mCherry expression, which is encoded in the *Bmal1* stop cassette. Thus, only KO epidermis expressed mCherry, as the cassette is absent in the WT and removed by the Cre recombinase in the RE epidermis (Figure 4A & Figure 5C).

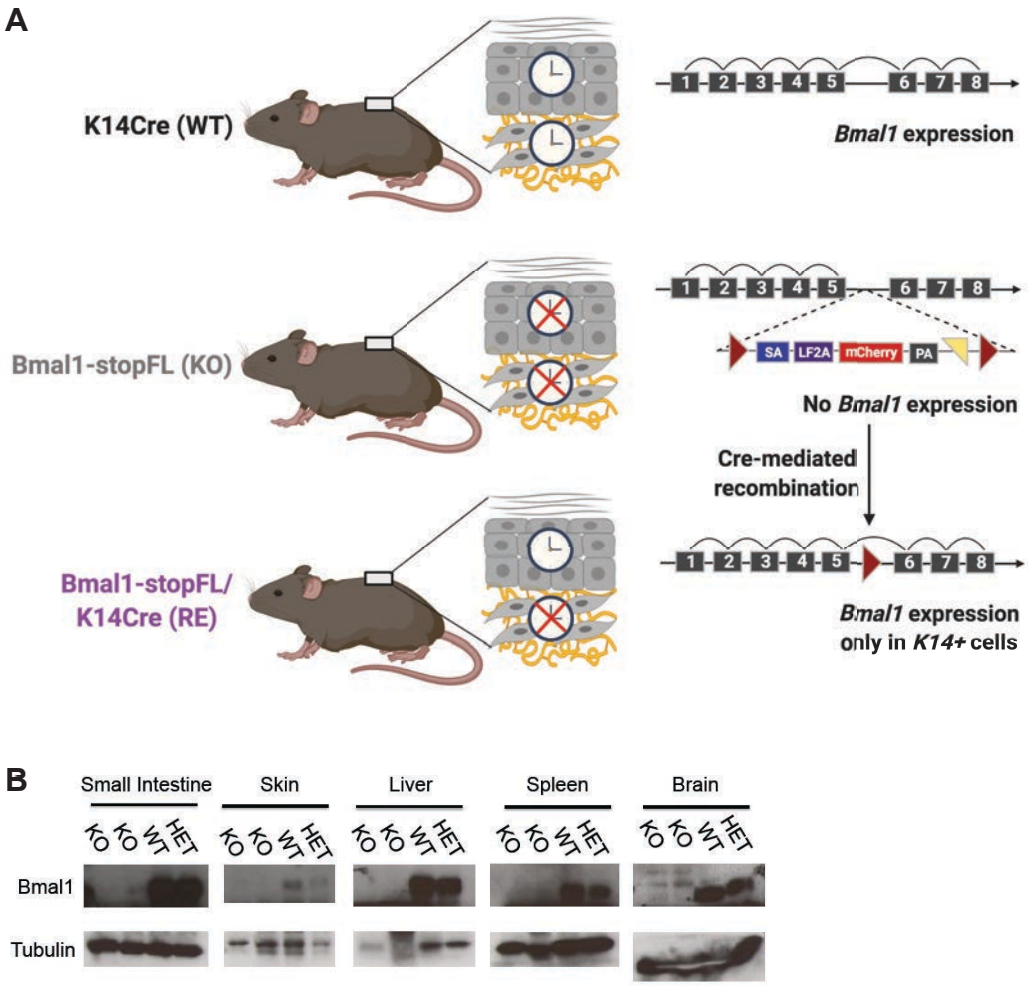

Figure 4. The novel *Bmal1-stopFL* mouse model

(**A**) Schematic of the genomic targeting of *Bmal1-stopFL* mouse. The *Bmal1-stopFL/K14-Cre* mouse model allows the endogenous expression of *Bmal1* only in K14+ cells (RE). Heterozygous K14-Cre (WT) and homozygous *Bmal1-stopFL* (KO) mice were used as experimental controls. (**B**) Immunoblots of Bmal1 from the indicated tissues taken from WT, heterozygous for the stop cassette (HET), and *Bmal1-stopFL* (KO) mice. Tubulin was used as loading control.

We also crossed *Bmal1-stopFL* mice with mice that express the Cre recombinase under the artificial Albumin-α-fetoprotein (Alfp) promoter (generated by combining parts of the albumin and the α-fetoprotein promoter region[299]), thereby obtaining animals with endogenous *Bmal1* expression reconstituted in the hepatocytes of the liver (hereby named Liver-RE mice; for details, refer to[319]). Finally, we checked for BMAL1 expression in different tissues of the RE mice, and found it expressed in the epidermis of *Bmal1-stopFL/K14Cre* mice and in the liver of *Bmal1-stopFL/AlfpCre* mice, but not in spleen or brain (Figure 5D).

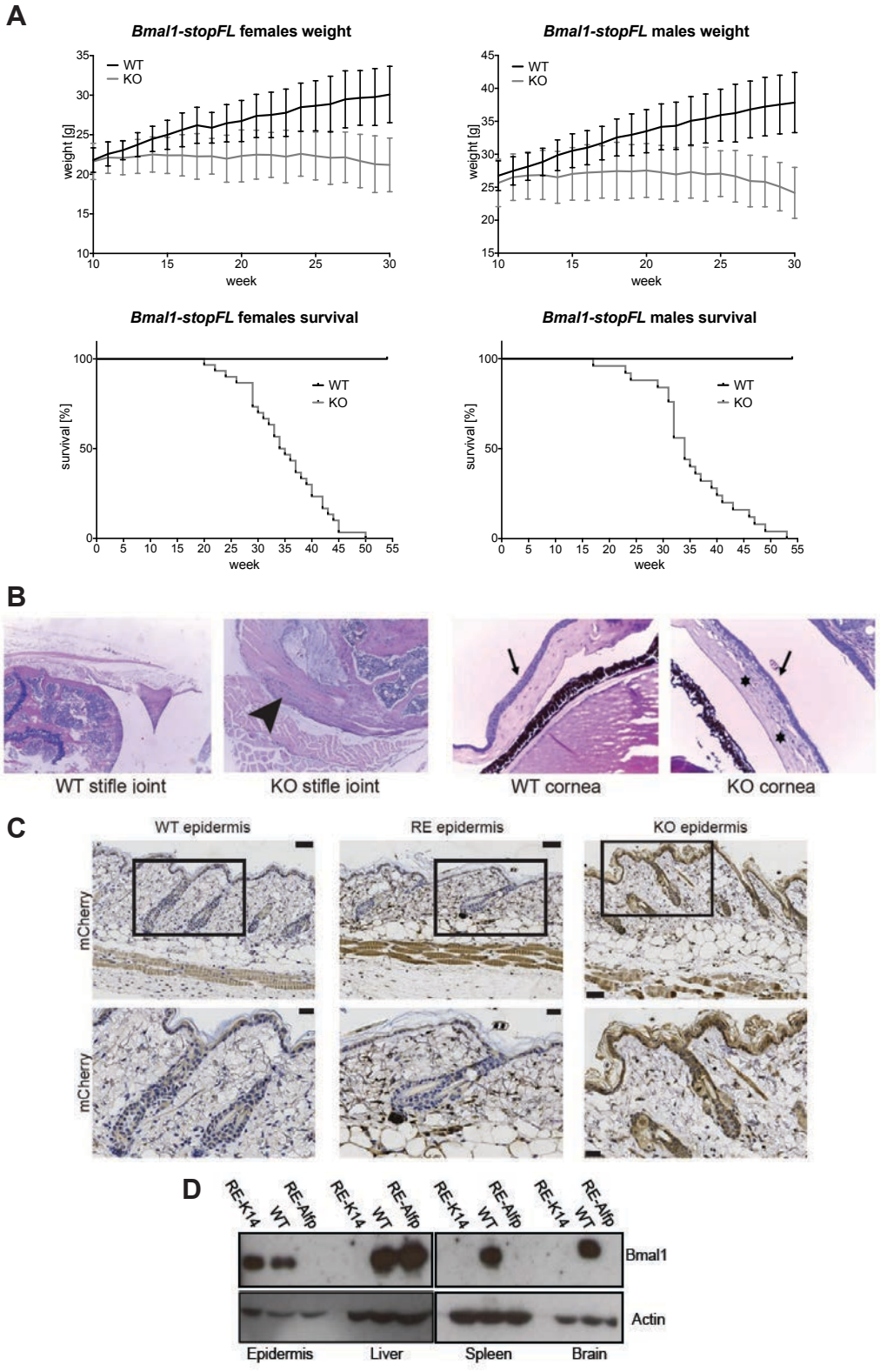

Figure 5. A novel *Bmal1-stopFL* mouse model recapitulates the ageing phenotype of full-body *Bmal1*-KO mice

(**A**) Upper graphs represent weight curves for WT and *Bmal1-stopFL* (KO) female and male mice. Females: n(WT) = 25, n(KO) = 30; males: n(WT) = 26, n(KO) = 25; data are represented as mean ± SD. Lower graphs represent Kaplan Meier survival curves for WT and KO female and male mice. Females: n(WT) = 25, n(KO) = 30, average lifespan (KO) = 34.9

± 7.3 weeks; males: n(WT) = 26, n(KO) = 25, average lifespan (KO) = 35.3 ± 8.2 weeks. (**B**) Haematoxylin/Eosin (H/E)–stained sections: On the left, figures display stifle joint sections showing severe arthropathy in 35-week-old KO mice (indicated by arrow); on the right, figures display cornea (indicated by arrows) showing inflammatory infiltrates and neovascularization (indicated by stars) in 30–35 weeks old KO mice. (**C**) mCherry staining in the epidermis of WT, KO and RE mice. mCherry is contained in the stop cassette, thus its expression is visible in KO epidermis, but disappears in RE epidermis thanks to the removal of the mCherry-containing stop cassette exclusively in K14+ cells; scale bar = 50mm. Second row of pictures shows a higher magnification; scale bar = 20µm. (**D**) Immunoblots of Bmal1 in various tissues of WT mice, as well as mice expressing K14-Cre, hence Bmal1 in the epidermis (RE-K14); or mice expressing Alfp-Cre, hence Bmal1 in the liver (RE-Alfp). Actin was used as loading control.

4.1.2 Light can entrain peripheral clocks independently of BMAL1 activity in other tissues

Having confirmed that the RE mouse model allowed tissue-specific reconstitution of BMAL1, we aimed at addressing the question whether the epidermis requires communication with other tissue clocks to maintain a robust clock machinery. Therefore, we performed a first circadian study where WT mice ($Arntl^{wt/wt}$, K14-$Cre^{tg/wt}$), RE mice (with epidermis-restricted *Bmal1* expression; $Arntl^{stopFL/stopFL}$, K14-$Cre^{tg/wt}$), and *Bmal1-stopFL* mice (KO; $Arntl^{stopFL/stopFL}$, K14-$Cre^{wt/wt}$) were kept under a standard 12h light/12h dark (LD) photoperiod. We then collected the epidermis at six different time points, or *Zeitgeber* Times (ZT), around the clock (i.e. every 4h) and performed RNA-sequencing, in order to obtain the epidermal transcriptome over the 24h cycle (Figure 6A). We analysed the transcriptional data pooled from four mice per genotype per time point. Using this dataset as an input, the algorithm JTK_CYCLE was utilised to identify oscillating transcripts[312].

As expected, WT epidermis expressed strong transcriptional rhythmicity of the main core clock genes, which oscillated with the correct amplitudes and phases as previously reported[183] (Figure 6B). Surprisingly, the core clock machinery oscillated in a circadian manner also in the epidermis of RE mice, despite the absence of a functional clock in any other tissue (Figure 6B). The observed transcriptional oscillations in RE epidermis were found to be in phase with the WT ones, i.e. peaking at the same time of the day (Figure 6B & Figure 7A), albeit with a lower amplitude compared to the WT (Figure 6B & Figure 7C).

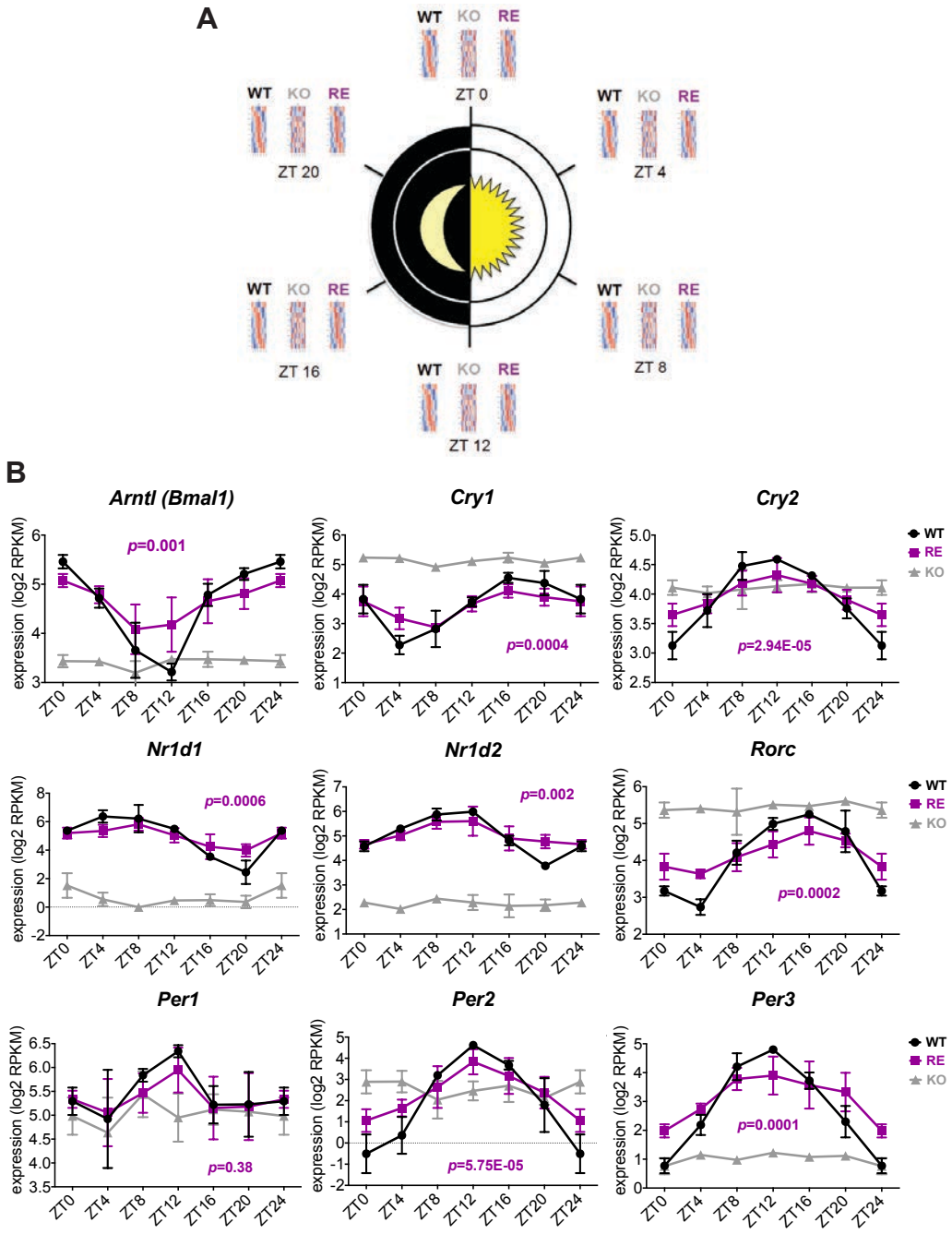

Figure 6. Light can entrain the epidermis independently of BMAL1 activity in other tissues

(**A**) Experimental setup scheme of the 12h Light/12h Dark (LD) study: Interfollicular epidermis was isolated at six different time points around the clock, i.e. every 4h, from 8-week-old WT, RE, and KO females kept under LD photoperiod. The obtained tissue was subsequently submitted for RNA-sequencing to establish the circadian transcriptome, which was determined by using the JTK_CYCLE algorithm[312]. (**B**) Core clock gene expression from the epidermis of WT, RE, or KO mice (n = 3 or 4 mice per time point and genotype). Adjusted *p* values relative to RE epidermis are shown; data are represented as mean ± SD. ZT: *Zeitgeber* Time.

The transcriptional fluctuations of *Bmal1* in the epidermis of both WT and RE mice were also observed at the protein level (Figure 7B). BMAL1 activity is tightly regulated by post-translational modifications, such as phosphorylation at serine residue 42[320] and acetylation at lysine residue 538[45]. When we carried out western blots of the modified forms of BMAL1, i.e. p-BMAL1 and ac-BMAL1 respectively, we further confirmed a rhythmic protein activity (Figure 7B).

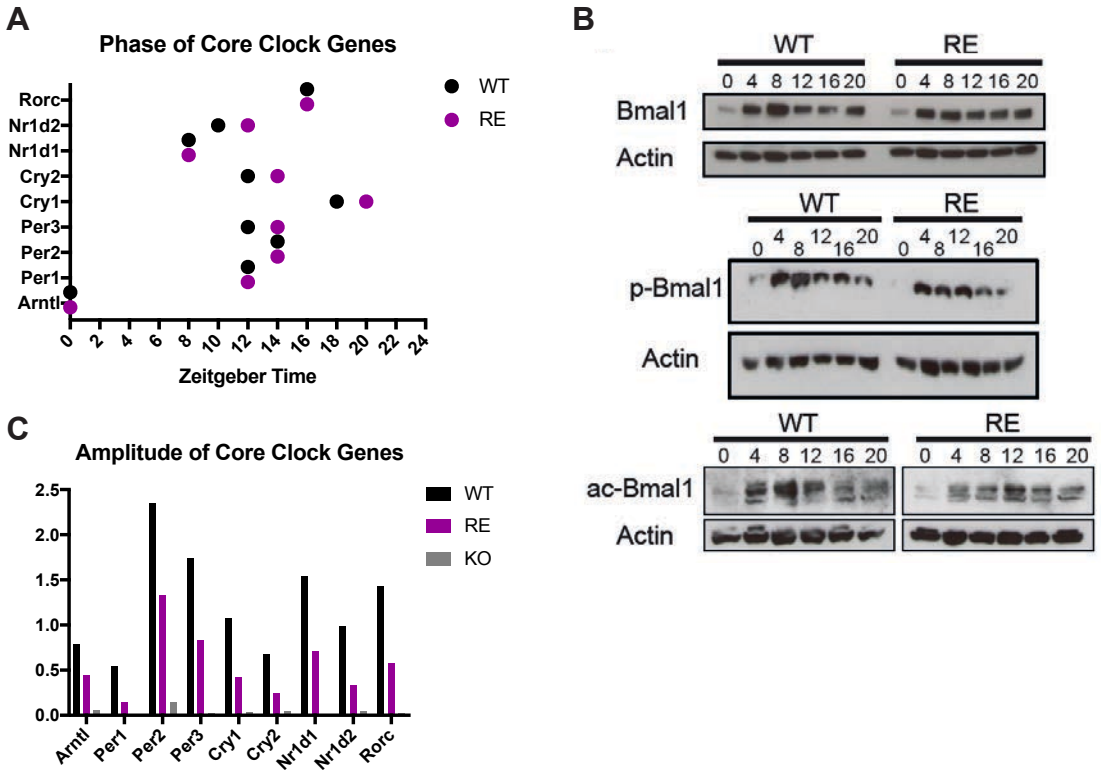

Figure 7. The tissue-autonomous clock sustains the core circadian machinery both at gene and protein level

(**A, C**) Phase and amplitude of core clock genes in WT and RE epidermis from the LD study. (**B**) Immunoblots of Bmal1, phosphorylated Bmal1 (p-Bmal1), and acetylated Bmal1 (ac-Bmal1) extracted from WT or RE epidermis at six different time points around the clock from mice kept under LD conditions. Actin was used as loading control.

A similar outcome was obtained when analysing the core clock genes of livers collected around the clock from Liver-RE mice (Arntl$^{stopFL/stopFL}$, Alfp-Cre$^{tg/wt}$) kept under LD conditions. Here, the circadian machinery maintained solid transcriptional oscillations, though with a 4h phase advance compared to WT livers (Figure 8)[319]. Altogether, these results point to a strong independence of the tissue-intrinsic rhythmic clock, which can align to the external time without the need of functional clocks in any other tissue[198].

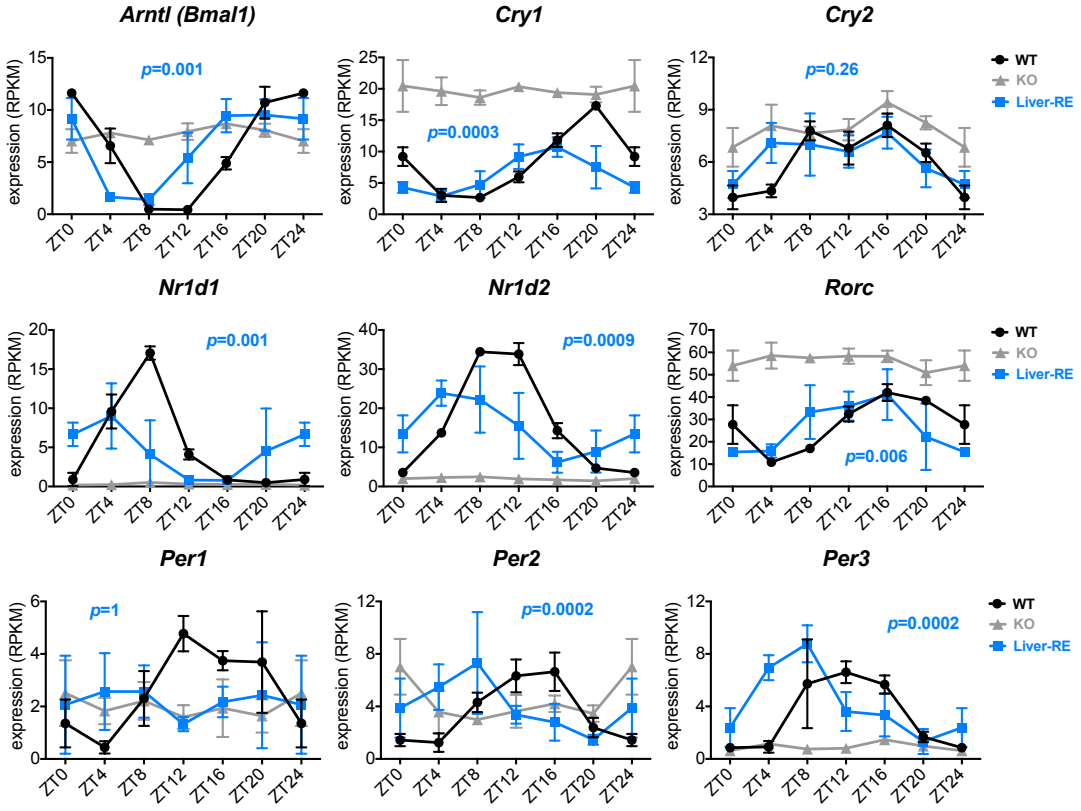

Figure 8. Light can entrain the liver independently of BMAL1 activity in other tissues

Core clock gene expression from the liver of WT, KO or Liver-RE (*Bmal1* expression only in *Alfp*-Cre+ cells) mice kept under LD photoperiod (n = 3 mice per time point and genotype). Adjusted *p* values relative to Liver-RE are shown; data are represented as mean ± SD. ZT: *Zeitgeber* Time.

4.1.3 Homeostatic circadian functions of the epidermis are maintained even in the absence of non-epidermal clocks

In the light of the first results of this project, we set out to explore the physiological relevance of the tissue-autonomous clock. Characterising the circadian transcriptome, we found that WT epidermis rhythmically expressed 2,970 transcripts, whereas the RE epidermis expressed 1,107 significantly oscillating transcripts ($p \leq 0.01$) (Figure 9A&C). Of this, 392 transcripts were found to also be circadian in WT, constituting 13.2% of the overall circadian transcriptome of WT epidermis (Figure 9A&C). Interestingly, KO epidermis showed 1,018 rhythmic genes, of which 224 were shared with WT and RE (Figure 9A&C). This suggests that 7.5% of the WT epidermal transcriptome exhibits a rhythmic behaviour in a BMAL1-independent fashion. Moreover, the different classes of oscillating genes were particularly evident when the expression of all WT circadian genes was plotted for each genotype (Figure 9B). Interestingly, RE circadian genes displayed an oscillatory trend even within genes scored as circadian in WT only, while KO were completely arrhythmic (Figure 9B). Therefore, a greater number of RE epidermal genes than those scored by the JTK_CYCLE algorithm are actually expressed in a circadian manner.

As previously described[183], the phase distribution of circadian genes in WT epidermis showed a clear separation into two main peaks: A morning peak of genes at ZT0-ZT4, i.e. at the beginning of the light phase, and an evening peak at ZT12-ZT16, i.e. when the dark phase starts (Figure 10A). This separation was also observed for all circadian genes in RE epidermis, circadian genes unique to WT or RE, and shared genes (Figure 10A). Conversely, KO epidermal gene expression peaked at ZT4-ZT6, thus 4h later than WT and RE transcripts, while the phase distribution of rhythmic genes unique to KO was sparse (Figure 10A). Nevertheless, the overall amplitude of all and shared circadian genes in RE was lower than in WT, similar to the patterns observed for the core clock machinery (Figure 10B&C).

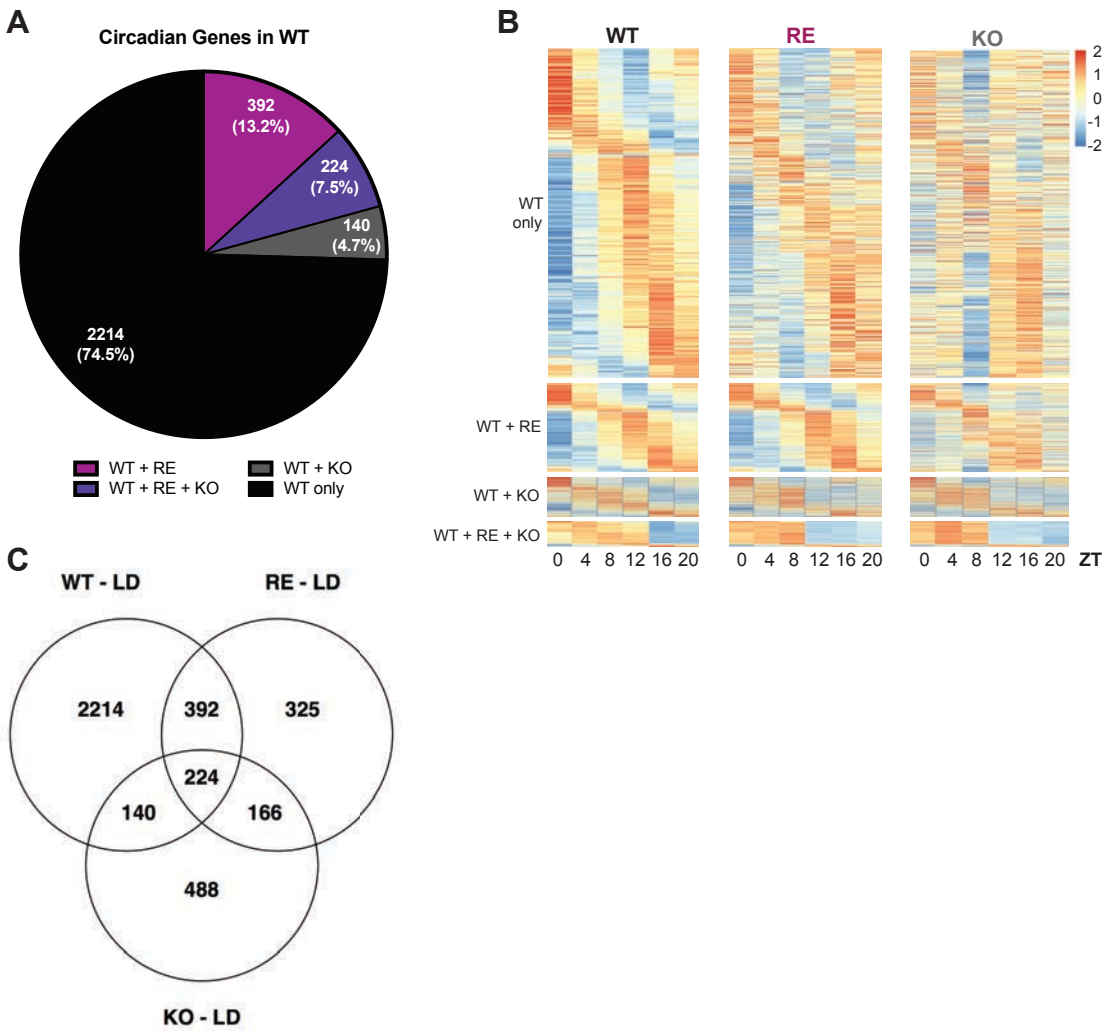

Figure 9. A portion of the WT circadian transcriptome is rescued by reconstituting only the epidermal clock

(**A**) Pie chart displaying the circadian genes of the LD study expressed in WT epidermis and their overlap with rhythmic genes in RE and KO epidermis. (**B**) Heatmaps showing the circadian expression in the different genotypes of transcripts that are rhythmic in (from top to bottom): WT only, WT + RE, WT + KO, and WT + RE + KO, respectively. ZT: *Zeitgeber* Time. (**C**) Venn diagram of circadian genes found in the epidermis of WT, RE and KO mice kept under LD conditions; $p \leq 0.01$.

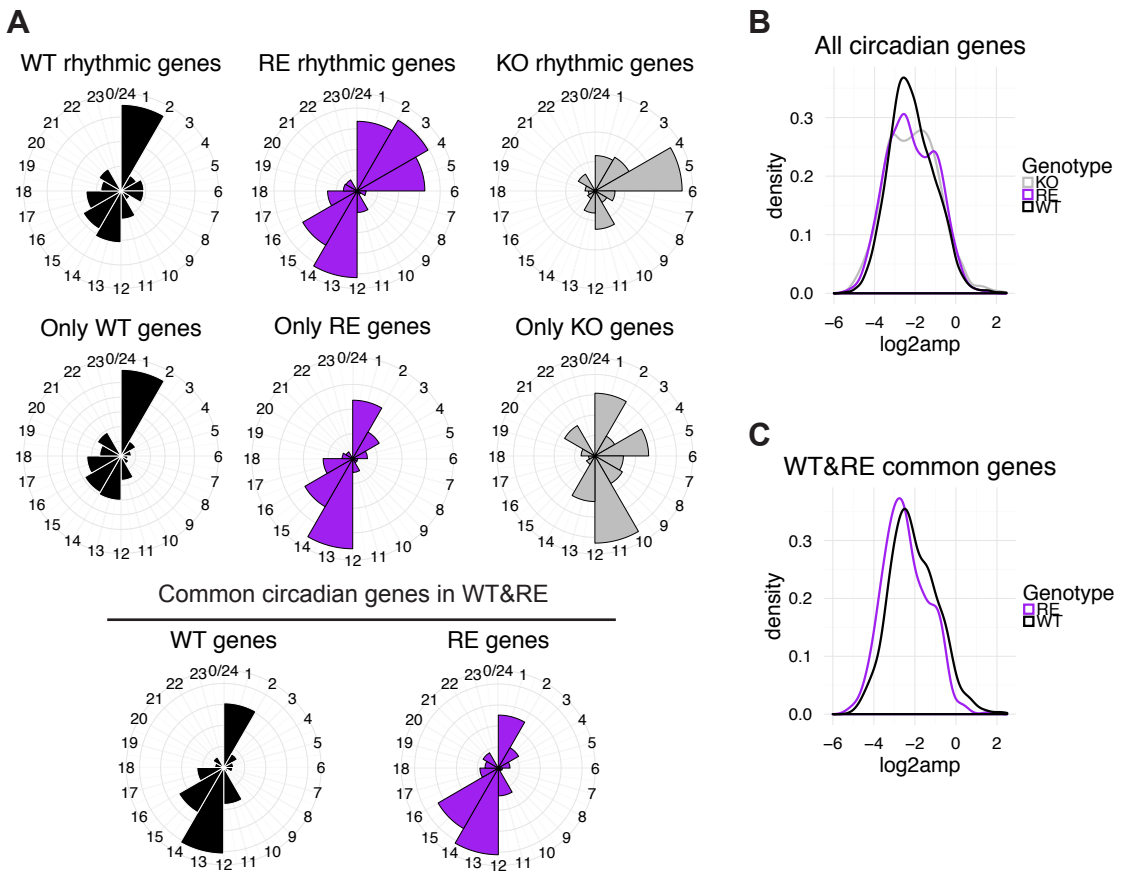

Figure 10. Phase and amplitude of RE rhythmic genes are similar to WT rhythmic genes

(**A**) Phase distribution of circadian genes in the indicated genotypes and groups. (**B**) Amplitude of rhythmic transcripts in WT, RE and KO epidermis. (**C**) Amplitude of genes that are oscillating in both WT and RE epidermis.

We additionally compared WT with KO and RE epidermis to analyse the transcriptional changes given by the absence or presence of a systemic versus tissue-specific functional clock. To do so, we performed differential gene expression analyses, regardless of the time of the day, hereby pooling the transcriptional data from the different time points of each genotype. In this context, we found greater changes in gene expression between KO and WT epidermis, with a total of 4,826 differentially expressed genes (DEGs), in contrast to RE and WT, with only 248 genes (q-value ≤ 0.05). (Figure 11A&B). Specifically, 2,282 transcripts were upregulated in KO epidermis compared to WT, while 2,544 were downregulated (Figure 11A&B). Conversely, only 119 genes were upregulated in the RE epidermis relative to the WT, whereas 129 were downregulated (Figure 11A&B). The majority of up- or downregulated transcripts in RE were included in the KO DEGs (Figure 11A&B), indicating that some RE transcriptional features result from the lack of non-epidermal *Bmal1*. Nevertheless, the overall outcome points to a greater transcriptional similarity between WT and RE, than

between WT and KO, suggesting that the local epidermal clock can, to a certain extent, sustain a physiological transcriptome[198].

To validate the homeostatic potential of a tissue-autonomous functional clockwork, we decided to study the biological processes related to the uncovered rhythmic genes. Therefore, we performed Gene Ontology (GO) analyses using the genes scored as circadian in WT only (2,214 genes), shared between WT and RE epidermis (392 genes), or circadian in all genotypes (224 genes) (Figure 9A&C, Figure 11C). We found that the circadian genes in WT only are involved in a diverse range of processes including: metabolic processes and signalling pathways, cell cycle and DNA repair processes, as well as cytoskeleton and ECM organisation (Figure 11C). This suggests that the clock in the WT epidermis regulates the very basic epidermal clock functions, such as the high cellular turnover, while receiving systemic and niche-derived rhythmic signals. In agreement with this, we found that the downregulated DEGs in both RE and KO compared to WT (Figure 11B) were mainly involved in cellular communication and regulation of signal transduction (data not shown). In contrast, the shared circadian genes between WT and RE fall into categories of cell cycle and DNA repair, as well as circadian regulation of gene expression (Figure 11C). These results point to a core circadian program of the epidermis to sustain its homeostasis even in the absence of clocks elsewhere. In this line, it was previously described that a core rhythmicity is maintained in the epidermis of aged mice or mice exposed to different diets[183]. Lastly, the circadian genes shared by all genotypes included metabolic processes, as well as translation and oxidative phosphorylation categories (Figure 11C). This suggests that daily rhythms in protein translation and mitochondrial oxidative metabolism are likely modulated by a BMAL1-independent mechanism, contrasting with previous reports that have suggested that BMAL1 is involved in the regulation of translation[321] and mitochondrial energetics[200,322,323].

The cell cycle appeared in both the WT and RE epidermis as one of the most important processes to ensure daily renewal and turnover of the cellular protective layers. Therefore, we decided to validate the transcriptional data by analysing the expression of a typical marker of mitosis, namely phosphorylated histone H3 (pHH3)[324]. Indeed, the number of $pHH3^+$ cells was rhythmic in both WT and RE (Figure 11D), further validating the observation that the tissue-autonomous clock is sufficient to maintain core homeostatic processes like cell cycle.

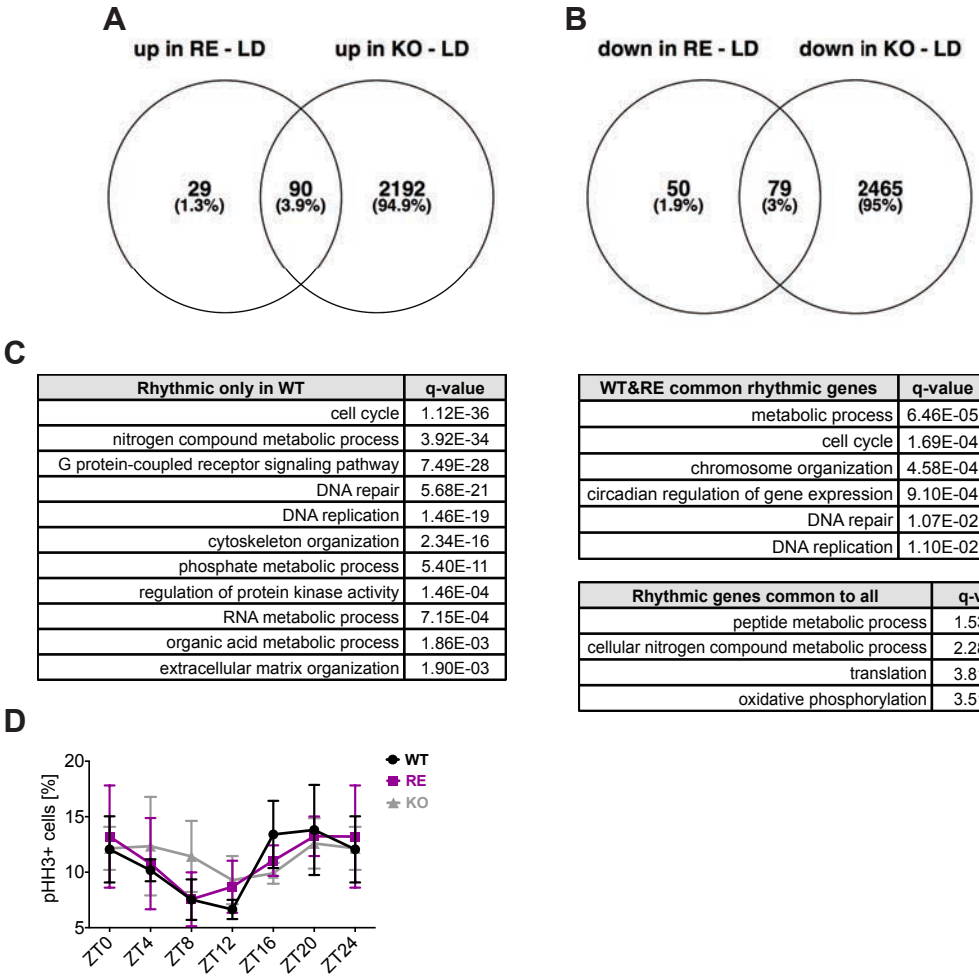

C

Rhythmic only in WT	q-value
cell cycle	1.12E-36
nitrogen compound metabolic process	3.92E-34
G protein-coupled receptor signaling pathway	7.49E-28
DNA repair	5.68E-21
DNA replication	1.46E-19
cytoskeleton organization	2.34E-16
phosphate metabolic process	5.40E-11
regulation of protein kinase activity	1.46E-04
RNA metabolic process	7.15E-04
organic acid metabolic process	1.86E-03
extracellular matrix organization	1.90E-03

WT&RE common rhythmic genes	q-value
metabolic process	6.46E-05
cell cycle	1.69E-04
chromosome organization	4.58E-04
circadian regulation of gene expression	9.10E-04
DNA repair	1.07E-02
DNA replication	1.10E-02

Rhythmic genes common to all	q-value
peptide metabolic process	1.53E-10
cellular nitrogen compound metabolic process	2.28E-10
translation	3.81E-10
oxidative phosphorylation	3.51E-03

Figure 11. Tissue-autonomous basic homeostatic functions are preserved in the epidermis in the absence of non-epidermal rhythmicity

(**A**) Venn diagram representing the overlap between genes that are significantly upregulated in RE or KO epidermis as compared to WT epidermis of mice kept under LD photoperiod (n = 23 per genotype); q-value ≤ 0.05. (**B**) Venn diagram representing the overlap between genes that are significantly downregulated in RE or KO epidermis as compared to WT epidermis of mice kept under LD photoperiod (n = 23 per genotype); q-value ≤ 0.05. (**C**) Representative GO terms relative to genes that are rhythmic only in WT (n = 2,214 genes, refer to Figure9A&C), commonly circadian in both WT and RE epidermis (n = 392 genes, refer to Figure9A&C), or rhythmic in all three genotypes (WT, RE and KO) (n = 224 genes, refer to Figure9A&C), respectively. (**D**) Percentage of phospho-histone H3-positive (pHH3+) cells around the clock in the epidermis of WT, RE and KO; data are represented as mean ± SD. ZT: *Zeitgeber* Time.

4.1.4 Differential chromatin dynamics do not account for the reduced circadian output of clock-reconstituted epidermis

To account for the reduced transcriptional output observed in RE epidermis relative to WT (Figure 9A&C), we hypothesised that differential chromatin opening could explain these differences in circadian output. This hypothesis aligns with the known pioneer factor properties of BMAL1, which allow it to open chromatin *de novo*, initiating transcription[46,47,325,326]. To assay changes in chromatin dynamics, we performed ATAC-seq (Assay for Transposase-Accessible Chromatin using sequencing) to assess genome-wide chromatin accessibility[302]. We performed ATAC-seq on IFE cells of WT, RE, and KO mice, kept under a standard LD photoperiod, at ZT0 and ZT12. These time points correspond to the peak and the trough of *Bmal1* expression, respectively, allowing the greatest possibility of observing changes in chromatin accessibility.

WT epidermis presented 2,567 more open areas at ZT0 than at ZT12, while 1,567 more accessible regions were seen in RE epidermis at ZT0 compared to ZT12 (Figure 12B). This was further validated by the high consistency observed between replicates (Figure 12A), while KO mice exhibited no differential genome accessibility between the two time points, likely due to the lack of *Bmal1*. Hence, these results indicate that cell-intrinsic BMAL1 may drive daily opening of chromatin.

The differentially opening peaks between WT at ZT0 vs ZT12 and RE at ZT0 vs ZT12 showed literal similarities, with an overlap of only 537 peaks (21% of overall WT peaks and 34% of the RE-related ones) (Figure 12B). The genomic distribution of these peaks was enriched at 5'UTR (untranslated region) and promoter regions (defined as -1kb/+100bp from TSS) (Figure 12D), suggesting a role in regulating active transcription. We therefore annotated the genes with a differential peak in the promoters, and found that 321 genes overlapped between the WT at ZT0 vs ZT12 and the RE at ZT0 vs ZT12 (Figure 12C), 769 were specific to the WT at ZT0 vs WT at ZT12 (Figure 12C), and 598 genes with a differential peak in the promoter were unique to the RE at ZT0 vs RE at ZT12 (Figure 12C). In order to find evidence for a relationship between chromatin dynamics and circadian transcription, we intersected those genes having a differential peak in the promoter with the genes circadian in WT or RE (Figure 12F&G). Less than 10% of the genes rhythmically expressed in WT or RE epidermis were found within differentially opening promoter regions of the chromatin (Figure 12F&G). This suggests that there is no apparent correlation between the chromatin accessibility at promoter and the rhythmic transcriptional output.

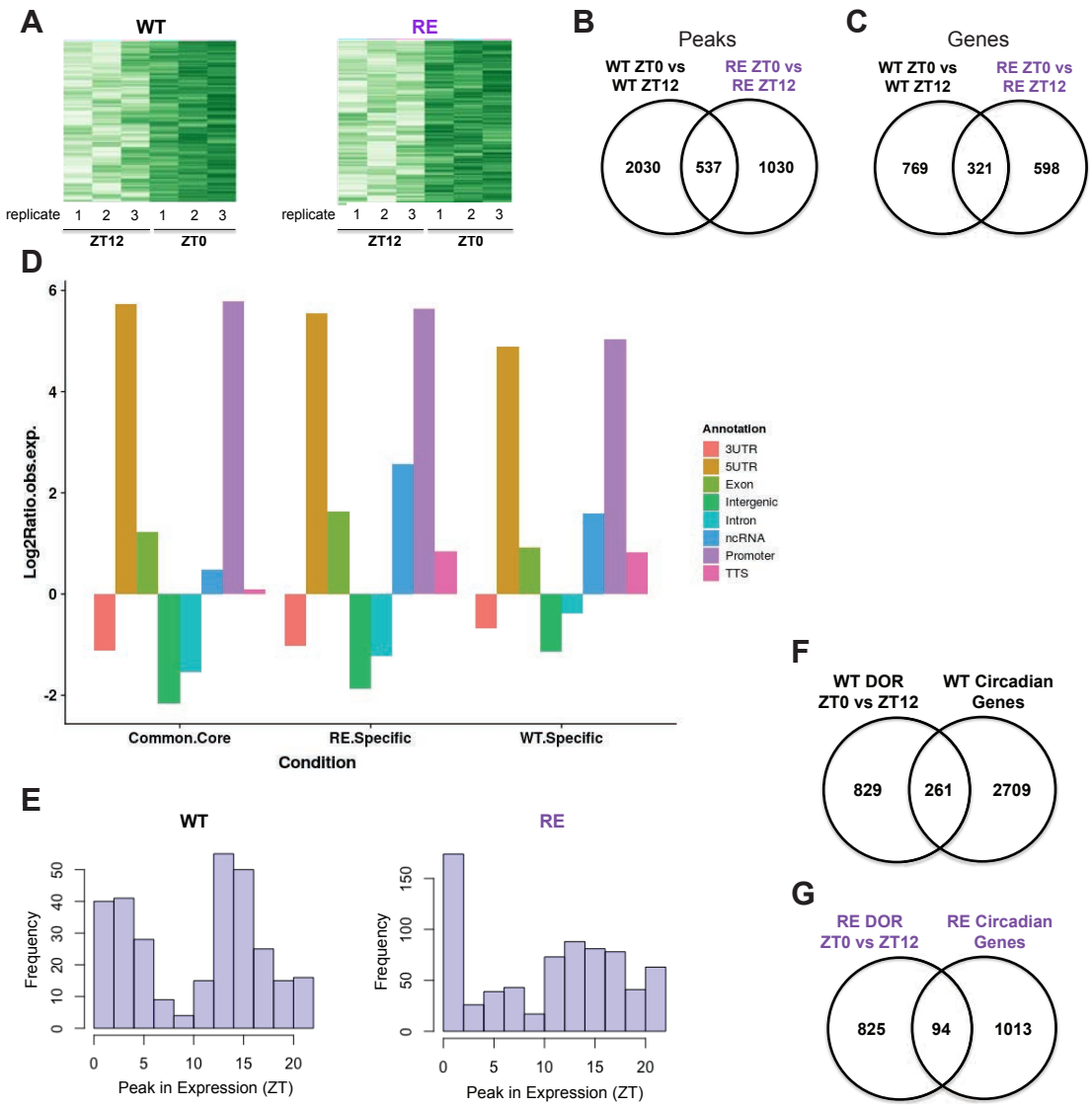

Figure 12. Tissue-intrinsic BMAL1 sustains daily chromatin dynamics

(**A**) Heatmap affinity binding plots displaying three replicates of WT or RE differential opened regions at ZT12 and ZT0. (**B**) Venn diagram representing the overlap between the number of differentially opened peaks in the WT between ZT0 and ZT12 and the number of differentially opened peaks in the RE between ZT0 and ZT12. (**C**) Venn diagram representing the overlap between the number of genes with a differential peak in the promoter, between the WT at ZT0 vs ZT12 and the RE at ZT0 vs ZT12. (**D**) Annotation of the differentially opened genomic regions in the WT at ZT0 vs ZT12 and the RE at ZT0 vs ZT12 (refers to the numbers displayed in **B**), normalised by the representation of these regions along the genome. (**E**) Graphs showing peak in expression of the genes with a differential peak in WT or RE. (**F**) Venn diagram representing the overlap between the number of genes with a differential opening region (DOR) in the promoter of the WT between ZT0 and ZT12 and the number of circadian genes in the WT. (**G**) Venn diagram representing the overlap between the number of genes with a differential opening region (DOR) in the promoter of the RE between ZT0 and ZT12 and the number of circadian genes in the RE.

Given that we observed changes in chromatin accessibility to represent closing from ZT0 to ZT12, we anticipated that any gene with circadian transcription linked to this differential opening of chromatin would show a morning peak in expression (i.e. at ZT0). However, when we analysed the peak expression of the nearest circadian gene to all differential opening regions, we found that there was no such relationship (Figure 12E). In other words, the expression of the total genes with a differential opening chromatin did not peak at ZT0 (Figure 12E), as one would expect from the observed chromatin opening at this time of the day as opposed to ZT12 (Figure 12A).

Despite our analysis being limited to only two time points, these results suggest that the presence of a tissue-specific clock ensures rhythmic chromatin dynamics, in agreement with the results obtained from chromatin immunoprecipitation (ChIP)-sequencing experiments performed on Liver-RE mice[319]. Nevertheless, differential chromatin opening cannot explain the reduced circadian transcriptional output observed in RE epidermis as compared to WT epidermis.

4.2 Non-epidermal clocks are required to maintain circadian behaviour in response to light and for epidermal rhythmicity in the absence of light

Valentina M. Zinna[1*], Patrick-Simon Welz[1*], Aikaterini Symeonidi[1], Kevin B. Koronowski[2], Kenichiro Kinouchi[2], Jacob G. Smith[2], Inés Marín Guillén[1], Andrés Castellanos[1], Georgiana Crainiciuc[3], Juan Martín Caballero[4], Andrés Hidalgo[3,5], Paolo Sassone-Corsi[2], and Salvador Aznar Benitah[1,6]

[*] These authors contributed equally

Affiliations:

[1]Institute for Research in Biomedicine (IRB Barcelona), Barcelona Institute of Science and Technology, 08028 Barcelona, Spain

[2]Center for Epigenetics and Metabolism, University of California, Irvine, CA 92697, USA

[3]Area of Developmental and Cell Biology, Centro Nacional de Investigaciones Cardiovasculares Carlos III (CNIC), 28029 Madrid, Spain

[4]PCB-PRBB Animal Facilities, 08028 Barcelona, Spain

[5]Institute for Cardiovascular Prevention, Ludwig-Maximilians University, 80336 Munich, Germany

[6]ICREA, Catalan Institution for Research and Advanced Studies, 08010 Barcelona, Spain

4.2.1 Non-epidermal clocks are required to drive behavioural rhythmicity

Since peripheral clocks can be entrained by different *Zeitgebers*, including light and food[3,125], we hypothesised that rhythmic behaviour and/or metabolism could account for the observed circadian oscillations in the *Bmal1*-RE epidermis (and liver) (Figure 6B & Figure 8). To test this hypothesis, we measured various behavioural rhythms that are known to play a role in the entrainment of the circadian clock, such as locomotor activity, feeding and drinking behaviours, as well as metabolism.

Starting with the locomotor activity, we observed that WT mice were more active in the dark hours, as expected, and also their drinking behaviour had a clear nocturnal increase (Figure 13A&B&E). Therefore, feeding behaviour and the corresponding metabolic cycles of oxygen consumption, respiratory exchange ratio and energy expenditure showed a peak at night as well (Figure 13D). Rhythms of locomotor and drinking behaviours were maintained in complete darkness experimental conditions (Figure 13A&B&E). Conversely, in LD and DD conditions, both RE and KO mice displayed an overall lower activity than their WT counterparts with less pronounced day:night changes in activity (Figure 13A&B). We also observed signs of light masking[93], whereby KO and RE mice experienced a minor increase of locomotor activity in the nocturnal phase when under LD photoperiod (Figure 13A&B). However, this phenomenon was highly variable among mice and across the different days of measurements, with several hours of fluctuations in activity onset from initiation of the dark phase (Figure 13C). In contrast, food intake and drinking behaviour, and related metabolic parameters, such as oxygen consumption, respiratory exchange ratio and energy expenditure, were entirely arrhythmic in KO and RE mice (Figure 13D&E).

These observations were consistent with those found for Liver-RE mice, whose activity and feeding behaviours stayed largely arrhythmic, further strengthening our conclusions (data not shown, refer to[319]). Taken together, these results demonstrate that the BMAL1-driven transcriptional oscillations in the epidermis (and the liver) do no depend on rhythmic signals coming from the food intake and corresponding metabolism[198].

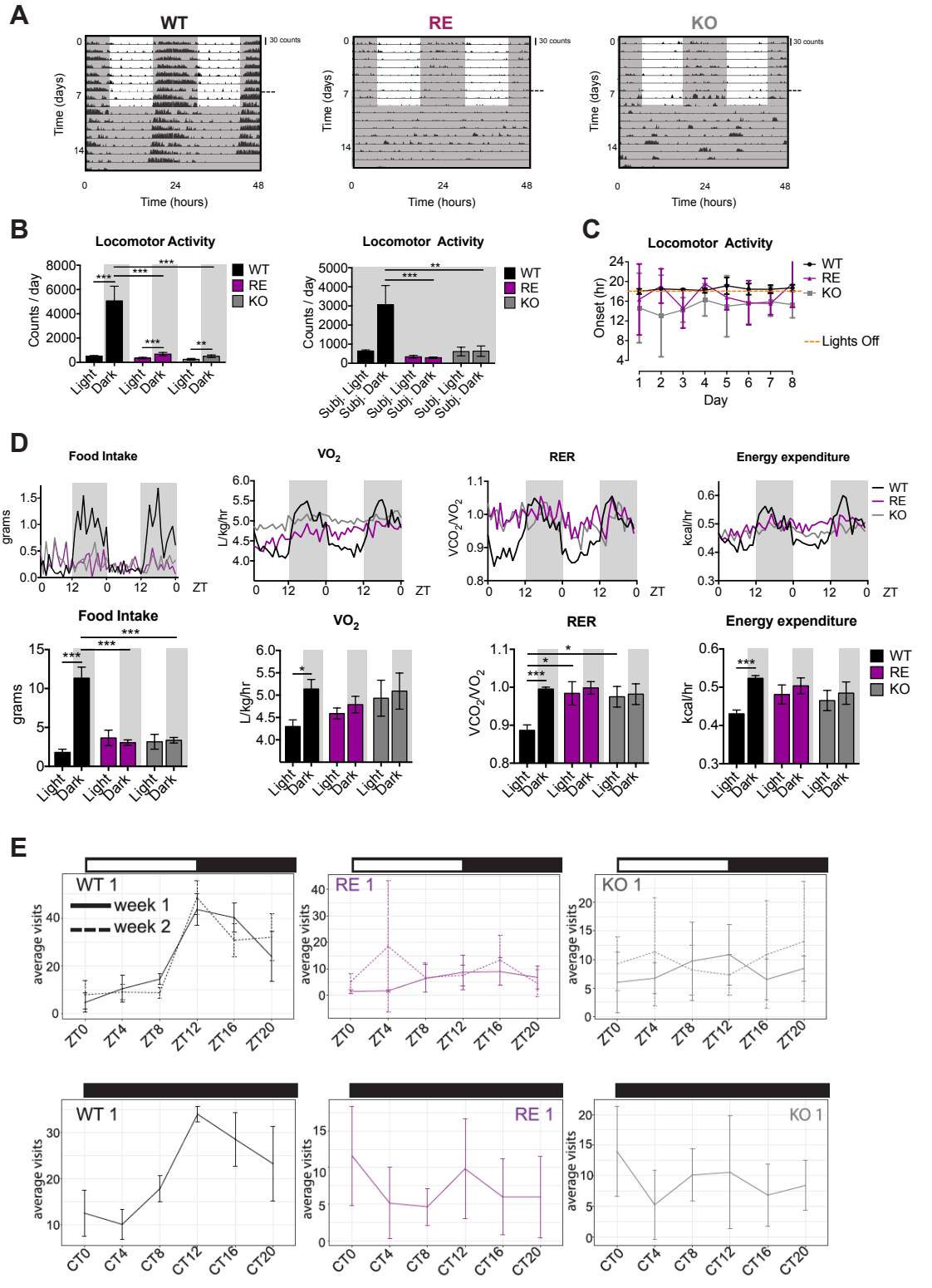

Figure 13. Non-epidermal clocks are required to preserve behavioural rhythmicity

(**A**) Representative actograms showing locomotor activity of one WT, one RE, and one KO replicate, respectively, duplicated over two days for visualisation. Joint data from two experiments: For the first measurement, mice were kept in LD conditions for seven days, while for the second measurement, mice were kept in LD for two days, then for seven days in DD. Joining of the two experiments is marked by a horizontal dashed line on the right side of the graphs. Scale bar: 30 counts. (**B**) Quantification of the locomotor activity measurements in LD cycle and DD conditions. LD: n(WT) = 5, n(KO) = 5, n(RE) = 4; DD: n(WT) = 3, n(KO) = 4, n(RE) = 3. Two-way ANOVA, $^{**}p \leq 0.01$, $^{***}p \leq 0.001$; data are

represented as mean ± SEM. (**C**) Locomotor activity onset in LD conditions as determined by Clocklab. n(WT) = 5, n(KO) = 5, n(RE) = 4; data are represented as mean ± SD. (**D**) Metabolic characterisation of *ad libitum* fed mice kept in LD conditions for two days. Traces of group averages are shown on the top graphs, while quantification is displayed on the lower graphs. RER: respiratory exchange ratio. Food intake and energy expenditure: n = 4 for all genotypes; VO2 and RER: n(WT) = 5, n(KO) = 5, n(RE) = 4. Two-way ANOVA, $*p \leq 0.05$, $***p \leq 0.001$. (**E**) Top: Behavioural activity measured over 24h as average visits per day to the drinking bottles of each individual WT, RE, or KO mouse kept in LD conditions for two weeks (shown as average visits within 4h bins over all days from each week). Bottom: Behavioural activity measured as visits to drinking bottles by individual WT, RE, and KO mice kept in DD conditions. Data are represented as mean ± SD. ZT: *Zeitgeber* Time. CT: Circadian Time. Also refer to[198].

4.2.2 Non-epidermal clocks are required to preserve transcriptional rhythmicity in constant darkness

Having identified the existence of a tissue-autonomous clock, we next wanted to test the signals responsible for its entrainment to the external environment. One possibility was that transcriptional rhythmicity in RE epidermis was due to clock entrainment by external light signals. Thus, we placed the mice under conditions of constant darkness (DD) for one week (i.e. between 156h and 176h), and we followed the previous experimental procedure of epidermis collection at six different time points around the clock, in order to obtain the circadian transcriptome (Figure 14A). WT mice maintained a robust core circadian machinery even after one week of darkness (Figure 14B). However, KO and also RE mice in this case displayed no oscillations in core clock gene, with the exception of *Bmal1, Per2* and *Per3* that were scored as circadian by the JTK_CYCLE algorithm, though with a minor statistical significance (Figure 14B). Additionally, the amplitude of the rhythmic genes in RE and KO was marginal (Figure 14B); therefore, such rhythmicity would not translate into physiologically meaningful processes.

Furthermore, WT epidermis expressed 2,302 significantly oscillating transcripts, while the RE epidermis expressed 476 rhythmic genes ($p \leq 0.01$) (Figure 15A&C). Of this, only 53 transcripts were circadian also in WT (Figure 15A&C), indicating that the physiological epidermal transcriptome of these mice is largely lost in the absence of light stimulus. KO epidermis expressed 836 rhythmic genes, of which only 21 were shared with WT and RE (Figure 15A&C).

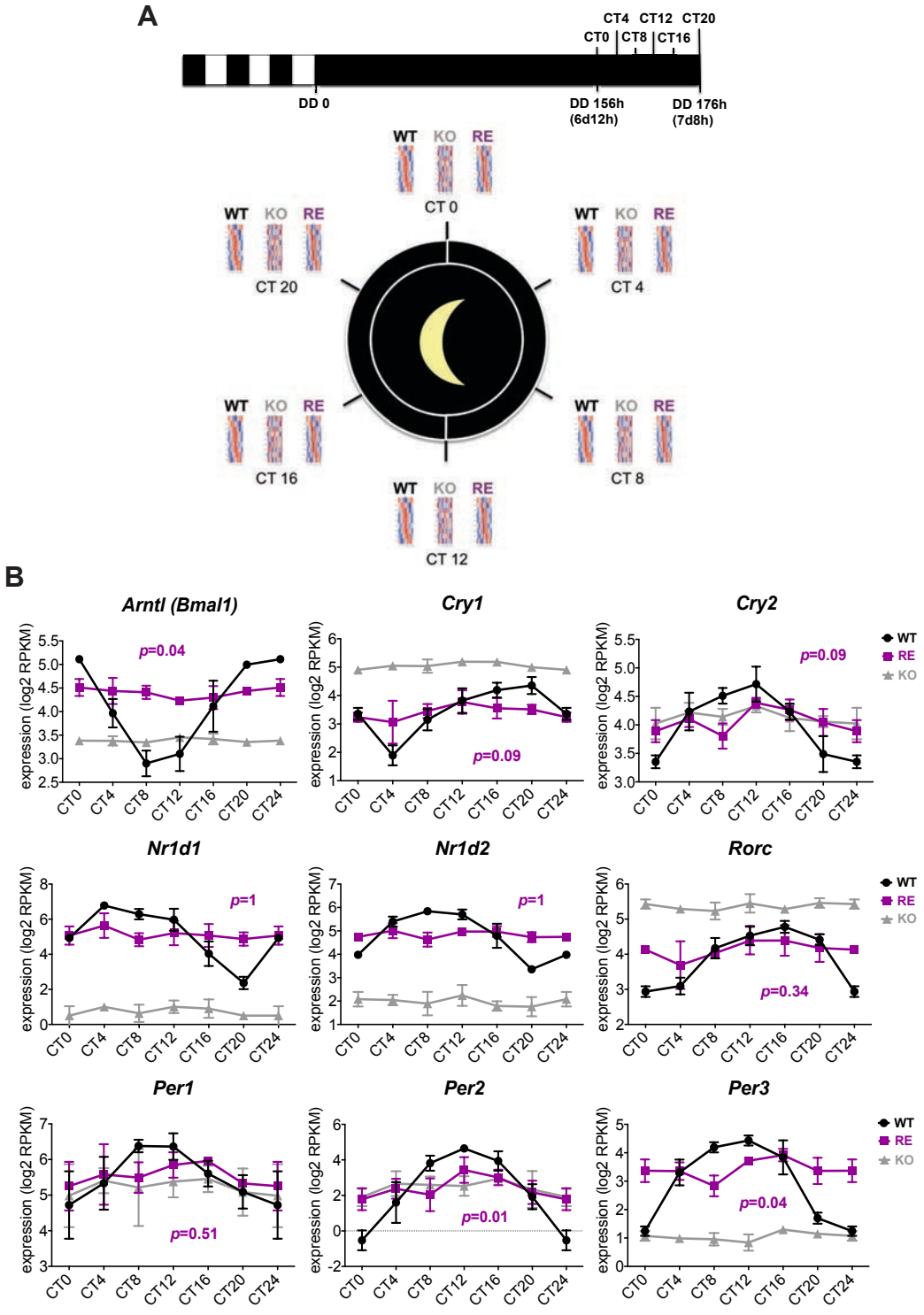

Figure 14. Non-epidermal clocks are required to preserve transcriptional rhythmicity in constant darkness

(**A**) Experimental setup scheme of the 12h Dark /12h Dark (DD) study: After standard LD photoperiod, 8-week-old WT, RE, and KO female mice were transferred to conditions of constant darkness for 6-7 days; interfollicular epidermis was then isolated at six different time points around the clock, i.e. every 4h. The obtained tissue was subsequently submitted for RNA-sequencing to establish the circadian transcriptome, which was determined by using the JTK_CYCLE algorithm[312]. (**B**) Core clock gene expression from the epidermis of WT, RE, or KO mice (n = 3 or 4 mice per time point

and genotype). Adjusted *p* values relative to RE epidermis are shown; data are represented as mean ± SD. CT: Circadian Time.

We carried out GO analysis on the rhythmic genes in WT only and found similar circadian categories to the ones obtained for the LD experiment, namely cell cycle, DNA replication and repair, circadian rhythms, but also cytoskeleton organisation, signalling and metabolic pathways (Figure 15D). In contrast, since only 53 of the 476 significantly oscillating transcripts in RE epidermis overlapped with the WT circadian output, we could not carry out GO analysis on them (Figure 15A&C).

In this regard, the RE transcriptomic distribution displayed a highly arrhythmic trend when plotted against the WT-only circadian genes, in contrast with what was found in the LD experiment (Figure 9B), and similar to the KO transcriptome (Figure 15B). A comparable transcriptional arrhythmia resulted in livers collected from Liver-RE mice kept in darkness (data not shown, refer to[319]). Therefore, light is indispensable to entrain the tissue-specific circadian system in absence of clocks in other tissues, according to the external time[198].

Differential gene expression analyses performed on the DD experiment dataset reflected a similar trend to that seen in the LD experiment. KO and WT epidermis displayed substantial changes in gene expression, with 5,236 DEGs, of which 2,597 were upregulated in KO epidermis compared to WT, whereas 2,639 were downregulated (Figure 15E). Interestingly, these downregulated DEGs showed a 30% overlap with the DEGs of the LD experiment found in the KO compared to WT, while no overlap was obtained between the LD and DD upregulated DEGs of KO compared to WT (data not shown). However, RE epidermis showed 1,107 DEGs compared to the WT (10% of which overlapped with the DEGs found in the LD experiment), with 490 upregulated transcripts, and 617 downregulated (Figure 15E). This indicates that the RE epidermis kept in absence of light presents a more different transcriptome than the WT, as compared to the RE epidermis under LD conditions, which only expressed 248 DEGs compared to the WT (Figure 11A&B). Nevertheless, the RE epidermal transcriptome in DD still appears more similar to the WT transcriptome, as compared to the KO, further underlying the importance of BMAL1 at the tissue level. Additionally, also in the context of absence of light we found that the downregulated DEGs in both RE and KO compared to WT were mainly included in biological processes of cytoskeleton organisation, extracellular communication and regulation of signal transduction (data not shown). Moreover, the downregulated DEGs in KO compared to

WT were further involved in the basic homeostatic functions of the epidermis, such as cell cycle, DNA replication and repair (data not shown). This further supports that even in the absence of external cues, the clock in the WT epidermis sustains epidermal physiology, while perceiving extracellular rhythmic signals.

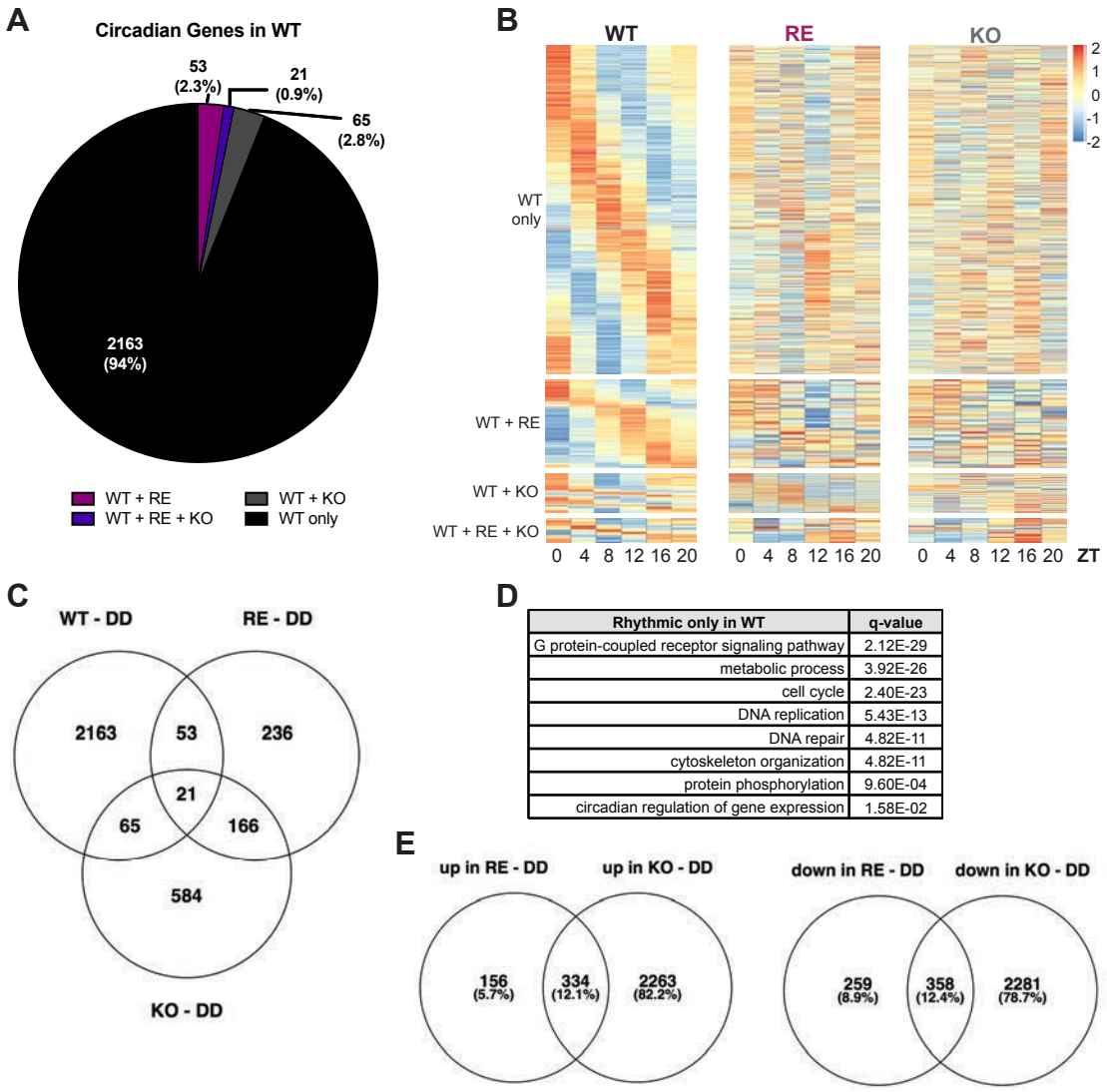

Figure 15. The rhythmic transcriptional output of BMAL1-driven epidermis is lost in constant darkness

(**A**) Pie chart displaying the circadian genes of the constant darkness (DD) study expressed in WT epidermis and their overlap with rhythmic genes in RE and KO epidermis. (**B**) Heatmaps showing the circadian expression in the different genotypes of transcripts that are rhythmic in (from top to bottom): WT only, WT + RE, WT + KO, and WT + RE + KO, respectively. ZT: *Zeitgeber* Time. (**C**) Venn diagram of circadian genes found in the epidermis of WT, RE and KO mice kept under DD conditions. (**D**) Representative GO terms relative to genes that are rhythmic only in WT (n = 2,302 genes). (**E**) Venn diagram representing the overlap between genes that are significantly upregulated (left diagram) or downregulated (right diagram) in RE or KO epidermis as compared to WT epidermis of mice kept under DD photoperiod (n = 22-23 per genotype).

The outcome observed in RE mice within the DD experiment can be attributed to: 1) a phase dispersion phenomenon between different mice; 2) a phase dispersion between cells of the tissue; 3) a flattening of the cellular clock gene rhythms due to the absence of light signal. Since the circadian experiments were done by pooling transcriptional data from several mice, it would be impossible to discern a possible desynchronisation between mice. Nevertheless, the high coherence that emerged in the gene expression data pointed against the first hypothesis (Figure 14B). However, a potential loss of tissue synchrony could still have happened in each individual mouse. To test this, we carried out a further darkness experiment, where we collected ear snip epidermal samples coming from the same individual WT, RE, or KO mouse at six consecutive time points, after one week of complete darkness. Despite the variability caused by handling the same mouse every 4h over a period of 20h, *Bmal1* expression was circadian in the WT mice and arrhythmic in each KO and RE mouse (Figure 16). This outcome further strengthened the results previously obtained, whereby light is the entraining factor for BMAL1-driven epidermis[198].

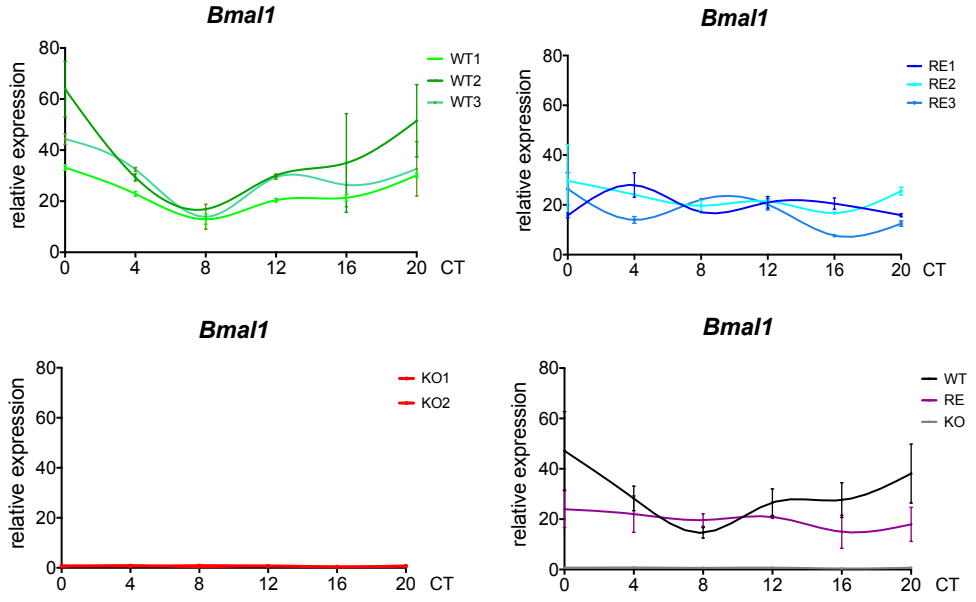

Figure 16. Non-epidermal clocks are required to maintain *Bmal1* rhythmicity in constant darkness

Relative expression of *Bmal1* in ear snip epidermis isolated at six consecutive time points over one day from the same individual mice that were kept in DD for 156h-176h; data are represented as mean ± SD. CT: Circadian Time.

4.2.3 The tissue-autonomous clock adjusts to jet lag conditions independently of the presence of other body clocks

In the light of the results obtained from the DD experiment, we hypothesised that the RE epidermis might respond faster to changes in the light regimen as compared to the WT. Therefore, under a different photoperiod, light-driven entrainment of epidermis would likely happen faster than if light had to re-entrain the central clock, which in turn had to re-entrain the peripheral clocks. To test our hypothesis, we performed a time-shift experiment that would resemble the jet lag situation.

We kept WT and RE mice under standard LD conditions, and then advanced the light cycle by 12 hours, mimicking “westward” traveling (Figure 17A). We then collected the epidermis of these mice in 4h intervals at twelve time points for the two days following the 12h shift, and for another seven time points corresponding to day 4 after the time-shift exposure (Figure 17A). In doing so, we hoped to observe whether there was a faster phase advance in the transcriptional rhythms of RE epidermis than in the WT tissue. However, by quantifying the expression phases of the core clock genes by qPCR, we noticed that the clock of RE epidermis did not respond faster than the WT to the new light regimen (Figure 17B). Instead, the rate of re-adjustment to the opposite light cycle was similar between the two genotypes, and only at day 4 we observed a 4h advance in gene expression with respect to the previous light schedule (Figure 17B).

In contrast to the slow shift in clock gene phase, the locomotor behaviour of WT mice rapidly shifted within two days to the new light regime of exposure (Figure 17C). This was strikingly observed in locomotor activity onset, which shifted to the new starting time of the darkness phase after two days from the shift (Figure 17D). In contrast, the RE mice, even before the time-shift, did not exhibit a rhythmic locomotor activity, nor a consistent activity onset at the beginning of the darkness (Figure 17C&D).

Altogether our findings confirm that the SCN clock re-entrains faster to a new light schedule than the peripheral clocks, thus quickly adjusting the behavioural rhythms dependent on it. In contrast, peripheral transcriptional rhythms re-adjust more slowly to new light conditions, and this is independent of the presence of other tissue clocks.

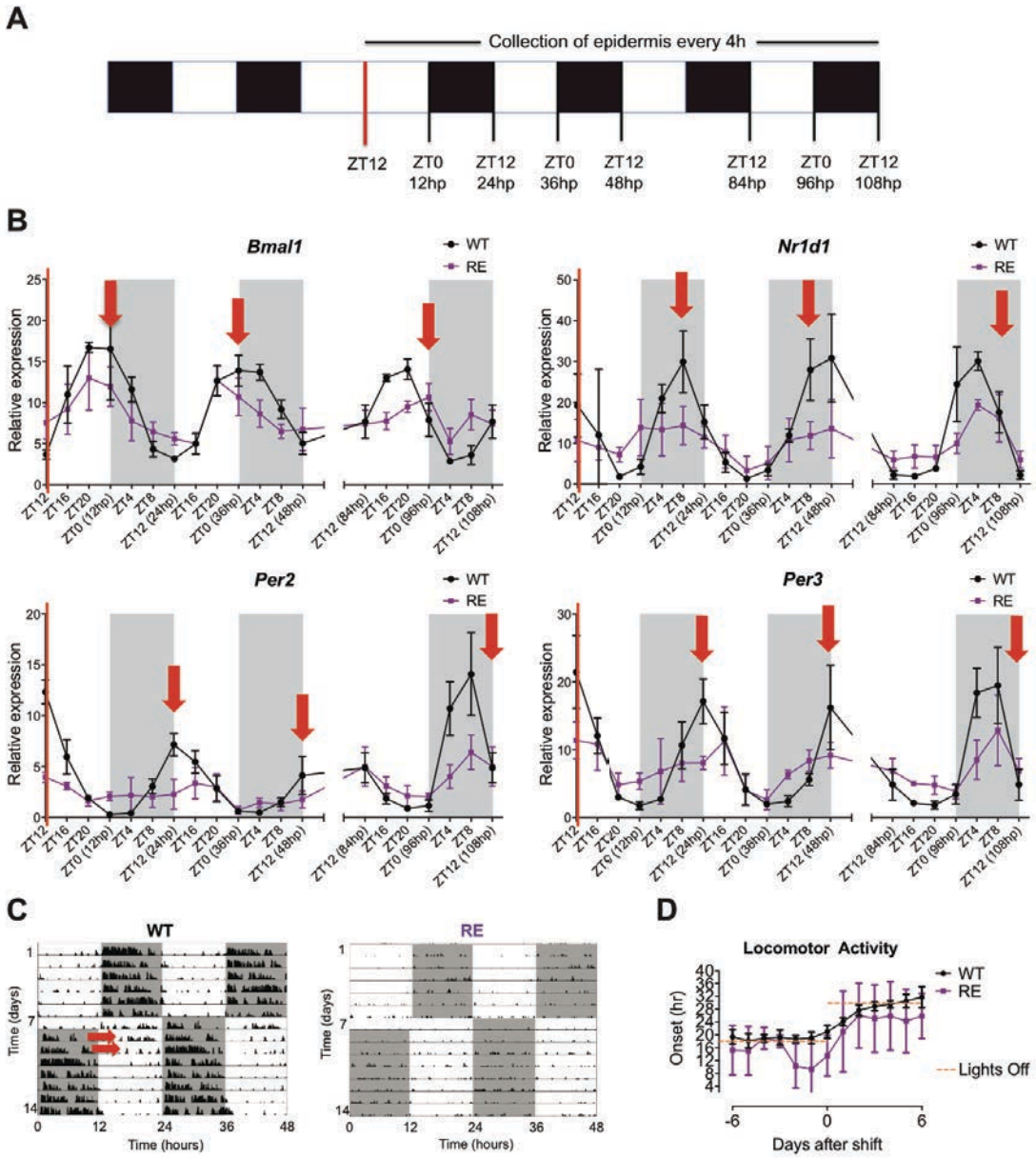

Figure 17. The tissue-autonomous clock adjusts to jet lag conditions independently of the presence of other body clocks

(**A**) Experimental setup scheme of the time-shift study: After standard LD photoperiod, 8-week-old WT and RE female mice underwent prolonged light exposure of 12 additional hours (i.e. 24h of continuous light) and were then kept under opposite LD schedule. Interfollicular epidermis was isolated every 4h at twelve time points for the two days following the 12h shift, and for another seven time points corresponding to day 4 after the time-shift exposure. The beginning of the shifted light regimen is highlighted by the red line; hp = hours after 12h shift. ZT: *Zeitgeber* Time. (**B**) Relative expression of core clock genes from the epidermis of WT and RE mice (n = 4 mice per time point and genotype). The red line on the y-axis represents the beginning of the 12h-shifted light schedule; red arrows represent expected expression peak for each gene according to the light regimen prior to the shift; data are represented as mean ± SD. ZT: *Zeitgeber* Time. (**C**) Representative actograms showing locomotor activity of one WT and one RE replicate, respectively, duplicated over two days for visualisation. The time-shift, i.e. the 24h of continuous light exposure, was performed at day 7, and mice were then kept under the new photoperiod for one week. Red arrows point at locomotor activity of mice over two days after the 12h shift. (**D**) Locomotor activity onset in LD conditions and upon 12h shift at day 0 as determined by Clocklab. n(WT) = 5, n(RE) = 3; data are represented as mean ± SD.

4.3 Communication between the SCN and the epidermal clock is sufficient to maintain a robust epidermal transcriptional output

Valentina M. Zinna[1*], Thomas Mortimer[1*], Carmelo Laudanna[1], Paul Petrus[2], Kevin B. Koronowski[2], Jacob G. Smith[2], Carolina Greco[2], Mireia Vaca Dempere[3], Arun Kumar[3], Jesus Gonzalez[4], Paolo Sassone-Corsi[2], Pura Muñoz-Cánoves[3,5,6], Patrick-Simon Welz[1], and Salvador Aznar Benitah[1,6]

[*] These authors contributed equally

Affiliations:

[1]Institute for Research in Biomedicine (IRB Barcelona), Barcelona Institute of Science and Technology, 08028 Barcelona, Spain

[2]Center for Epigenetics and Metabolism, University of California, Irvine, CA 92697, USA

[3]Universitat Pompeu Fabra (UPF), Department of Experimental and Health Sciences (DCEXS) and CIBER on Neurodegenerative Diseases (CIBERNED), 08003 Barcelona, Spain

[4]PCB-PRBB Animal Facilities, 08028 Barcelona, Spain

[5]Centro Nacional de Investigaciones Cardiovasculares Carlos III (CNIC), 28029 Madrid, Spain

[6]ICREA, Catalan Institution for Research and Advanced Studies, 08010 Barcelona, Spain

4.3.1 Communication between the SCN and the epidermal clock is sufficient to maintain a robust epidermal clock output

Having defined the degree of autonomy of peripheral tissue clocks, we then set out to establish the interactions they require with the rest of the clock network for full physiological circadian functionality. In the light of our published results[198,319] (see Results sections 4.1 and 4.2), we wondered whether the SCN clock is sufficient to maintain synchrony of peripheral clocks and drive their functional outputs, even when external cues like light are lacking. Specifically, we asked whether the central clock of the SCN is sufficient to obtain a WT circadian transcriptional output in the epidermis.

To study this interaction, we generated a further mouse model, in which circadian clock activity was reconstituted in the SCN and epidermis. We achieved this by driving the expression of Cre recombinase under both the Synaptotagmin10 (Syt10)[298] and the K14 promoter, respectively. We termed this mouse "double reconstituted" (RERE) (Figure 18A). Of note, Syt10-Cre activity mostly concentrates in the SCN cells, in the testis, and in very few other neural areas, like the olfactory bulbs[218].

Subsequently, we performed an LD circadian experiment using WT mice (Arntl$^{wt/wt}$, K14-Cre$^{tg/wt}$, Syt10-Cre$^{tg/wt}$), RE mice (with epidermis-restricted *Bmal1* expression; Arntl$^{stopFL/stopFL}$, K14-Cre$^{tg/wt}$, Syt10-Cre$^{wt/wt}$), SCN-RE mice (with SCN-restricted *Bmal1* expression; Arntl$^{stopFL/stopFL}$, K14-Cre$^{wt/wt}$, Syt10-Cre$^{tg/wt}$), and RERE mice (with epidermis- and SCN-restricted *Bmal1* expression; Arntl$^{stopFL/stopFL}$, K14-Cre$^{tg/wt}$, Syt10-Cre$^{tg/wt}$) (Figure 18A). As previously performed (and as schematically shown in Figure 6A), the experimental mice were kept under 12h light/12h dark (LD) photoperiod. We then collected the epidermis at six different time points around the clock (i.e. every 4h) and performed RNA-sequencing, in order to obtain the related circadian transcriptome. The algorithm JTK_CYCLE was then applied to identify the significantly oscillating transcripts[312].

Remarkably, and in contrast to the RE mice, the core circadian machinery oscillated in the epidermis of RERE mice in a WT-like manner (Figure 18B). In contrast, the *Bmal1*-deficient epidermis of SCN-RE mice did not display significant rhythmic oscillations of the main core clock genes, thereby indicating that *Bmal1* expression in SCN and epidermis is sufficient to achieve WT transcriptional oscillations of the core clock machinery in the epidermis (Figure 18B).

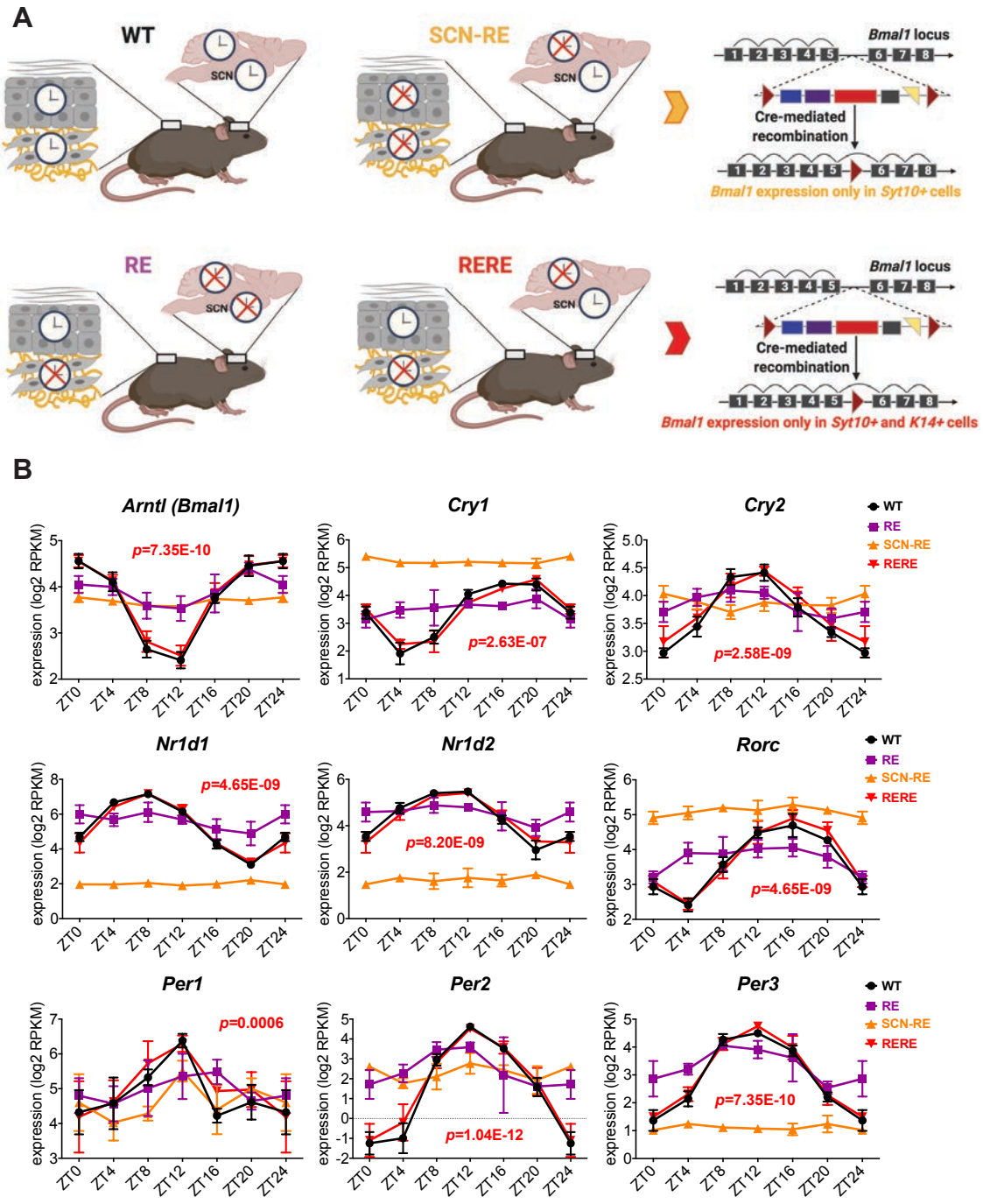

Figure 18. Communication between the SCN and the epidermal clock is sufficient to maintain a robust epidermal clock machinery

(**A**) Schematic of the *Bmal1-stopFL*-derived mouse models. The RE mouse allows the endogenous expression of *Bmal1* only in K14+ cells, the SCN-RE mouse allows the endogenous expression of *Bmal1* only in Syt10+ cells, while the RERE mouse allows the endogenous expression of *Bmal1* only in Syt10+ and K14+ cells. Heterozygous K14-Cre/Syt10-Cre (WT) mice were used as experimental controls. (**B**) Core clock gene expression from the epidermis of WT, RE, SCN-RE or RERE male mice kept under LD standard photoperiod (n = 4 mice per time point and genotype). Adjusted *p* values relative to RERE epidermis are shown; data are represented as mean ± SD. ZT: *Zeitgeber* Time.

We next set out to analyse the transcriptomic impact of such inter-tissue communication and clock robustness observed in the RERE. To achieve this, we studied how the whole circadian transcriptional output differed between the various animals. In this context, we found that the rhythmic transcriptome of WT epidermis consisted of 3,115 circadian genes, whereas the RERE epidermis exhibited 1,862 significantly oscillating transcripts (Figure 19A&B). Of this, 1,060 transcripts were found to also be circadian in the WT, making it a 34% of the overall circadian transcriptome of WT epidermis (Figure 19A&B). 651 rhythmic genes of the WT oscillating transcriptome were uniquely rescued by the RERE, thus they strictly derive from the SCN and epidermal clocks communication. RE epidermis solely expressed 756 rhythmic genes in total, with only 177 being shared with the WT (Figure 19A&B). These results underlie the importance of central:peripheral clock interaction for circadian transcriptional output. Strikingly, SCN-RE epidermis expressed 1,662 oscillating transcripts, of which 628 were common to the WT (20% of the total WT circadian transcriptome) (Figure 19A&B). Of this, 287 genes were uniquely rescued by the SCN-RE, which therefore included all the epidermal transcripts that are directly controlled by the SCN. Interestingly, 67 rhythmic genes were shared between all genotypes, suggesting that 2% of the overall WT transcriptional output remains circadian with either a functional central or peripheral clock activity (Figure 19A&B).

Additionally, RERE epidermal transcripts revealed a robust oscillatory trend within genes scored as circadian in WT only, whereas RE- and SCN-RE-derived transcriptional heatmaps exhibited an overall arrhythmic distribution (Figure 19C). Therefore, also in this case a greater number of RERE epidermal genes than those scored by the JTK_CYCLE algorithm are actually expressed in a circadian manner.

Of note, the rhythmic genes shared by all genotypes displayed an opposite phase when plotted against the SCN-RE transcriptome, as compared to all the other genotypes (Figure 19C). This feature became more evident when studying the circadian phase distribution of the various genotypes' transcriptome (Figure 20A). Here, we observed a clear peak of expression at the beginning of the light phase (i.e. ZT0-2) that was consistent across all genotypes, with the exception of the RE epidermal transcriptome, which peaked at the beginning of the dark phase (i.e. ZT12-14) (Figure 20A). However, the circadian genes common in all genotypes exhibited a different phase distribution, with a peak in the evening in all the genotypes but the SCN-RE one, which instead displayed a morning peak (Figure 20A).

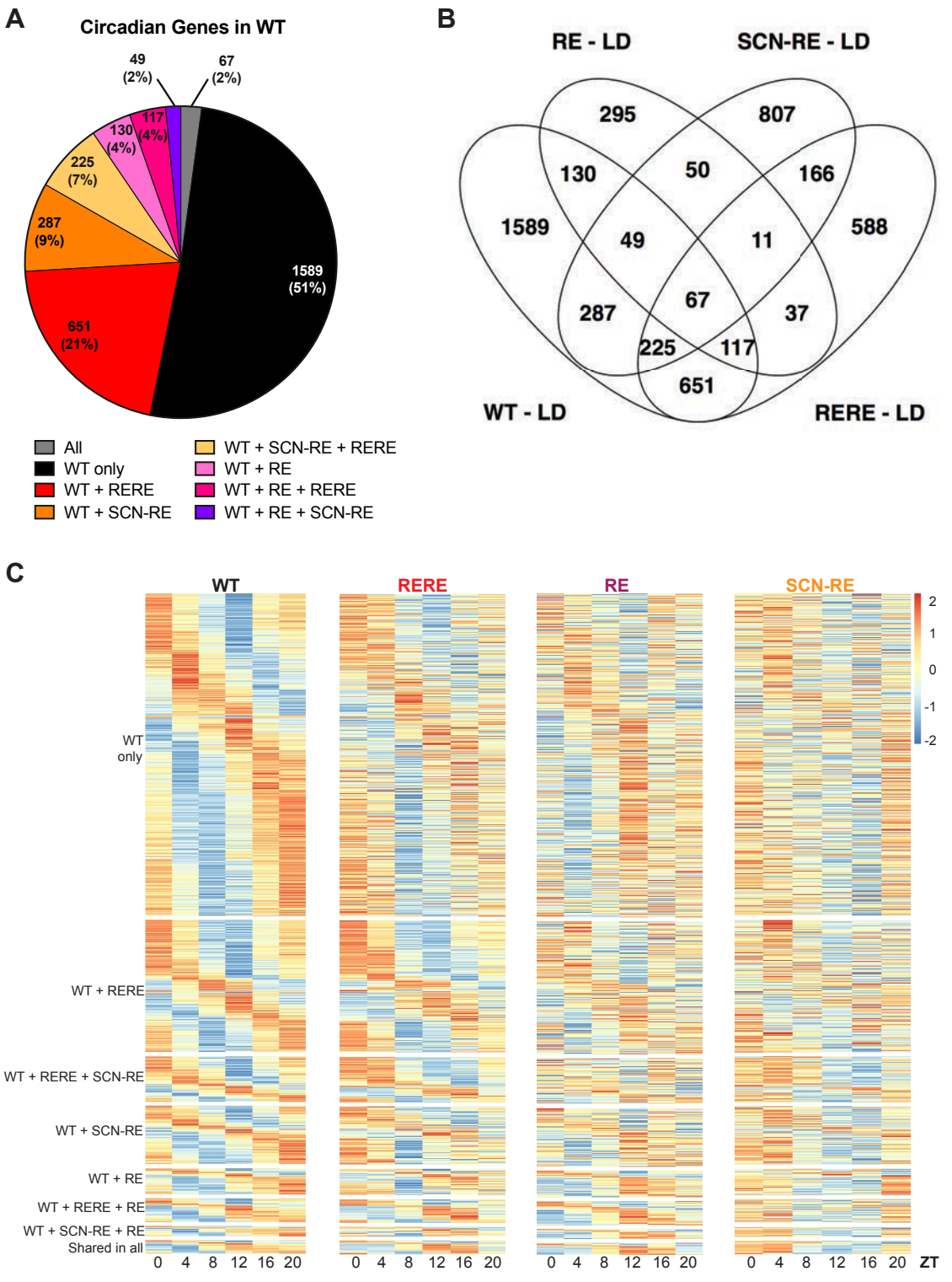

Figure 19. Communication between the central and epidermal clock largely rescues the circadian transcriptional output driven by the tissue-autonomous clock

(**A**) Pie chart displaying the circadian genes of the LD study expressed in WT epidermis and their overlap with rhythmic genes in RE, RERE and SCN-RE epidermis. (**B**) Venn diagram of circadian genes found in the epidermis of WT, RE, SCN-RE and RERE mice kept under LD conditions. (**C**) Heatmaps showing the circadian expression in the different genotypes of transcripts that are rhythmic in (from top to bottom): WT only, WT + RERE, WT + RERE + SCN-RE, WT + SCN-RE, WT + RE, WT + RERE + RE, WT + SCN-RE + RE, and WT + RERE + SCN-RE + RE, respectively. ZT: *Zeitgeber* Time.

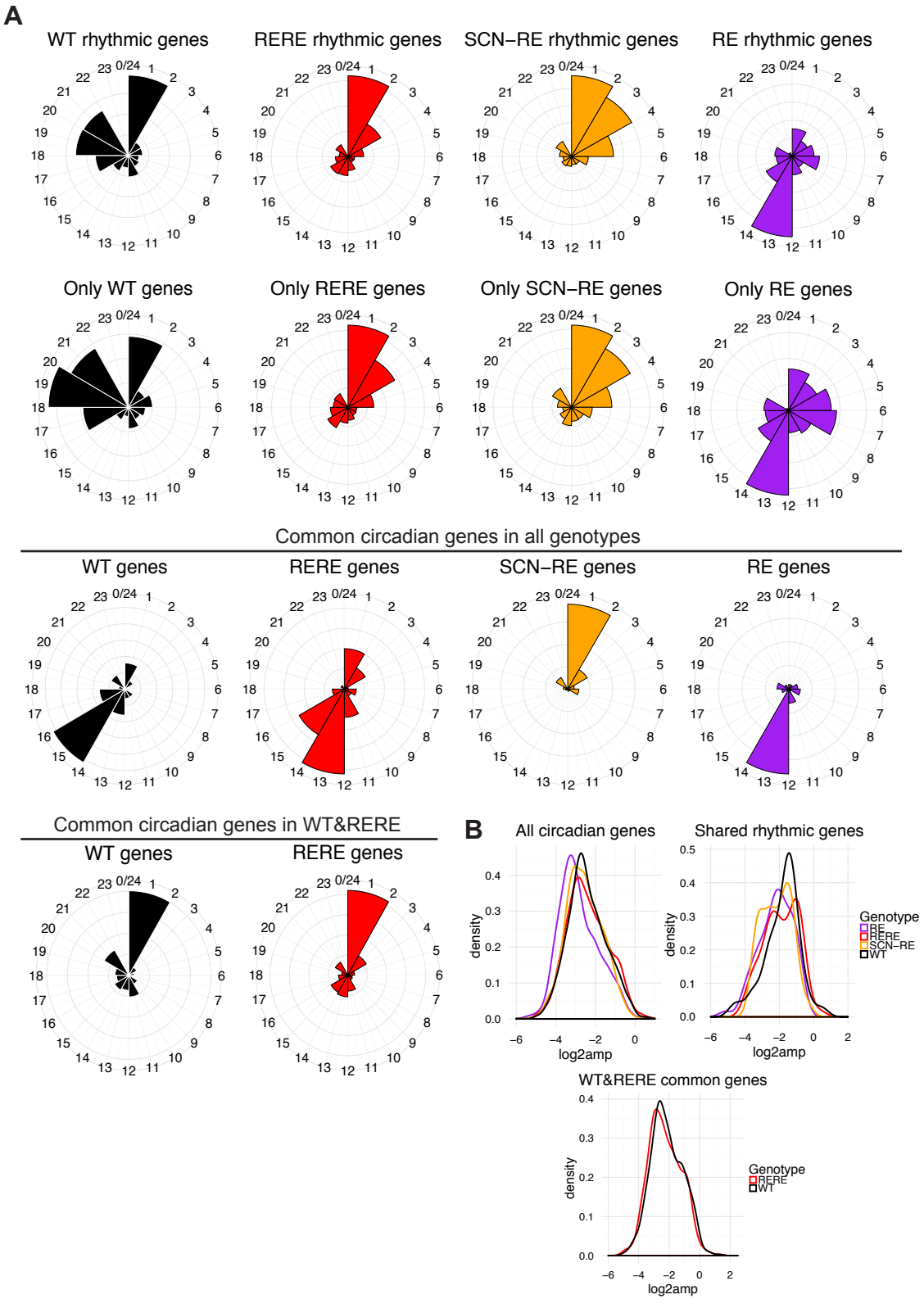

Figure 20. Phase and amplitude of RERE rhythmic genes are similar to WT rhythmic genes

(**A**) Phase distribution of circadian genes in the indicated genotypes and groups. (**B**) Amplitude of rhythmic transcripts in WT, RE, RERE and SCN-RE epidermis; Amplitude of shared rhythmic genes between WT, RE, RERE and SCN-RE; Amplitude of genes that are oscillating in both WT and RERE epidermis

Of note, the phase patterns of WT and RE transcripts from this experiment differed from the previous LD experiment (Figure 10A), likely due to the different sex of mice used for the two studies (females for the first and males for the second LD study). The amplitude of the rhythmic genes in the various genotypes other than WT was overall lower, particularly in the case of the oscillating transcripts shared by all (Figure 20B). Nevertheless, the amplitude of RERE genes was similar to the WT in the case of the common rhythmic transcripts between RERE and WT (Figure 20B).

At this point, we wanted to unveil which physiological processes rely on clock:clock communication or on other types of signals. Therefore, we looked at processes enriched in rescued circadian genes. In line with our previous results (Figure 11C), we found that the circadian transcripts in WT only (1,589 genes) were involved in a plethora of metabolic processes and signalling pathways, as well as in cell cycle and DNA repair processes (Figure 21A). Additionally, we further uncovered categories related to post-transcriptional processes, such as protein translation and modification, as well as epigenetic regulation processes (Figure 21A). These results highlight the importance of systemic BMAL1, thus of interactions within the body clock network, for full circadian physiology in WT epidermis. However, the genes circadian only in RERE (588 genes) solely comprised weakly enriched GO categories, mainly involved in metabolic processes and signalling pathways (Figure 21A). In contrast, the oscillating genes that were shared only between WT and RERE (651 genes), hence solely rescued by the RERE, fell into categories of cell cycle, cytoskeleton organisation and circadian regulation of gene expression (Figure 21A), suggesting that these biological processes predominantly require communication between the central and the peripheral clock. No significant categories were found regarding rhythmic genes shared between RE and RERE, RE and SCN-RE, or SCN-RE and RERE. Nevertheless, the transcripts that commonly oscillated in WT, RE and RERE epidermis (117 genes), or even in all genotypes (67 genes), were found to be mainly involved in cell cycle and DNA replication and repair (Figure 21A). The significant enrichment in these categories strongly points to a core circadian program of the epidermis to sustain its homeostasis regardless of the presence of either the central or the local clock. This stands in slight disagreement with what was previously hypothesised, according to which the basic cellular turnover of the epidermis is driven by the tissue-specific clock[198] (and see Results section 4.1.3 of this thesis).

To validate the GO results obtained by studying the biological processes behind the rhythmic genes shared in all genotypes, we analysed some of the genes involved in cell cycle and DNA replication. Strikingly, the phase of these genes was consistently

similar in WT, RE and RERE epidermis, where BMAL1 is locally present, whereas it was completely reversed in the SCN-RE epidermis that lacks local BMAL1 (Figure 21B). This finding is in line with the observations that SCN-RE epidermal transcriptome displayed an opposite phase concerning the distribution of circadian transcripts shared by all genotypes (Figure 19C & Figure 20A), and warrants further studies in order to uncover the reason and the consequences of this anti-phasic transcriptional output.

A

Rhythmic only in WT	q-value
metabolic process	1.93E-48
G protein-coupled receptor signaling pathway	3.08E-25
RNA processing	7.51E-16
ribosome biogenesis	2.89E-13
protein modification process	9.93E-13
cell cycle	3.22E-05
translation	1.51E-04
chromatin organization	1.02E-03
DNA repair	1.11E-03
histone modification	5.87E-03

Rhythmic only in RERE	q-value
sensory perception	6.86E-07
protein transport	4.26E-04
G protein-coupled receptor signaling pathway	5.98E-04
metabolic process	5.23E-03

WT&RERE common rhythmic genes	q-value
cell cycle	3.93E-30
cytoskeleton organization	2.17E-17
G protein-coupled receptor signaling pathway	8.91E-08
circadian regulation of gene expression	6.35E-05
protein modification	1.84E-04
rhythmic process	5.21E-04

WT&RE&RERE common rhythmic genes	q-value
DNA replication	4.55E-07
DNA metabolic process	7.94E-05
cell cycle	1.44E-04
rhythmic process	2.53E-03
DNA repair	1.80E-02

Rhythmic genes common to all	q-value
DNA replication	4.13E-23
DNA repair	8.58E-20
metabolic process	6.42E-19
cell cycle	2.19E-14

B

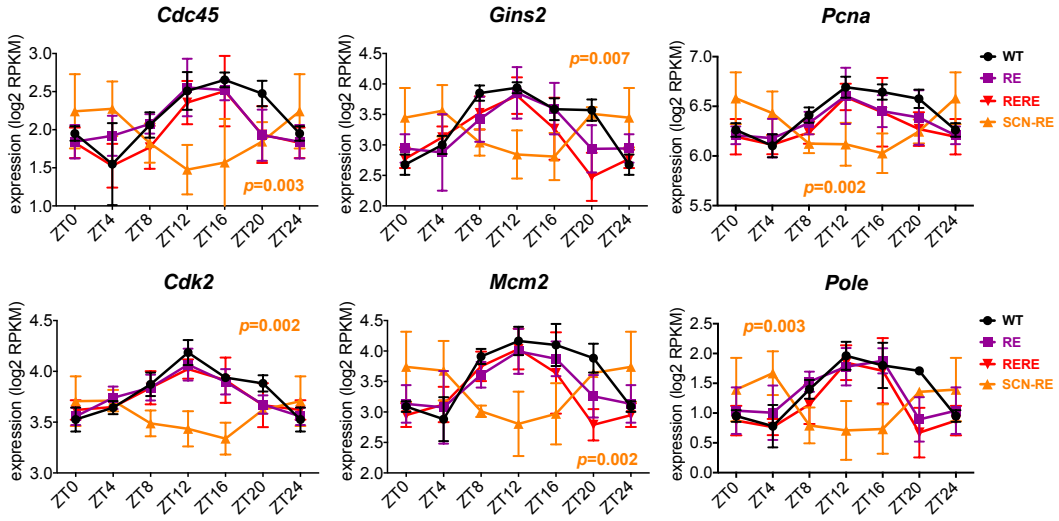

Figure 21. Communication between the central and epidermal clock preserves basic homeostatic functions in the epidermis

(**A**) Representative GO terms relative to genes that are rhythmic only in WT (n = 1,589 genes, refer to Figure19A&B), rhythmic only in RERE (n = 588 genes, refer to Figure19B), commonly circadian in both WT and RERE epidermis (n = 651 genes, refer to Figure19A&B), commonly circadian in WT, RE and RERE epidermis (n = 117 genes, refer to Figure19A&B), or rhythmic in all four genotypes (WT, RE, RERE and SCN-RE) (n = 67 genes, refer to Figure19A&B), respectively. (**B**) Cell cycle gene expression from the epidermis of WT, RE, RERE or SCN-RE mice (n = 4 mice per time point and genotype). Adjusted *p* values relative to SCN-RE epidermis are shown; data are represented as mean ± SD. ZT: *Zeitgeber* Time.

4.3.2 Communication between the SCN and the epidermal clock is sufficient to maintain epidermal clock output in the absence of light

The following question that we addressed was whether signals coming from the central clock are sufficient to maintain peripheral clock rhythmicity in absence of external environmental entraining stimuli. Hence, we kept the experimental mice in DD for one week (i.e. between 156h and 176h), and just like previously, we collected the epidermis at six different time points around the clock, in order to obtain the circadian transcriptome (Figure 22A). Remarkably, RERE mice maintained a robust core circadian machinery even after one week of darkness, similar to WT mice (Figure 22B). In line with the previous DD results of the present project, clock gene rhythmicity was flattened in RE epidermis after the period of constant darkness (Figure 22B).

WT epidermal transcriptome comprised 2,669 significantly oscillating transcripts, while 1,896 rhythmic genes were preserved in the RERE epidermis despite the DD conditions (Figure 23A&B). In this context, the RERE epidermis shared 1,079 circadian genes with the WT, accounting for a 40% of the overall WT transcriptional output (Figure 23A&B). 939 rhythmic transcripts of the WT circadian transcriptome were uniquely rescued by the RERE, pointing again at the key interaction between central and epidermal clock to attain a substantial circadian output in the epidermis. In contrast, SCN-RE epidermis lost 65% of its circadian output observed in the LD experiment, with only 579 significantly oscillating transcripts in DD (8% of total WT circadian transcriptome) (Figure 23A&B). In line with the previous DD experiment, the RE epidermis lost its circadian output, with a total of 256 genes oscillating in darkness conditions (Figure 23A&B). These results strongly point to a reliance on SCN clock for light-dependent peripheral circadian transcription.

Many of those genes classified as uniquely circadian in WT also showed pattern of rhythmicity in RERE, as opposed to RE and SCN-RE gene sets that appeared arrhythmic (Figure 23C). Altogether, this outcome implies that communication between the SCN and the epidermal clock is sufficient to preserve a robust circadian transcriptional output even in the absence of external entraining cues.

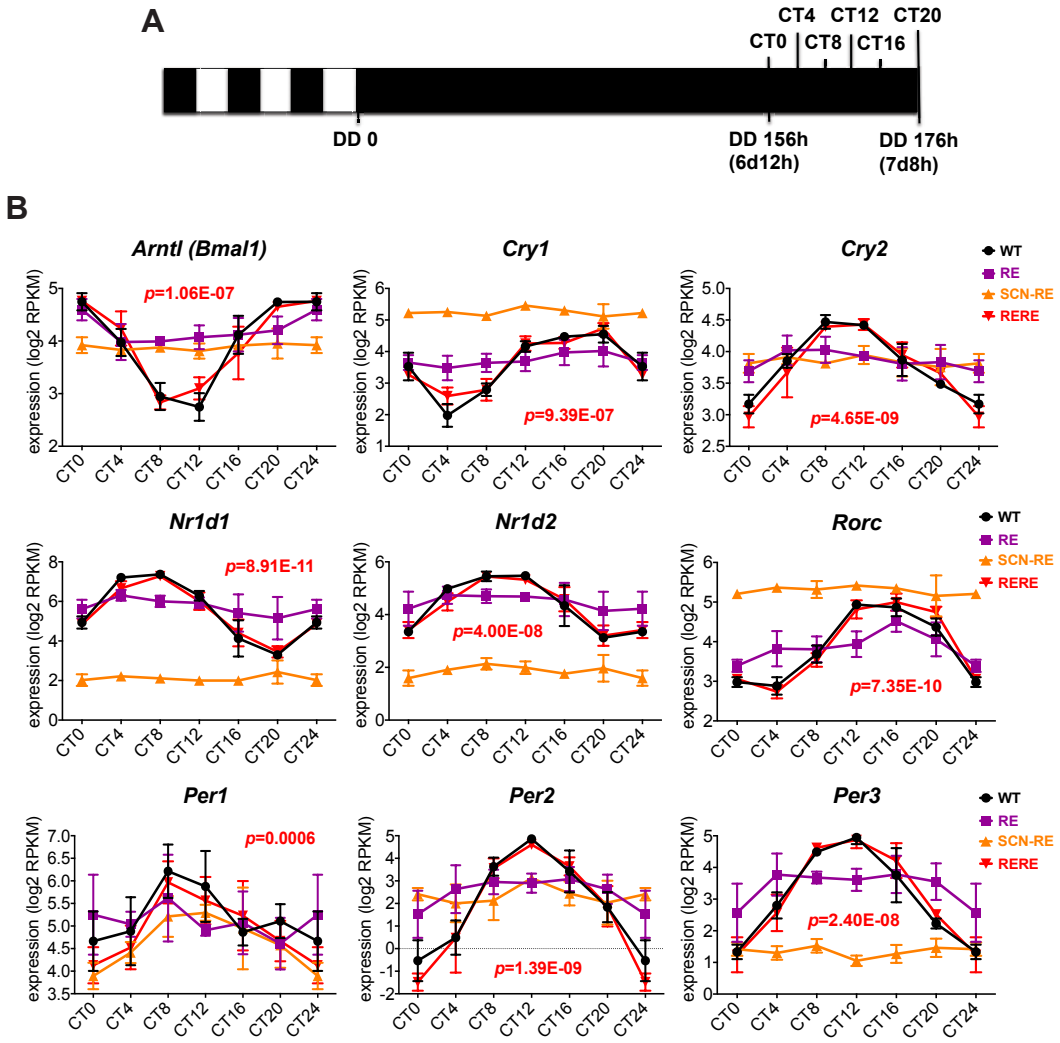

Figure 22. Communication between the SCN and the epidermal clock is sufficient to maintain a robust epidermal clock machinery in the absence of light

(**A**) Experimental setup scheme of the 12h Dark /12h Dark (DD) study: After standard LD photoperiod, 8-week-old WT, RE, RERE and SCN-RE female mice were transferred to conditions of constant darkness for 6-7 days; interfollicular epidermis was then isolated at six different time points around the clock, i.e. every 4h. The obtained tissue was subsequently submitted for RNA-sequencing to establish the circadian transcriptome, which was determined by using the JTK_CYCLE algorithm[312]. CT: Circadian Time. (**B**) Core clock gene expression from the epidermis of WT, RE, SCN-RE or RERE mice (n = 4 mice per time point and genotype). Adjusted *p* values relative to RERE epidermis are shown; data are represented as mean ± SD. CT: Circadian Time.

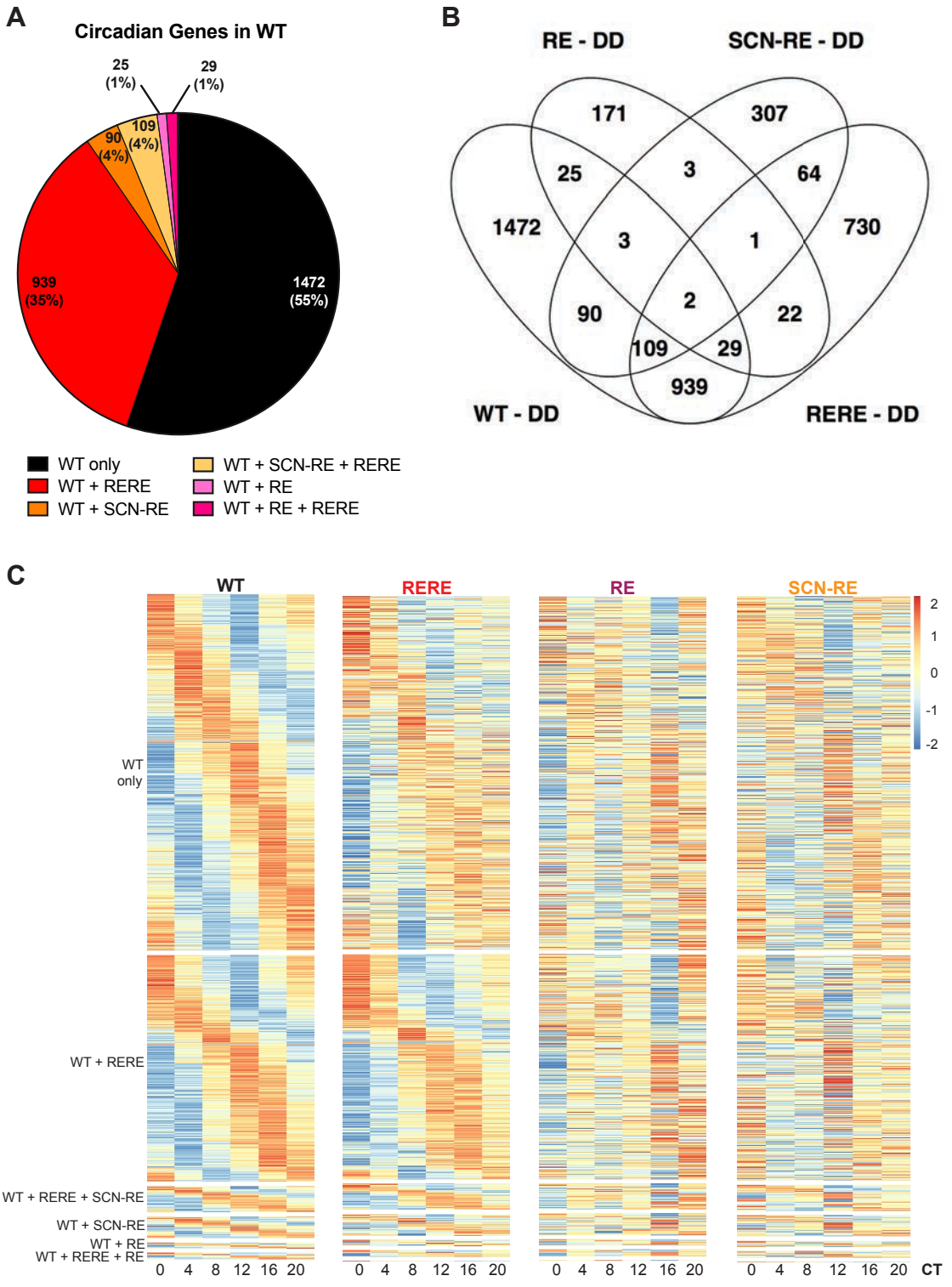

Figure 23. Communication between the central and epidermal clock largely preserves the circadian transcriptional output in the absence of light

(**A**) Pie chart displaying the circadian genes of the DD study expressed in WT epidermis and their overlap with rhythmic genes in RE, RERE and SCN-RE epidermis. (**B**) Venn diagram of circadian genes found in the epidermis of WT, RE, SCN-RE and RERE mice kept under DD conditions. (**C**) Heatmaps showing the circadian expression in the different genotypes of transcripts that are rhythmic in (from top to bottom): WT only, WT + RERE, WT + RERE + SCN-RE, WT + SCN-RE, WT + RE, WT + RERE + RE, WT + SCN-RE + RE, and WT + RERE + SCN-RE + RE, respectively. CT: Circadian Time.

Regarding the phase distribution of the various outputs, all genotypes showed a clear separation into two main peaks, at the beginning of the light and of the dark time, with the exception of the RE epidermis, which exhibited a clock-wise phase shift (Figure 24A). Of note, the phase distribution of WT transcripts from this DD experiment confirmed the phase pattern observed in the first LD experiment performed (Figure 10A), likely because the same sex of mice was used in this context (females). Importantly, all subsets of RERE rhythmic genes showed a similar phase distribution to the WT (Figure 24A). Once again, the circadian genes shared by WT, RERE and SCN-RE epidermis exhibited an opposite phase distribution, with WT and RERE transcripts mainly peaking in the evening, while the SCN-RE epidermal transcriptome displayed a morning peak instead (Figure 24A). Moreover, the amplitude of all circadian genes in RE, SCN-RE and RERE epidermis was reduced compared to the WT (Figure 24B).

Next, we performed GO analyses and uncovered that, similar to the LD experiment, the circadian transcripts in WT only (1,472 genes) were involved in cell cycle, metabolic processes and signalling pathways (Figure 25A). In addition, categories of sensory perception and epithelium development were also enriched (Figure 25A). These results suggest that, even in the absence of external light, the WT epidermal circadian transcriptome is in charge of extracellular interactions and signal perception that ensure proper tissue turnover and maintenance. Moreover, the 730 circadian transcripts in RERE only were involved in cytoskeleton organisation, as well as signalling pathways and metabolic processes (Figure 25A). These categories point to a dynamic state underlying inter-tissue communication. Furthermore, 939 oscillating genes (i.e. 35% of the overall WT rhythmic transcriptome) were uniquely rescued by the RERE, and included core physiological functions, such as cell cycle, DNA replication and repair, cytoskeleton organisation, epigenetic regulation, and circadian rhythms (Figure 25A). This underlies the great relevance of the communication between central and epidermal clock to sustain the epidermal physiological requirements. No significant categories were identified from the other subgroups of shared rhythmic genes, with the exception of the 109 transcripts (4% of WT output) commonly circadian between WT, RERE and SCN-RE, which were found to be involved in cell cycle and DNA replication and repair (Figure 25A). This strengthens what was already described for the LD experiment (Figure 21), thus, pointing once again to a core circadian program of the epidermis that can be maintained by either the peripheral or the central clock.

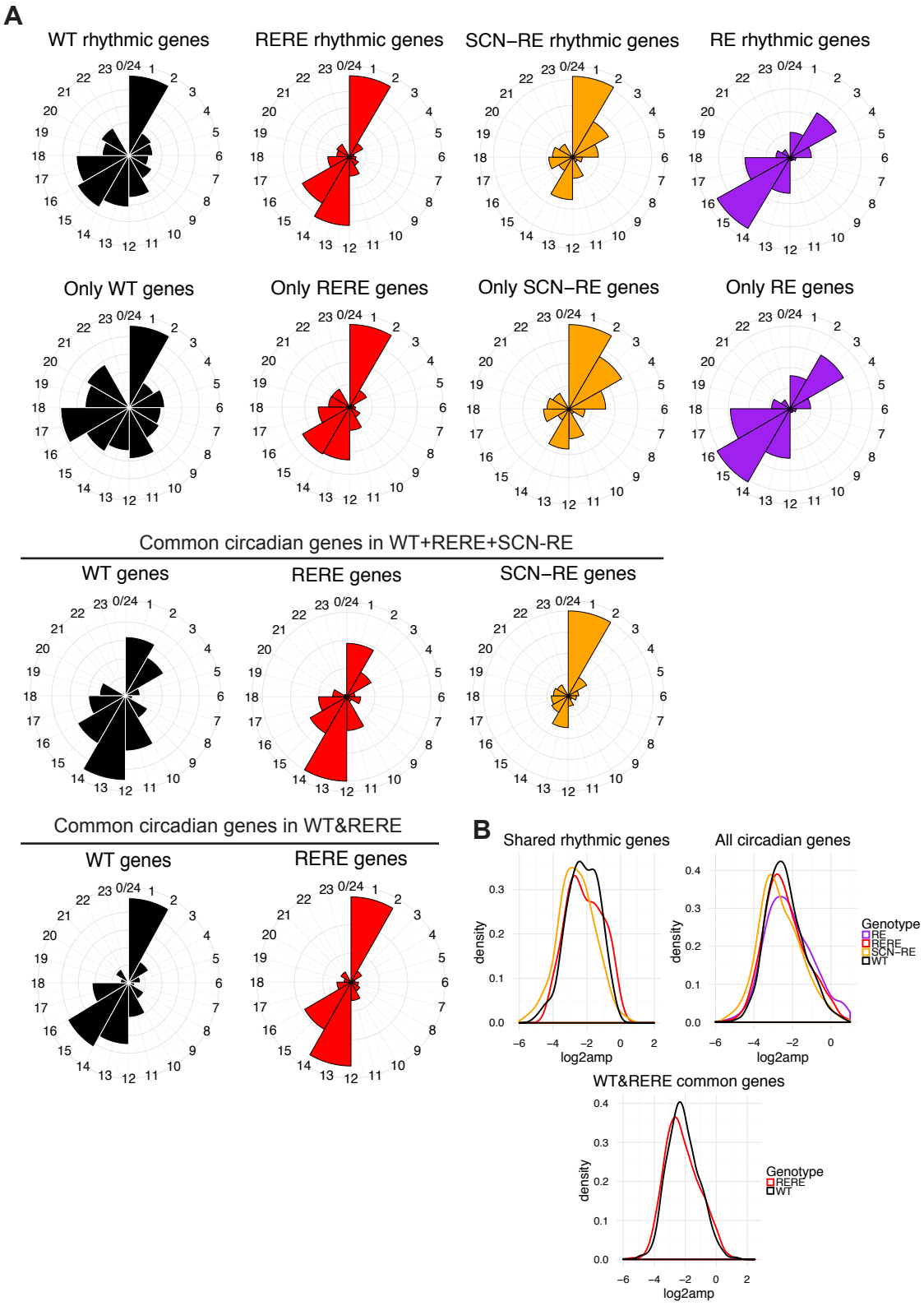

Figure 24. Phase and amplitude of RERE rhythmic genes are similar to WT rhythmic genes in conditions of constant darkness

(**A**) Phase distribution of circadian genes in the indicated genotypes and groups. (**B**) Amplitude of rhythmic genes that are shared between WT, RERE and SCN-RE epidermis; Amplitude of rhythmic transcripts in WT, RE, RERE and SCN-RE epidermis; Amplitude of genes oscillating in both WT and RERE epidermis.

To further validate the GO results, we analysed those same genes involved in cell cycle and DNA replication that we studied in the context of the LD experiment (Figure 21B). Notably, the phase of these genes was consistently similar in WT and RERE epidermis, while being completely opposite in the SCN-RE epidermis (Figure 25B).

A

Rhythmic only in WT	q-value
sensory perception	2.50E-23
G protein-coupled receptor signaling pathway	4.57E-18
metabolic process	3.43E-10
cell cycle	3.65E-10
protein transport	1.20E-06
cytoskeleton organization	8.71E-06
protein modification process	2.51E-05
epithelium development	2.56E-05

Rhythmic only in RERE	q-value
sensory perception	4.93E-11
metabolic process	7.19E-08
G protein-coupled receptor signaling pathway	1.45E-06
cytoskeleton organization	1.57E-05

WT&RERE common rhythmic genes	q-value
cell cycle	8.93E-39
DNA repair	2.64E-21
metabolic process	7.42E-20
cytoskeleton organization	6.98E-16
G protein-coupled receptor signaling pathway	1.09E-13
DNA replication	3.71E-13
histone phosphorylation	5.72E-04
chromatin organization	1.36E-03
circadian rhythm	5.00E-03

WT&SCN-RE&RERE common rhythmic genes	q-value
DNA replication	3.42E-10
cellular response to stress	8.24E-09
DNA repair	2.11E-08
metabolic process	8.86E-07
cell cycle	9.66E-04

B

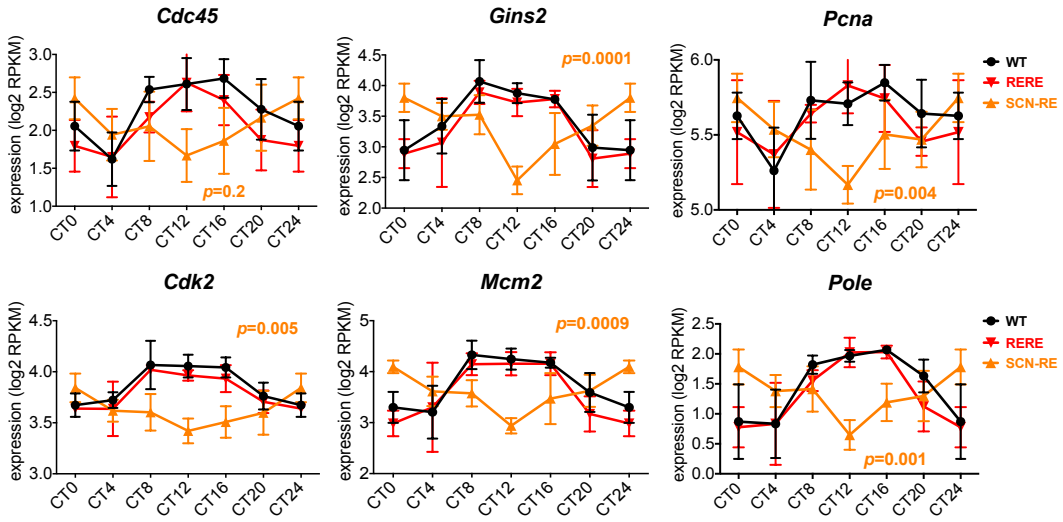

Figure 25. Communication between the central and epidermal clock preserves basic homeostatic functions in the epidermis in the absence of light

(**A**) Representative GO terms relative to genes that are rhythmic only in WT (n = 1,472 genes, refer to Figure23A&B), rhythmic only in RERE (n = 730 genes, refer to Figure23B), commonly circadian in both WT and RERE epidermis (n = 939 genes, refer to Figure23A&B), or commonly circadian in WT, SCN-RE and RERE epidermis (n = 109 genes, refer to Figure23A&B), respectively. (B) Cell cycle gene expression from the epidermis of WT, RERE or SCN-RE mice (n = 4 mice per time point and genotype). Adjusted *p* values relative to SCN-RE epidermis are shown; data are represented as mean ± SD. CT: Circadian Time.

This finding supports the previous LD outcome, and opens up new potential signalling pathways involved in peripheral clock entrainment. Additionally, it indicates that the SCN clock regulates the cell cycle machinery in an opposite circadian manner as compared to the local clock, and independently of light signalling. This could imply a dominance of the epidermal clock in the context of a possible conflict between pathways induced by systemic signals versus local input.

4.3.3 The SCN clock is sufficient to preserve behavioural rhythmicity

Having determined the epidermal circadian transcriptome of RERE mice, we next asked whether behavioural rhythms dependent on a functional central clock would enable such clock communication between SCN and epidermis. To address this question, we measured various behavioural rhythms that are known to play a role in the entrainment of the circadian clock, such as locomotor activity, food intake, as well as metabolism.

As expected, WT mice showed a rhythmic locomotor activity both under LD and DD conditions, counteracted by the arrhythmic behaviour of KO mice (Figure 26A&B). A similar outcome was observed with regard to the feeding behaviour and accompanying metabolism, which were robustly circadian in the WT mice, but not in the KO, and this held true both in LD and DD conditions (Figure 26C&D). Interestingly, SCN-RE mice were more active in the dark hours than in the light hours when placed under LD conditions (Figure 26A&B). However, a considerable variability was noticed between animals, which caused the lack of a statistical significant locomotor increase at night (Figure 26A&B). When the SCN-RE mice were transferred to constant darkness experimental conditions, a significant phase advance was noted, which shifted the behavioural rhythmicity of these animals (Figure 26A&B). On the other hand, their feeding behaviour and respiratory exchange ratio had a clear nocturnal increase, and these rhythms were strikingly preserved in conditions of constant darkness, with the only exception of energy expenditure rate that did not display a circadian trend in LD nor in DD (Figure 26C&D).

Taken together, these results indicate that the epidermal BMAL1-driven transcriptional oscillations reliant on central:peripheral clock communication may depend on central-clock-induced rhythmic behaviour.

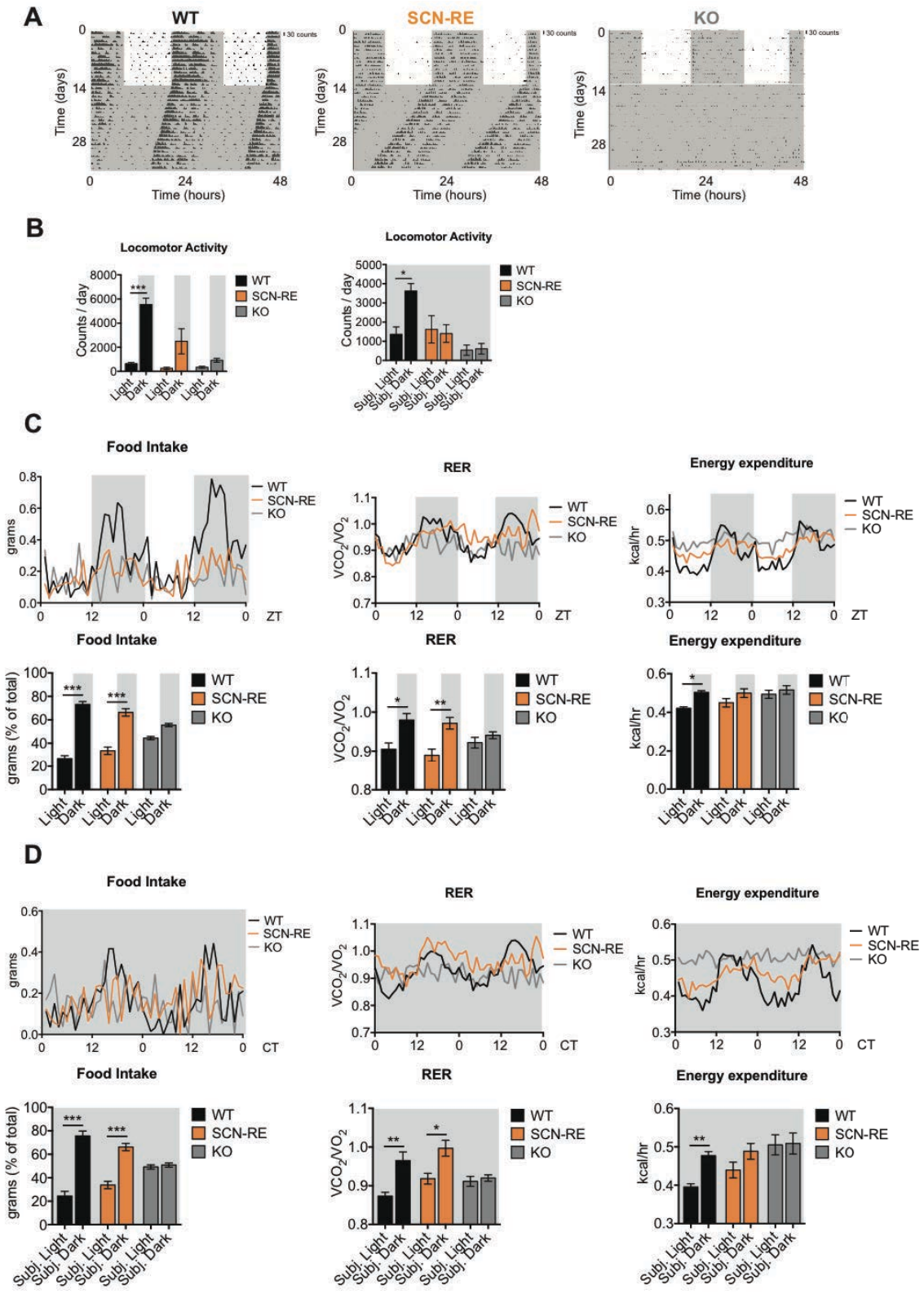

Figure 26. The SCN clock is sufficient to preserve behavioural rhythmicity

(**A**) Representative actograms showing locomotor activity of one WT, one SCN-RE, and one KO replicate, respectively, duplicated over two days for visualisation. Mice were kept in LD conditions for 14 days, and were then moved to DD. Scale bar: 30 counts. (**B**) Quantification of the locomotor activity measurements in LD and DD conditions. Six mice were used per genotype per experiment. Two-way ANOVA, $*p \leq 0.05$, $***p \leq 0.001$; data are represented as mean ± SEM. (**C**)

Metabolic characterisation of *ad libitum* fed mice kept in LD conditions for two days. Traces of group averages are shown on the top graphs, while quantification is displayed on the lower graphs. RER: respiratory exchange ratio. Food intake: n(WT) = 5, n(KO) = 5, n(SCN-RE) = 7; RER: n(WT) = 6, n(KO) = 6, n(SCN-RE) = 8; Energy expenditure: n(WT) = 6, n(KO) = 6, n(SCN-RE) = 7. Two-way ANOVA, *$p \leq 0.05$, **$p \leq 0.01$, ***$p \leq 0.001$. (**D**) Metabolic characterisation of *ad libitum* fed mice kept in DD conditions for two days. Traces of group averages are shown on the top graphs, while quantification is displayed on the lower graphs. RER: respiratory exchange ratio. Food intake: n(WT) = 6, n(KO) = 4, n(SCN-RE) = 6; RER: n(WT) = 7, n(KO) = 5, n(SCN-RE) = 7; Energy expenditure: n(WT) = 7, n(KO) = 5, n(SCN-RE) = 7. Two-way ANOVA, *$p \leq 0.05$, **$p \leq 0.01$, ***$p \leq 0.001$.

4.4 Tissue-autonomous clock entrainment is induced by light via the sympathetic nervous system

Valentina M. Zinna[1*], Thomas Mortimer[1*], Jesus Gonzalez[2], Paolo Sassone-Corsi[3], Pura Muñoz-Cánoves[4,5,6], Patrick-Simon Welz[1], and Salvador Aznar Benitah[1,6]

[*] These authors contributed equally

Affiliations:

[1]Institute for Research in Biomedicine (IRB Barcelona), Barcelona Institute of Science and Technology, 08028 Barcelona, Spain

[2]PCB-PRBB Animal Facilities, 08028 Barcelona, Spain

[3]Center for Epigenetics and Metabolism, University of California, Irvine, CA 92697, USA

[4]Centro Nacional de Investigaciones Cardiovasculares Carlos III (CNIC), 28029 Madrid, Spain

[5]Universitat Pompeu Fabra (UPF), Department of Experimental and Health Sciences (DCEXS) and CIBER on Neurodegenerative Diseases (CIBERNED), 08003 Barcelona, Spain

[6]ICREA, Catalan Institution for Research and Advanced Studies, 08010 Barcelona, Spain

4.4.1 BMAL1-driven epidermal oscillations are mediated by the sympathetic nervous system

The exact mechanisms mediating epidermal clock entrainment are yet to be elucidated. With the RERE mouse model, we uncovered that communication with the central clock is sufficient to maintain a robust circadian transcriptional output, even in the absence of environmental cues. On the other hand, with the RE mouse model, we unveiled that light can entrain the epidermal clockwork independently of other tissue clocks. Therefore, we attempted to dissect the mechanisms behind the light-driven epidermal transcriptional rhythmicity. In this regard, it has already been reported that proliferation of hair follicle stem cells is stimulated by external light via the sympathetic nervous system[327]. Moreover, the autonomic nervous system has been implicated in modulating the circadian control of physiological functions of peripheral organs, such as kidney and liver, among others[115,116].

Based on these findings, we hypothesised that the light-dependent mechanisms behind the transcriptional oscillations observed in the epidermis in the absence of a functional SCN clock could be of neuronal origin. Hence, we performed pharmacological sympathectomy on WT and RE mice placed under standard LD photoperiod, in order to explore the impact of sympathetic nerves on the epidermal-intrinsic circadian clock. Cutaneous denervation was carried out through subcutaneous injections of 6-hydroxydopamine (6-OHDA), which is a neurotoxin that selectively kills sympathetic nerves[328]. Efficacy of the chemical sympathectomy procedure was histologically assessed by staining for Tyrosine Hydroxylase (TH), which specifically labels sympathetic nerves, as it represents the rate-limiting enzyme for catecholamine biosynthesis (Figure 27A&B). Treatment with 6OHDA effectively depleted sympathetic innervation to the skin, as exemplified by the lack of TH staining contacting the hair follicles, as well as by a significant reduction of TH mRNA levels in the treated skin as opposed to the sham-injected counterparts (Figure 27). Recent studies have adopted a similar chemical approach and have also shown a similar selective ablation of the cutaneous sympathetic nervous system[235,327].

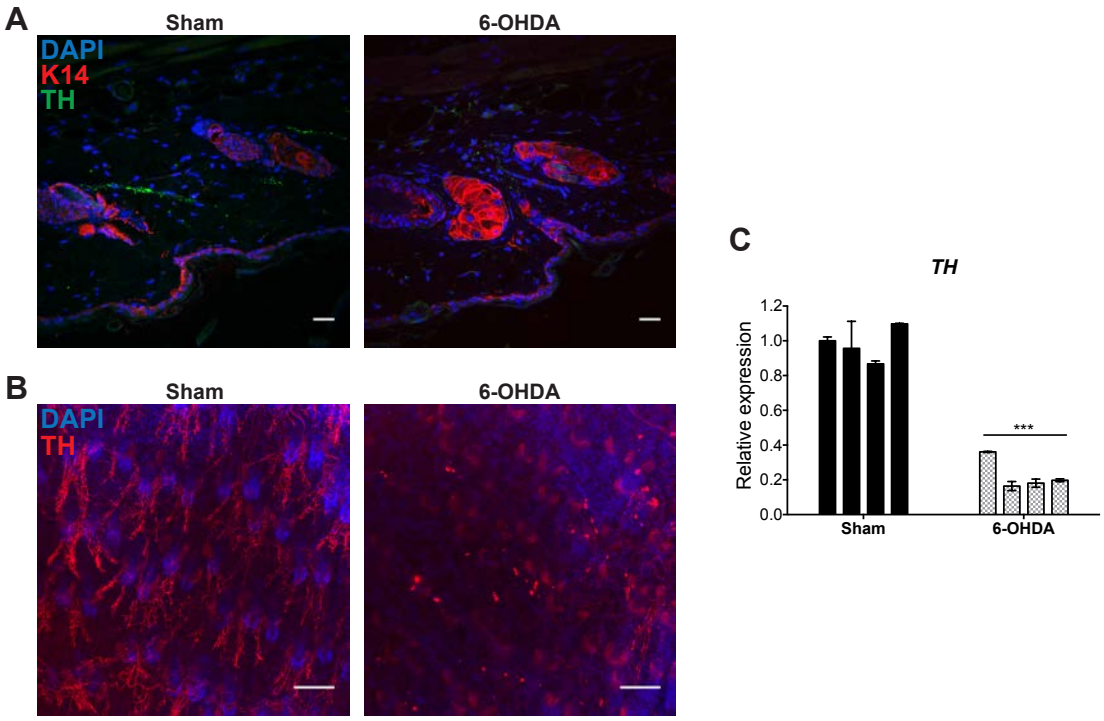

Figure 27. 6-OHDA treatment disrupts sympathetic innervation in the skin

(**A**) Representative immunofluorescence images of intensity levels of DAPI (blue, marker for nuclei), K14 (red, marker for basal cell layer), and Tyrosine Hydroxylase ([TH] green, marker for sympathetic nerves); scale bar = 50µm. Left picture represents a sham-injected WT skin section; right picture represents a 6-OHDA-treated WT skin section. (**B**) Representative whole-mount images of intensity levels of DAPI (blue, marker for nuclei), and TH (red, marker for sympathetic nerves); scale bar = 100µm. Left picture represents sham-injected WT skin; right picture represents 6-OHDA-treated WT skin. (**C**) Relative expression of *TH* in sham-injected and 6-OHDA-treated WT back skin; data are represented as mean ± SD; Unpaired t test, ***$p \leq 0.001$ compared to Sham.

We performed pharmacological cutaneous sympathectomy in WT and RE mice, kept under standard LD photoperiod, two weeks prior to the sacrifice time point (8 weeks of age). We then collected sham- and 6OHDA-injected epidermal samples at ZT0 and ZT12, representing peak and trough of *Bmal1* expression, and analysed gene expression levels of *Bmal1* (core clock gene), and of *Dbp* (a direct CCG). In line with our hypothesis, we observed a loss of day:night differences in these two genes in the epidermis of sympathectomised RE animals, but not in the WT (Figure 28). This might point to a disruption of transcriptional rhythmicity in RE epidermis caused by the sympathectomy procedure, while WT rhythms remain unaltered. Of note, RE epidermis in sham-injected animals displayed lower amplitudes of *Bmal1* and *Dbp* gene expression, as compared to the WT tissue, which is in line with what was already observed in the context of the RNA-sequencing experiment in LD conditions (Figure 6B). Yet, no significant difference in *Bmal1* and *Dbp* gene expression was found between ZT0 and ZT12 in sympathectomised RE epidermis (Figure 28). Thus, in absence of communication between clocks in different tissues, synchronisation of the circadian clockwork in the epidermal tissue might rely on the sympathetic nervous system. In contrast, the light signal entrained the WT epidermis albeit the absence of local sympathetic innervation, suggesting that further signalling pathways might be involved in peripheral clock entrainment.

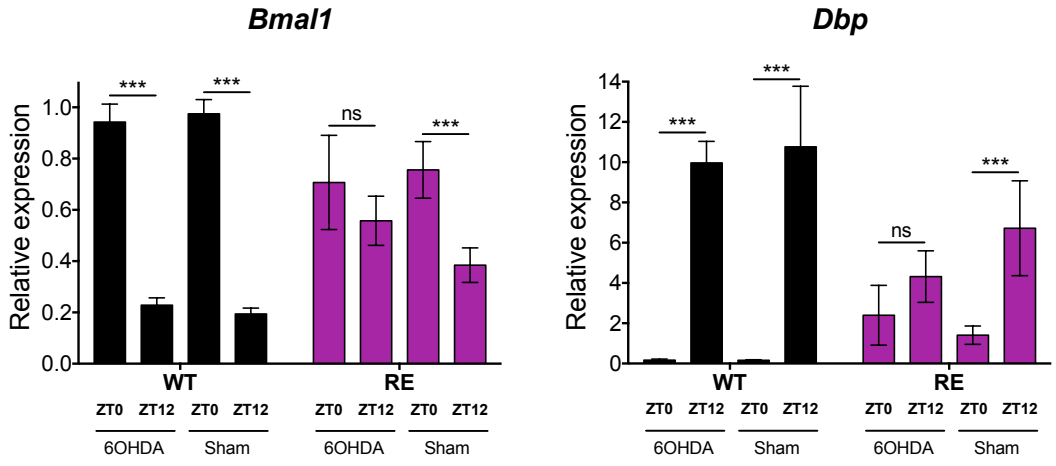

Figure 28. *Bmal1* and *Dbp* rhythmic expression in BMAL1-driven epidermis is mediated by the sympathetic nervous system

Relative expression of *Bmal1* and *Dbp* in sham-injected or 6-OHDA-treated WT or RE back skin epidermis collected at two time points, ZT0 and ZT12; n = 3 mice per time point, genotype and treatment; data are represented as mean ± SD; Two-way ANOVA with Tukey's multiple comparisons test, ***q-value ≤ 0.001, ns: non significant. ZT: *Zeitgeber* Time.

4.4.2 The epidermal clock machinery may require sympathetic innervation to oscillate in free-running conditions

Based on the results obtained from the first sympathectomy experiment, we wondered whether the sympathetic nervous system is required to communicate memory of external cycle to peripheral clocks. Therefore, we decided to perform a DD experiment with sympathectomised WT mice. We carried out cutaneous chemical sympathectomy on WT animals and kept them under standard LD photoperiod, before moving them to one week of constant darkness. We then collected the epidermis at CT0 and CT12 to analyse gene expression levels of *Bmal1* (core clock gene), and of *Dbp* (a direct CCG).

Remarkably, circadian oscillations of *Bmal1* and *Dbp* genes were lost in sympathectomised WT mice (Figure 29). Interestingly, the overall total levels of gene expression seemed to be impaired by the treatment (Figure 29). Hence, these results emphasise the importance of cutaneous sympathetic innervation to communicate light cycle memory to the local clock machinery.

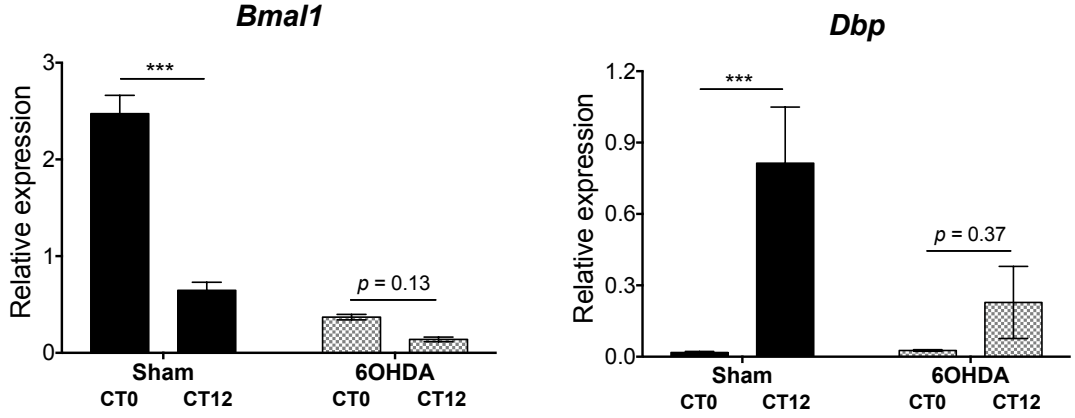

Figure 29. The epidermal clock machinery requires sympathetic innervation to robustly oscillate in the absence of light

Relative expression of *Bmal1* and *Dbp* in sham-injected and 6-OHDA-treated WT back skin epidermis collected at two time points, CT0 and CT12; n = 3 mice per time point and treatment; data are represented as mean ± SD; Two-way ANOVA with Tukey's multiple comparisons test, ***q-value ≤ 0.001. CT: Circadian Time.

4.5 Tissue-intrinsic BMAL1 ensures physiological epidermal ageing but is insufficient to drive correct wound healing

Valentina M. Zinna[1*], Thomas Mortimer[1*], Patrick-Simon Welz[1*], Carmelo Laudanna[1], Kevin B. Koronowski[2], Jacob G. Smith[2], Inés Marín Guillén[1], Andrés Castellanos[1], Neus Prats[1], Monica Aguilera[1], Esther Pintado[1], Juan Martín Caballero[3], Jesus Gonzalez[3], Pura Muñoz-Cánoves[4,5,6], Paolo Sassone-Corsi[2], and Salvador Aznar Benitah[1,6]

[*] These authors contributed equally

Affiliations:

[1]Institute for Research in Biomedicine (IRB Barcelona), Barcelona Institute of Science and Technology, 08028 Barcelona, Spain

[2]Center for Epigenetics and Metabolism, University of California, Irvine, CA 92697, USA

[3]PCB-PRBB Animal Facilities, 08028 Barcelona, Spain

[4]Universitat Pompeu Fabra (UPF), Department of Experimental and Health Sciences (DCEXS) and CIBER on Neurodegenerative Diseases (CIBERNED), 08003 Barcelona, Spain

[5]Centro Nacional de Investigaciones Cardiovasculares Carlos III (CNIC), 28029 Madrid, Spain

[6]ICREA, Catalan Institution for Research and Advanced Studies, 08010 Barcelona, Spain

4.5.1 Epidermal BMAL1 prevents tissue premature ageing

An impaired circadian clockwork leads to several signs of premature ageing, both at the systemic and local tissue level. For example, full-body *Bmal1*-KO mice have a shorter life expectancy compared to WT mice[196,197] (Figure 5A). Furthermore, they show a number of progressive premature ageing conditions, such as eye pathologies, weight loss, arthropathy, and osteoporosis[155] (Figure 5A&B). At the skin tissue level, *Bmal1*-KO mice experience decreased epidermal self-renewal, dampened hair growth and high epidermal differentiation[196,217], which are hallmarks of mammalian skin ageing[329–332]. Overall, the lack of *Bmal1* in $K14^+$ cells causes severe epidermal ageing, demonstrated by the expression of differentiation markers, like loricrin, and by a worsened epidermal cornification[217].

Therefore, we asked whether tissue-specific BMAL1 is sufficient for physiological ageing. To this aim, we measured organismal and epidermis-specific signs of ageing. Nevertheless, we did not observe any recovery in the life span of RE mice, nor did we obtain a rescue in the loss of body weight (Figure 30A). However, and strikingly, the expression of the core clock gene solely in the epidermis remarkably rescued the signs of epidermal tissue ageing, as exemplified by a thinner layer of epidermal cornification in aged RE mice compared to full-body *Bmal1*-KO mice (Figure 30C&D). Accordingly, LORICRIN, as a marker for terminally differentiated keratinocytes, was considerably less expressed in aged RE mice than in KO mice (Figure 30B).

Next, we integrated already published single-cell RNA-sequencing signatures of the keratinocyte differentiation process[333] with our transcriptomic data, in order to establish the impact of tissue-specific BMAL1 on the gene expression profile of epidermal cells. We found that markers for keratinocyte differentiation were markedly upregulated in the KO epidermis compared to the WT, while markers for stem and progenitor cells of the basal epidermal layer were downregulated (Figure 30E). In contrast, the RE epidermis displayed an intermediate gene signature between WT and KO, and the same held true for both LD and DD experimental conditions (Figure 30E). Therefore, *Bmal1* expression solely in the epidermis suffices to delay the signs of tissue ageing that prematurely appear in the KO epidermis[198]. Nevertheless, since RE epidermis is transcriptionally arrhythmic in DD (Figure 14B & Figure 22B), the observed rescue effects might be due to a non-circadian activity of BMAL1, or alternatively to circadian functions that are independent of BMAL1.

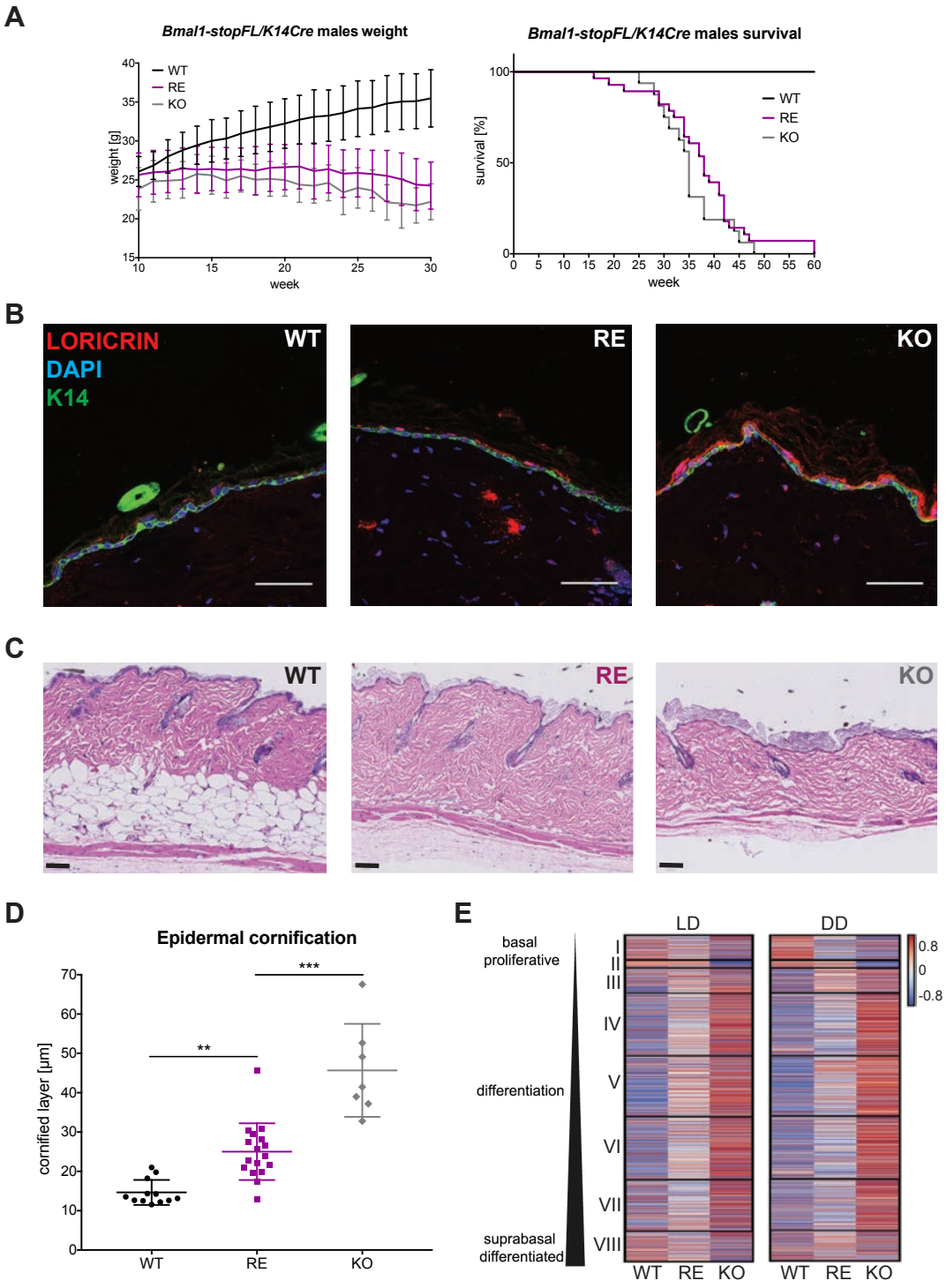

Figure 30. Epidermal BMAL1 is required to prevent premature tissue differentiation and ageing

(**A**) On the left: Weight curves for WT, *Bmal1-stopFL/K14* (RE), and KO males; n(WT) = 34, n(RE) = 28, n(KO) = 16; data are represented as mean ± SD. On the right: Kaplan-Meier survival curve for WT, RE, and KO males (no significant difference between RE and KO, p = 0.27); n(WT) = 34, n(RE) = 28, n(KO) = 16; average lifespan (RE) = 37.4 ± 9.8 weeks; average lifespan (KO) = 35.2 ± 6.3 weeks. (**B**) Representative images of intensity levels of DAPI (blue, marker for nuclei), K14 (green, marker for basal cell layer), and LORICRIN (red, marker for epidermal differentiation); scale bar = 50µm. (**C**) H/E–stained skin sections for visualisation of the cornified outer layer representing epidermal differentiation; scale bar = 100µm. (**D**) Epidermal cornification quantified as thickness of cornified layer between each hair follicle along an H/E–stained skin section; One-way ANOVA with Tukey's multiple comparisons test, q-value(RE vs WT) = 1.97*10^3,

q-value(RE vs KO) = 1.33*10^6, q-value(WT vs KO) = 8.79*10^10); data are represented as mean ± SD. (**E**) Heatmaps showing the expression in the different genotypes of clusters of markers that describe keratinocytes populations according to their differentiation status[333]. This characterisation was performed for both the LD (on the left) and the DD (on the right) experiment, by plotting the overall gene expression across all time points of WT, RE, and KO 8-week-old females.

4.5.2 The central SCN clock is not sufficient for physiological tissue ageing in the epidermis

The circadian experiments with RERE mice shed light on the contribution of tissue-autonomous clock versus central:peripheral clock communication on the epidermal transcriptome and related physiology. In this context, we found that light can entrain the epidermal clockwork independently of other tissue clocks, while allowing for core circadian tissue homeostasis. In addition, communication between central and peripheral clock is sufficient to maintain a robust circadian transcriptional output, even in the absence of environmental cues. Hence, we next tested whether communication between the SCN and the epidermal clock could further prevent premature epidermal ageing, as compared to the sole contribution of epidermis-restricted BMAL1 (Figure 30). Firstly, we closely monitored the survival rate and weight of SCN-RE mice, compared to the KO prematurely ageing animals. We hypothesised that the presence of a functional clock, even if only in a restricted area of the brain, could impact the life span of these mice. However, we did not obtain any recovery in the life span of SCN-RE mice, nor did we observe a rescue in body weight, which stayed constant throughout the life span of the mice (Figure 31A). Thus, a functional central clock is not sufficient to rescue the shortening of life span occurring in KO mice. A further analysis including the life span and weight measurement of RERE mice would be needed, albeit no differences are likely to be observed compared to the results obtained from RE and SCN-RE mice. That is, physiological ageing in terms of life span and body weight likely requires systemic BMAL1, as opposed to the sole rescue of BMAL1 in the SCN and/or the epidermis.

In addition, the SCN clock alone could not prevent the histological signs of epidermal tissue ageing, and therefore the epidermal cornification state was comparable between SCN-RE and KO mice (Figure 31B&C). In contrast, RERE mice exhibited a thinner cornified layer compared to SCN-RE and KO mice (Figure 31B&C). However, the epidermal ageing rescue observed in these mice was similar to the one achieved by reconstituting *Bmal1* expression only in the epidermis (RE mice) (Figure 31B&C).

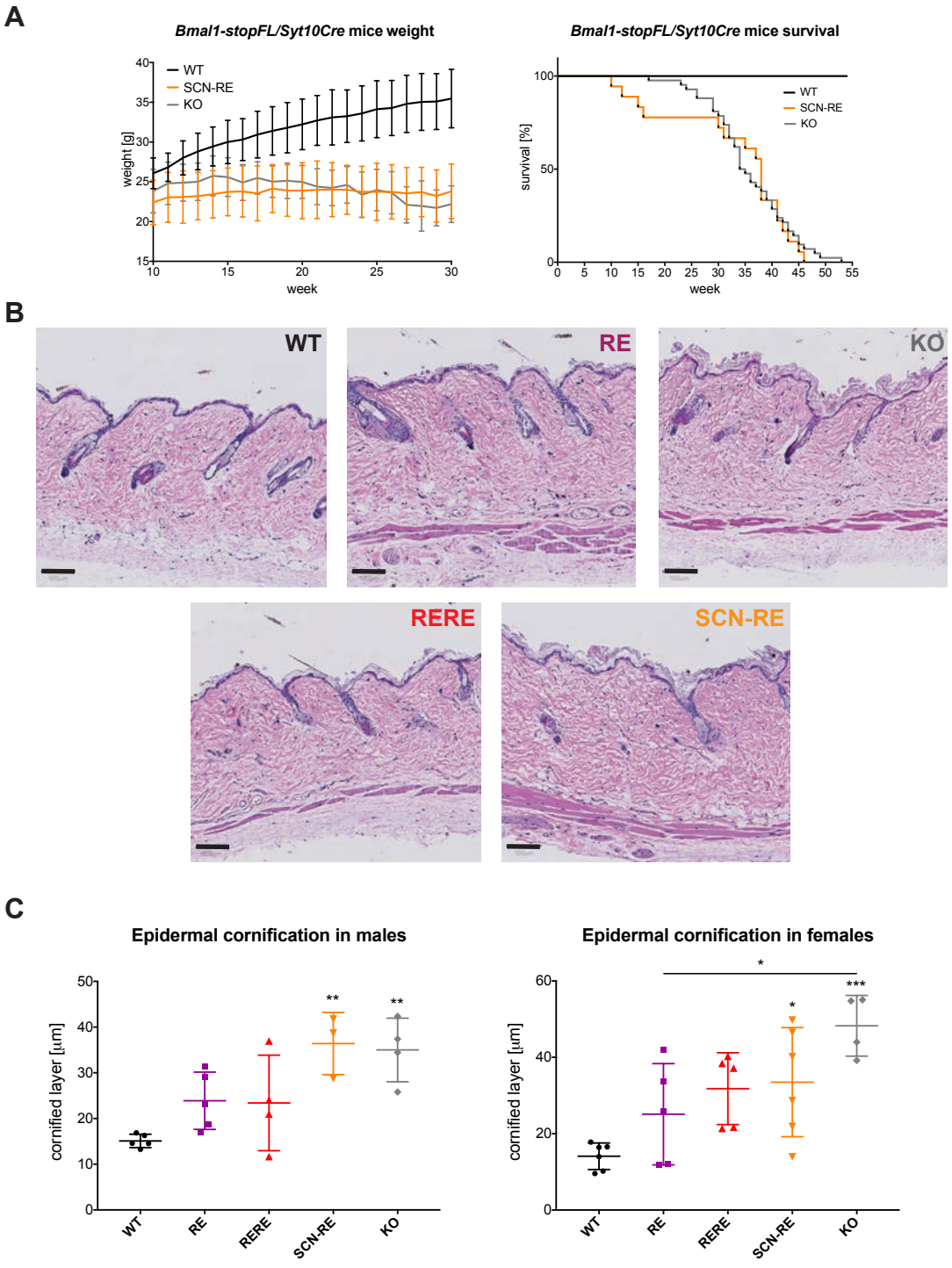

Figure 31. Communication between the SCN and the epidermal clock is not sufficient to restore physiological tissue ageing

(**A**) On the left: Weight curves for WT, *Bmal1-stopFL/Syt10Cre* (SCN-RE), and KO mice; n(WT) = 34, n(SCN-RE) = 21, n(KO) = 16; data are represented as mean ± SD. On the right: Kaplan-Meier survival curve for WT, SCN-RE, and KO mice (no significant difference between SCN-RE and KO); n(WT) = 34, n(SCN-RE) = 18, n(KO) = 42; average lifespan (SCN-RE) = 33.1 ± 11.7 weeks; average lifespan (KO) = 35.9 ± 7.6 weeks. (**B**) H/E–stained skin sections for visualisation of the cornified outer layer representing epidermal differentiation; scale bar = 100µm. (**C**) Epidermal cornification quantified as thickness of cornified layer between each hair follicle along an H/E–stained skin section; data are represented as mean ± SD; One-way ANOVA with Tukey's multiple comparisons test; *q-value ≤ 0.05, **q-value ≤

0.01, ***q-value ≤ 0.001. Males: q-value(RERE vs WT) = 0.39, q-value(RERE vs KO) = 0.16, q-value(RERE vs RE) = 1, q-value(RERE vs SCN-RE) = 0.13, q-value(SCN-RE vs WT) = 0.004, q-value(SCN-RE vs KO) = 1, q-value(SCN-RE vs RE) = 0.13; Females: q-value(RERE vs WT) = 0.07, q-value(RERE vs KO) = 0.17, q-value(RERE vs RE) = 0.85, q-value(RERE vs SCN-RE) = 1, q-value(SCN-RE vs WT) = 0.03, q-value(SCN-RE vs KO) = 0.23, q-value(SCN-RE vs RE) = 0.68.

This outcome suggests that the epidermal clock can contribute to a slower epidermal ageing; however, communication between the SCN and the epidermal clock is not sufficient to attain WT-like physiological tissue ageing. Hence, interactions with other tissue clocks are required for physiological ageing, as opposed to solely a central:peripheral interaction.

4.5.3 Communication between the SCN and the epidermal clock improves physiological ageing

Given the substantial rescue of WT circadian transcription achieved by restoring central:peripheral clock communication, we wondered whether this would also rescue the premature epidermal ageing observed in KO animals. Hence, we performed RNA-sequencing of epidermis collected at the same time point of the day, i.e. ZT16, from WT, KO, SCN-RE, RE, and RERE 26-week-old mice. In this regard, 26 weeks old KO, RE and SCN-RE mice are already to be considered old animals, as they die at around 35 weeks of age (Figure 30A & Figure 31A). We then carried out differential gene expression analyses on the obtained transcriptomes. As expected, there was a higher number of DEGs between WT and KO as compared to RERE and KO, with 2,439 DEGs in WT vs KO and 1,773 DEGs in RERE vs KO, whereas RE exhibited only 831 DEGs and SCN-RE presented 967 DEGs compared to KO (Figure 32A). Next, we performed hierarchical clustering of the DEGs identified between WT and KO on all the other genotypes (Figure 32B). Here, we noted that KO and SCN-RE clustered together as opposed to RE and RERE genes, which were closer to each other and to the WT aged transcriptome (Figure 32B). Therefore, the presence of epidermal BMAL1 leads to a more WT-like epidermal ageing also at the transcriptional level.

To elucidate the functional meaning of the results obtained from our DEG analysis, we compared the transcriptional changes observed in our aged RNA-sequencing data with published signatures describing epidermal differentiation[333]. Once again, we noticed that KO and SCN-RE clustered closer to each other, and so did RE and RERE, with the WT being closer to RE and RERE (Figure 32C). Additionally, we further compared

our ageing data against the ageing signature that our laboratory published in 2017 describing the circadian transcriptional reprogramming of aged epidermal stem cells[183], yet no different outcome was achieved in this context (Figure 32D). In other words, KO and SCN-RE aged epidermal transcriptomes consistently clustered together, while the WT distributed closer to RERE and RE (Figure 32B-D). Taken together, these analyses suggest that BMAL1-driven epidermis ages in a more physiological manner than the epidermis lacking a functional local clock.

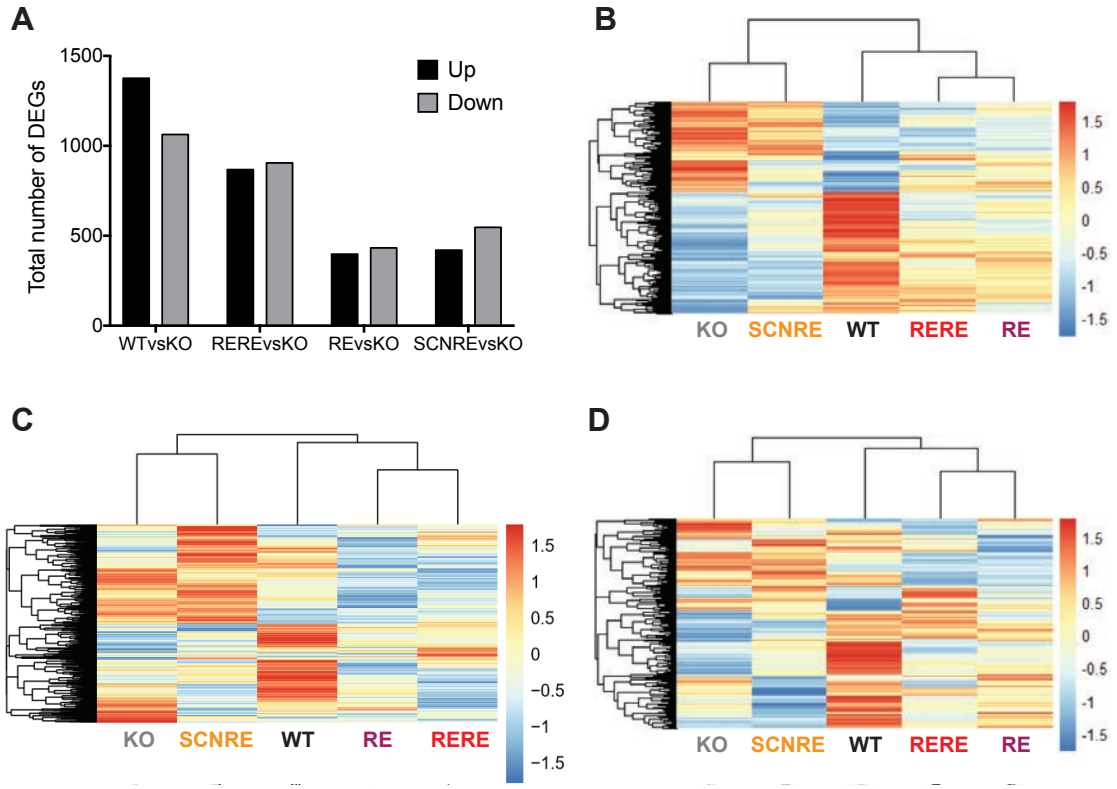

Figure 32. Aged RERE and RE epidermal transcriptomes are similar to the WT

(**A)** Number of differentially expressed genes (DEGs) in the various genotypes compared to the KO. (**B**) Heatmap showing the expression of WT vs KO DEGs in all genotypes. (**C**) Heatmap showing the expression profile of the aged epidermal RNA-sequencing data compared with the epidermal differentiation signature published by Joost *et al.*[333] (**D**) Heatmap showing the expression profile of the aged epidermal RNA-sequencing data compared with the ageing signature published by Solanas *et al.*[183].

At this point, we decided to undertake a different type of analysis; thus, we classified the ageing data gathered in the present project, in order to generate our own transcriptional signatures based on the aged RNA-sequencing results. Since both females and males were used for this experiment, batch correction for sex was applied. Next, we performed an sPLS Discriminant Analysis, which identifies key variables that drive the discrimination of the various genotypes, in order to uncover the molecular signatures associated to them. This discriminant analysis provided a transcriptional classification, where we could appreciate that KO and SCN-RE consistently classified together, whereas WT and RERE clustered closer to each other (Figure 33A). RE could not be clearly discriminated from the other genotypes by the classification, thus it distributed closer to the WT that is to be considered the reference genotype (Figure 33A). Next, we set out to identify gene signatures discriminating the different genotypes, in turn identifying three signatures contributing to the observed variations (Figure 33C). Signature 1 contained 20 genes and solely discriminated between WT/RERE and KO/SCN-RE; signature 2 was composed of 40 genes and largely separated RERE/SCN-RE from the other genotypes; lastly, signature 3 was characterised by 30 genes and mainly discriminated between WT and RE (Figure 33C). The way the samples classified based on the gene signatures could also be noticed by the heatmap depicted in Figure 33B.

Signature 1 mostly included core clock genes or CCGs, such as *Npas2, Per3, Nr1d1, Nr1d2, Dbp*, and therefore provided a circadian discrimination between genotypes owning an epidermal functional clock and genotypes without epidermal BMAL1 (Figure 33C). Signature 2 distinguished the activities controlled by an SCN clock, whereby genes discriminating SCN-RE and RERE from the rest of the groups were involved in cytoskeleton organisation and signalling pathways (e.g. *Eps8l2, Rgl2, Stk25, Tpra1, Gtpbp2, Ipo13*) (Figure 33C). Finally, Signature 3 mostly discriminated between systemic and epidermis-restricted BMAL1 activity, whereby genes distinguishing RE epidermis were mainly involved in transcription (e.g. *Zfp961, Zfp72, Zfp867*), whereas the WT epidermis was characterised by signalling pathways-related transcripts (e.g. *Sar1b, Flot2, Arhgap8*) (Figure 33C). Taken together, these results point at a similarity between WT and RERE over the process of ageing, which nevertheless is not sufficient for the RERE to attain a WT-like physiological ageing.

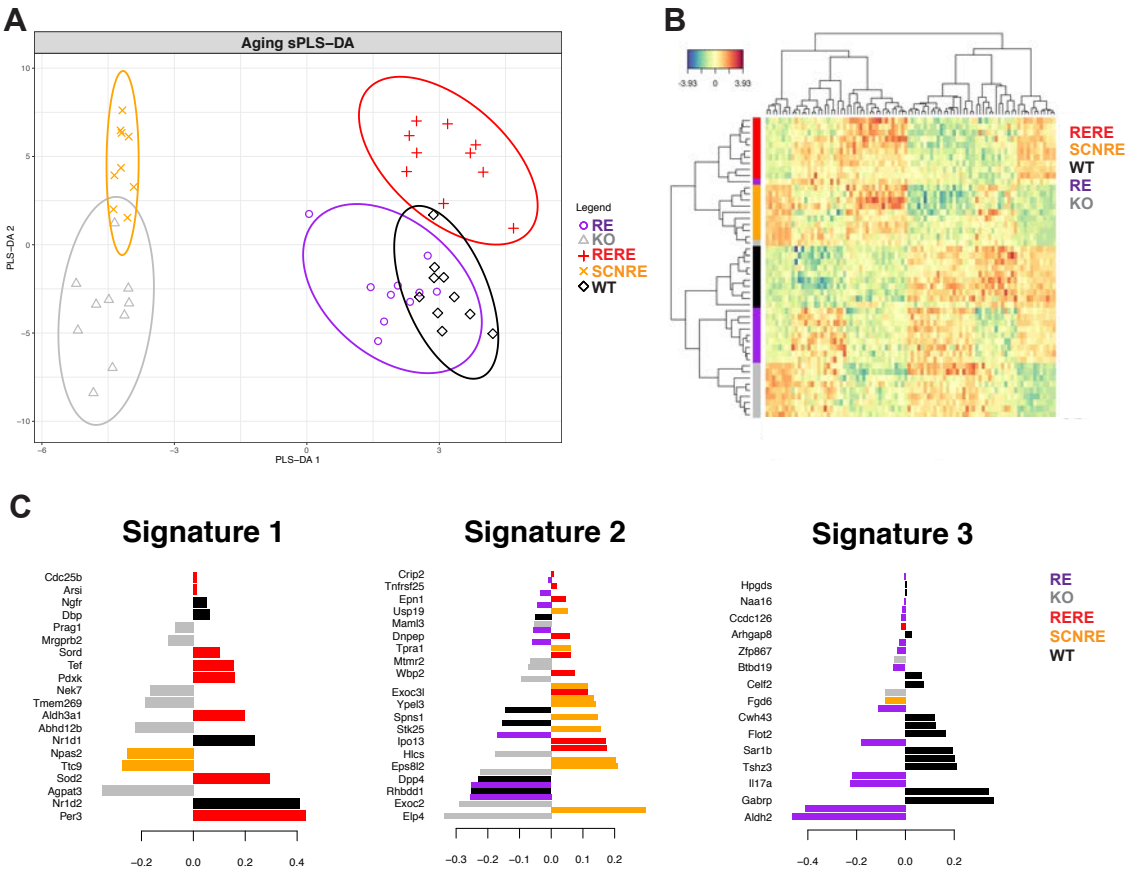

Figure 33. WT and RERE epidermal transcriptomes similarly age

(**A)** sPLS-DA plot displaying the distribution of the different genotypes. (**B**) Heatmap showing the clustering of the different genotypes based on the discrimination criteria given by the contributing signatures shown in **C**. (**C**) Contributing molecular signatures discriminating the distinct genotypes. n(WT) = 5 females, 5 males; n(RE) = 5 females, 5 males; n(SCN-RE) = 4 females, 5 males; n(KO) = 5 females, 5 males; n(RERE) = 5 females, 5 males.

4.5.4 A functional epidermal clock does not drive physiological wound healing

Next, we asked whether the presence of a functional clock in the epidermis would improve the outcome of regenerative processes, such as wound healing. Many studies have suggested that wound repair mechanisms are tightly coordinated in time and space[334]. Importantly, it has been shown that BMAL1 modulates epidermal regeneration[288], while lack of BMAL1 impairs wound closure[284].

To address this in the context of the present project, we carried out a wounding assay with young WT, KO, RE, SCN-RE, and RERE 8-week-old mice, and also with older 16-week-old mice, as accumulated damage from circadian misregulation may lead to an impairment of wound healing over time. In this regard, 16 weeks old KO, RE and SCN-RE mice are already to be considered middle-aged animals, as they die at around 35 weeks of age (Figure 30A & Figure 31A). Thus, we performed two symmetrical 5mm biopsy punches on the lower back skin of these mice (Figure 34A). We then monitored the wound closure rate by measuring the size of the lesions every two days over the healing time (Figure 34). In this context, we observed that the healing rate was similar between KO and RE 8-week-old mice, whilst being slower than in WT, SCN-RE, and RERE 8-week-old mice (Figure 34B). However, when we measured the wound closure progress of 15 weeks old mice, no significant differences were reported across the different modified genotypes, which all displayed a significantly slower healing rate as compared to WT mice (Figure 34B). This outcome suggests that the role of the central clock in the healing process in young mice appears to be important, but this effect is reduced by the ageing-related decline.

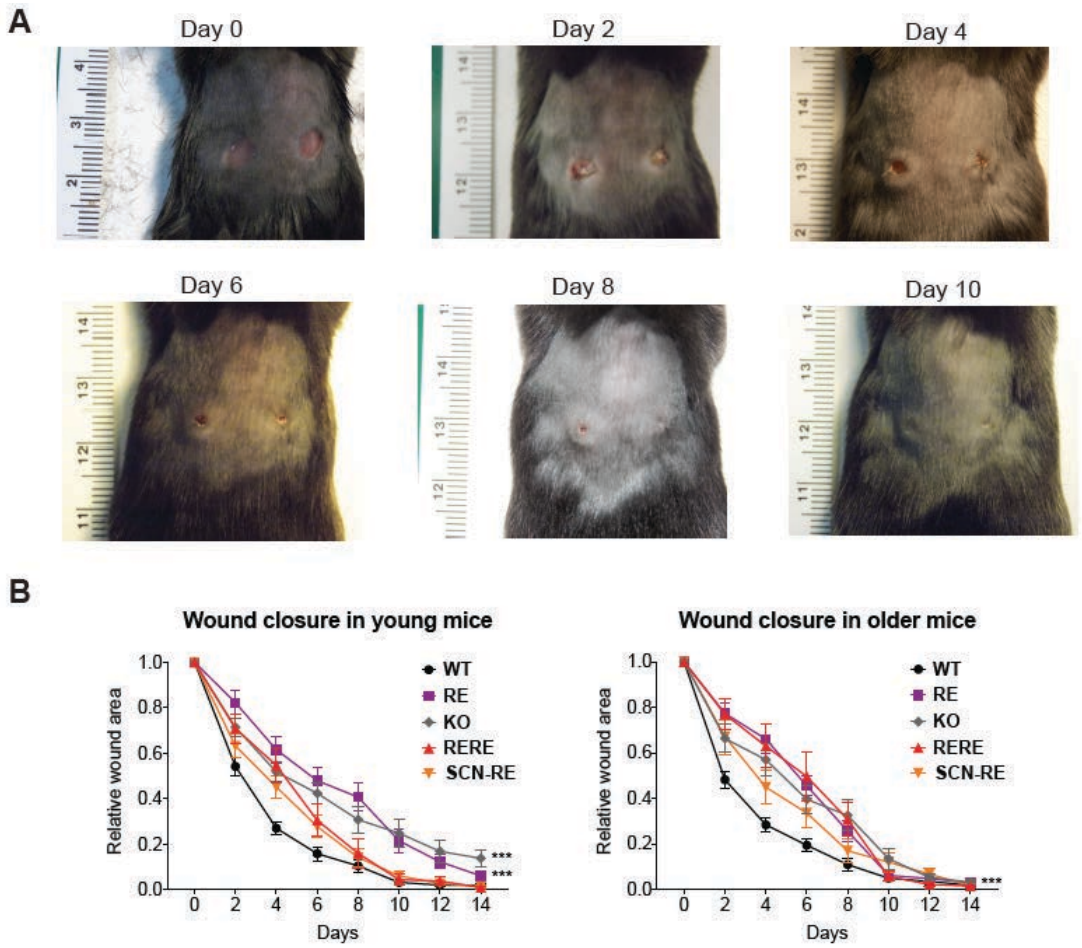

Figure 34. A functional epidermal clock does not drive physiological wound healing

(**A)** Representative images of back skin wounding and monitoring of wound closure over time. (**B**) Monitoring of wound closure over time in young (8-week-old) and older (16-week-old) males; data are represented as mean ± SD; One-way ANOVA with Tukey's multiple comparisons test. Young mice: q-value(WT vs RE) < 0.0001, q-value(WT vs KO) < 0.0001, q-value(WT vs RERE) = 0.001, q-value(WT vs SCN-RE) = 0.03, q-value(RE vs KO) = 0.66, q-value(RE vs RERE) < 0.0001, q-value(RE vs SCN-RE) < 0.0001, q-value(SCN-RE vs KO) < 0.0001, q-value(SCN-RE vs RERE) = 0.81, q-value(RERE vs KO) = 0.0007; Older mice: q-value(WT vs RE) < 0.0001, q-value(WT vs KO) < 0.0001, q-value(WT vs RERE) < 0.0001, q-value(WT vs SCN-RE) = 0.0008, q-value(RE vs KO) = 0.96, q-value(RE vs RERE) = 1, q-value(RE vs SCN-RE) = 0.07, q-value(SCN-RE vs KO) = 0.31, q-value(SCN-RE vs RERE) = 0.14, q-value(RERE vs KO) = 0.97.

Physiological wound healing is characterised by four main stages: haemostasis, inflammation, proliferation and remodelling[334,335]. During haemostasis, vascular constriction is tightly linked to platelet deposition, tissue degranulation and fibrin clot formation[334,335]. The inflammation phase is triggered by the release of pro-inflammatory cytokines that lead to the infiltration of several cell types into the lesioned dermal area[334,335]. This phase is followed by the proliferation step that consists of re-epithelialization, angiogenesis and ECM synthesis[334,335]. Lastly, wound resolution is accompanied by remodelling, in order to provide the correct organisational architecture to the regenerated skin tissue[334,335]. In abnormal wound repair, cell proliferation can be characterised by hyperplasia, i.e. hyperproliferation of the basal epidermal layer[336], and by hyperkeratosis, i.e. keratin overproduction and thickening of the stratum corneum[337].

Based on the knowledge about the various wound closure stages, we decided to histologically analyse processes that are known to play a role in wound healing. Strikingly, we found no significant differences in the quality of the repair process across the various groups of mice (Figure 35). We noticed lower indices of hyperkeratosis and hyperplasia in lesioned WT mice as compared to all the other genotypes, but these differences were not scored as statistically significant (Figure 35A).

Furthermore, inflammation indices, as quantified by the number of infiltrating cells into the lower and upper wounded dermal area, were similar across the different genotypes (Figure 35A). In accordance with these results, we could not identify any significant difference in cell proliferation, by quantifying $Ki67^+$ cells in the lesioned area, nor in newly vessel formation, by quantifying $CD31^+$ cells (Figure 35B). Therefore, further analyses are warranted in order to uncover the systemic and tissue-autonomous circadian clock contribution to the regenerative potential of peripheral tissues, like the epidermis.

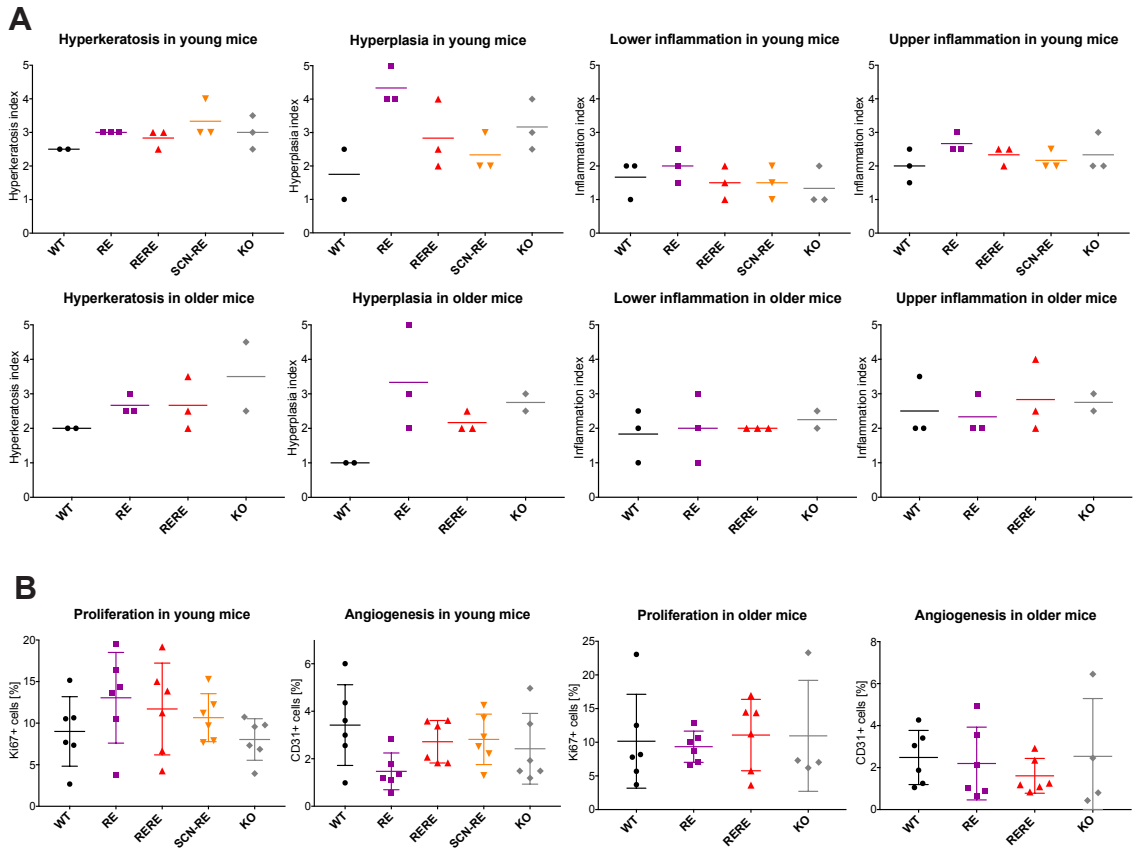

Figure 35. A functional epidermal clock does not drive physiological wound healing

(**A)** Assessment of the changes detected in epidermis and dermis 15 days after wounding in young (8-week-old) and older (16-week-old) males of the indicated genotypes, quantified according to the following scoring system: 1 = Minimal; 2 = Mild; 3 = Moderate; 4 = Marked; 5 = Severe. Each symbol represents a wound. (**B**) Percentage of positive cells for Ki67 (marker for cell proliferation) and Platelet and Endothelial Cell Adhesion Molecule 1 (CD31, marker for neovascularization), 15 days after wounding in young (8-week-old) and older (16-week-old) males of the indicated genotypes.

5. Discussion

5.1 Peripheral clocks respond independently to light to maintain homeostasis

The SCN has long been thought to function as the mammalian master clock regulator[3]. By directly receiving photic information from the external environment, its activity tightly synchronises with the daily light:dark cycles. In turn, the SCN synchronises the other brain areas, hereby coordinating behavioural rhythms, as well as the different peripheral tissue clocks, in order to achieve a temporal physiological organismal synchrony. Functional unidirectional connections have been described between the SCN and the various tissue clocks in mammals[28,338]. In contrast, prior studies have shown that individual cells possess clock systems that are cell-autonomous[84,339,340]. Moreover, evidence of circadian communication between peripheral oscillators has previously been reported[341]. Here, lung adenocarcinoma was found to distally reprogram the circadian homeostatic functions of the liver, while leaving unaltered the hepatic core clock machinery[341]. However, the degree to which peripheral tissues are autonomous from the central pacemaker remains controversial.

To address this question, we generated a novel mouse model that reconstitutes a BMAL1-driven clock in selected tissues of an otherwise full-body *Bmal1*-KO mouse, allowing an unprecedented dissection of inter-tissue clock communication. To achieve this, we leveraged Cre/loxP technology that, in the circadian field, has been widely adopted for tissue-specific deletions of *Bmal1*[144,216,218,342,343]. However, in our study, we generated a *Bmal1-stopFL* mouse with a stop cassette, flanked by loxP sites, inserted within the *Bmal1* locus (*Bmal1*$^{-/-}$). By crossing these *Bmal1-stopFL* mice with mice expressing Cre recombinase under a tissue-specific promoter, such as K14-Cre for the epidermis (RE mouse), or Alfp-Cre for the liver (Liver-RE mouse), the stop cassette was excised giving tissue-specific reconstitution of clock activity. As previously described[196], the *Bmal1-stopFL* mouse resembled the premature ageing phenotype of full-body *Bmal1*-KO mice, exhibiting weight loss, reduced life span, corneal degeneration and arthritis. On the other hand, the skin tissue developed without apparent abnormalities despite the absence of the main core clock gene, similar to what was reported in past work[196,260,269].

Using this novel mouse model, we provide evidence for the autonomy of single tissue clocks, such as epidermis and liver, in an unprecedented characterisation of tissue-intrinsic rhythmicity and related homeostasis[198,319]. Furthermore, we demonstrate for

the first time *in vivo* that, unexpectedly, light can synchronise the BMAL1-dependent circadian clockwork of single tissues, in spite of the absence of functional clocks elsewhere. Given that this observation was made in both the epidermis and the liver, we propose that this could represent a general entrainment mechanism of peripheral tissues in response to the environment.

We found that the tissue-specific clock machinery robustly oscillated without the need of *Bmal1* in other organs, and this held true both at the transcriptional and translational level. This remarkable finding provides new knowledge about clock autonomy that could not be achieved with previous murine models, hereby making the RE mouse essential for the circadian field in order to understand the molecular mechanisms of peripheral clock entrainment. Our outcome is in line with the discoveries that even cultured cells and tissue explants taken from a number of peripheral organs express rhythmic gene oscillations which, nevertheless, fade over time if not sustained by extrinsic entrainment stimuli[84,153,344,345]. Interestingly, prior studies had already attempted to describe an intrinsic circadian clock in the epidermis[268,269,346]. These studies focussed on understanding the circadian regulation of epidermal cell proliferation, and found that epidermal stem cells of clock-deficient mice fail to undergo rhythmic cycles of proliferation and differentiation[268,269]. Moreover, they found that HF cell cycle and DNA repair mechanisms are tightly coordinated by the circadian clock, further underlying the importance of a tissue-autonomous clock machinery to attain epidermal homeostasis[269,346]. In our study, strikingly, the phase of gene expression was preserved in the absence of non-epidermal clocks. However, it was shifted in the livers of Liver-RE mice, similar to what was reported regarding peripheral gene expression rhythms in SCN-lesioned rodents[84]. Here, the authors found robust rhythms of peripheral tissue explants from lesioned mice, albeit a significant phase dispersion was observed among the various tissues and between animals[84]. These results add an extra layer of complexity to the main circadian model, according to which light entrains the central hypothalamic clock, which subsequently sends synchronising signals to the different peripheral tissues.

In the present study, the overall circadian transcriptional output was, however, much reduced in RE epidermis and liver relative to WT[198,319]. Specifically, the RE epidermal transcriptome accounted for approximately 21% of the overall WT output, while the Liver-RE hepatic transcriptome reached as little as 10% of the WT circadian transcriptome[198,319]. Strikingly, the portion of transcriptome rescued in RE epidermis was found to be involved in the very basic physiological functions of the skin, e.g. cell cycle and DNA replication and repair, in order to sustain the high cellular turnover of

this tissue. As a functional readout of the GO analysis, we performed staining for pHH3, as a major marker for mitotic cell cycle, and indeed we could observe circadian fluctuations in the number of proliferating cells, as reported in previous studies of circadian characterisation of skin cells proliferation[268,269]. On the other hand, WT epidermis was able to coordinate broader biological processes, such as cytoskeleton and ECM organisation, as well as a number of metabolic and signalling pathways, together requiring incorporation of systemic and niche-derived signals. Therefore, while the tissue-intrinsic clock machinery does not require inter-tissue communication to synchronise with the external light regimen, correct circadian epidermal physiology entails communication with the clock network.

Similar hints were provided by previous studies, which highlighted the importance of peripheral and system-wide inter-tissue communication in order to attain an overall metabolic coordination[320,347]. Interestingly, Husse *et al.* demonstrated that peripheral organs, such as heart, adrenal glands, liver and kidney preserved rhythmic core clock gene expression in LD conditions, despite an SCN-restricted deletion of *Bmal1*[218]. This evidence further supports the existence of alternative pathways for the daily synchronisation of peripheral clocks in response to light, in an SCN-dependent or -independent fashion[223]. Furthermore, this evidence also led Husse *et al.* to propose a light-driven non-canonical pathway that goes through the SCN, albeit being independent of the SCN clock, in order to synchronise the peripheral clocks[218,223]. This non-canonical pathway is based on their studies, as well as on prior observations that SCN lesions impair peripheral rhythms under both LD and DD conditions, making the SCN network circuitry necessary for peripheral rhythmicity and synchrony[57,84,117,219–221,348]. However, their murine model of SCN-restricted deletion of *Bmal1* cannot distinguish the precise molecular mechanisms behind tissue-specific oscillations, as it is characterised by the presence of all peripheral clocks. In this context, our RE mice can be suitable models to dissect the mechanisms accounting for peripheral clock entrainment in a tissue-specific manner.

In light of the striking results obtained from our first LD experiment with RE mice, we hypothesised that the decreased rhythmic transcriptional output from the RE epidermis was due to a loss of circadian chromatin dynamics. Supporting this hypothesis, photic signalling has been shown to evoke dynamic chromatin remodelling in SCN neurons, in order to induce clock gene activation[349]. In line with this, prior ATAC-sequencing and ChIP-sequencing analyses performed on both WT and *Bmal1*$^{-/-}$ mice uncovered that the CLOCK/BMAL1 transcriptional complex is able to open chromatin at regulatory regions, making it permissive to further regulatory factors and for transcriptional

activation[325]. Furthermore, in the interfollicular epidermis, the CLOCK/BMAL1 heterodimer allows a dynamic chromatin state that favours its recruitment to cell cycle gene promoters, in order to maintain the transcription of cell cycle genes under circadian control[326]. Nevertheless, we found that different chromatin dynamics could not explain the differences that we observed at the transcriptomic level, as both WT and RE epidermis displayed chromatin opening between the two opposite time points analysed. However, no correlation was found between those genes that gain circadian rhythmicity upon epidermal clock reconstitution and the opening chromatin regions. Future ChIP-sequencing experiments will unveil the possible differential binding of BMAL1 to the chromatin and its potential effects on the epidermal circadian output. Interestingly, in liver of Liver-RE mice, recruitment of BMAL1 to clock and metabolic gene promoters took place rhythmically but with a 4h phase advance compared to WT liver that reflected the phase advance found in the transcriptional data[319]. Moreover, genome-wide BMAL1 recruitment displayed a highly similar pattern between WT and Liver-RE livers, accompanied by a 90% overlap between WT and Liver-RE BMAL1-target hepatic genes[319]. Therefore, tissue-autonomous BMAL1 drives the daily rhythms of circadian clock and metabolism in the liver[319].

Altogether, from these results we concluded that BMAL1-driven tissue clocks respond independently to light to maintain homeostasis, and this likely occurs through a novel SCN clock-independent pathway.

5.2 Non-epidermal clocks are required to maintain circadian behaviour in response to light and for epidermal rhythmicity in the absence of light

Food intake timing and rest-activity cycles have been established as prominent *Zeitgebers* for many peripheral tissues[261,350]. Indeed, experiments of time-restricted feeding showed that metabolic organs, such as pancreas and liver, adjusted their rhythms to the feeding schedule, whereas the SCN and other food-unaffected tissues remained synchronised to the light schedule[125,126]. In order to unveil the potential cause for the observed circadian transcriptional oscillations in RE epidermis under LD conditions, we decided to analyse the feeding and locomotor behaviours of these mice.

We hypothesised that a rhythmic activity and/or feeding could explain the entrainment of this peripheral tissue in the absence of functional clockworks elsewhere. Nevertheless, neither the RE nor the Liver-RE mice exhibited rhythmic metabolic or locomotor cycles, consistent with the results obtained from full-body *Bmal1*-KO mice[198,319]. These findings are also in line with previous experiments that suggested the SCN to be the key regulator of circadian behaviour, as SCN-lesioned rodents displayed a loss of circadian rest-activity cycle, feeding and drinking behaviours, as well as hormonal release[78–80]. However, and interestingly, we noticed that RE and KO mice experienced a minor increase in locomotor activity during the dark phase of the LD regimen. This phenomenon, known as “light masking”, has been previously reported[93,213,351]. Nevertheless, this event is unlikely to influence the gene expression of peripheral organs to the extent of instilling robust transcriptional oscillations, since locomotor rhythms in RE and KO mice were very weak. In agreement with this, in KO epidermis no clock genes oscillated and the circadian transcriptome was largely absent. Furthermore, light masked-locomotor activity could not explain the strong phase relationship between WT and RE epidermal rhythmic transcripts, given the highly variable onset of locomotor activity encountered in RE mice.

Based on the evidence that feeding, metabolic and locomotor behaviours do not determine epidermal transcriptional oscillations, we hypothesised that light itself could be directly entraining peripheral tissue clocks. As a result, we looked at circadian transcriptome under DD conditions in RE mice. In the context of *Bmal1*-KO restricted to the SCN, peripheral tissues preserved their gene expression rhythms, but their transcriptional oscillations were dampened under constant darkness conditions for 2 days[218]. Furthermore, SCN-ablated hamsters exposed to darkness failed to display locomotor rhythms, as well as clock gene expression rhythms of several organs[219].

Strikingly, one week of constant darkness was sufficient to eradicate the rhythmic transcriptional overlap of RE epidermis with the WT. This outcome is in line with what was described in the Liver-RE[319]. However, it contrasts with a recent publication showing that hepatocyte-restricted *Bmal1* expression is sufficient to maintain low-amplitude and phase-coherent transcriptional rhythms of the core clock machinery of the liver under constant conditions[80]. Here, the authors monitored single freely moving mice by real-time bioluminescence recording[352], and therefore claimed that the results obtained by Koronowski *et al.* could be due to potential inter-animal phase dispersion. In the context of the RE epidermis, the outcome obtained under DD conditions could be due to: 1) an inter-animal phase dispersion; 2) an inter-cellular phase dispersion; 3) a flattening of the cellular clock gene rhythms due to the absence of light. Nevertheless, inter-animal phase dispersion is unlikely to account for the observed DD arrhythmia, as our consecutive ear snip collection experiment demonstrated that individual RE animals lost circadian fluctuations of gene expression after seven days in darkness. However, we cannot formally exclude that inter-cellular phase dispersion could have caused the disrupted rhythmicity, similar to what happens *in vitro*[340,351]. Therefore, it could be plausible that even in constant darkness, individual epidermal cells continue oscillating but become desynchronised to one another, thereby leading to overall epidermal arrhythmia. In this context, phase dispersed oscillations in individual cells would likely be detrimental on the physiological level, similarly to a complete loss of rhythmicity.

Taken together, our results provide evidence for the existence of at least two entrainment pathways for the daily synchronisation of peripheral tissue clocks in response to light: An “autonomous response” and a “memory branch”[198]. On the one hand, the autonomous response pathway directly conveys changes in the light regimen, thereby explaining the dampening of transcriptional rhythmicity shown by the epidermis (and livers[319]) from RE mice kept in constant darkness. The SCN clock is redundant in this branch, which ensures peripheral circadian oscillations thanks to the presence of a tissue-autonomous BMAL1-dependent clock. By doing so, rhythmic physiology and homeostasis of the given tissue are preserved under standard LD photoperiod but would adapt to changes in environmental conditions even in the absence of clocks in any other tissue. In contrast, the memory branch relies on systemic BMAL1-driven clocks as cues that retain memory of the previous LD cycle. Hence, this pathway requires non-epidermal BMAL1 to function, in order to ensure robust circadian behaviour and transcriptional rhythmicity despite the lack of external signals, like light. In line with this, RE epidermis could not maintain a large part of the

circadian clock output, because of the memory branch that is dependent on BMAL1-driven clocks in other tissues. Finally, the coordination of these two entrainment branches would render peripheral clocks flexible enough to re-adjust to environmental changes, while maintaining an overall clock robustness. This concept is particularly relevant in the context of jet lag that challenges the circadian physiology of humans in the modern society.

To support the hypothesis that an autonomous response pathway would rapidly re-adjust to changes in environmental conditions, we performed a time-shift experiment, whereby we simulated westward traveling by 12h-shifting the light schedule that the mice were exposed to. According to our initial hypothesis, the RE mice only retain the autonomous response pathway; thus, they should more rapidly re-adjust their gene expression rhythms to the new LD cycle than their WT counterparts. However, no shift in transcriptional oscillations was observed in the core clock genes expression from RE epidermis up to two days after the time-shift. Only after four days, both WT and RE epidermal clockworks displayed a 4h phase advance with respect to the old LD cycle, suggesting an equivalent rate of re-adjustment to the new photoperiod. This contrasts with a previous study that demonstrated that the peripheral clocks of SCN-clock deficient mice re-adjust faster than in WT mice, when subjected to a new light regime[218]. In a further 6h-phase advancement experiment performed by the same group with WT mice, they confirmed that the rate of adaptation to changes in the light regime greatly differed between the SCN and the periphery, but also between the various peripheral organs[106]. Here, the authors demonstrated that the adrenal clock plays a key role in the resynchronisation of the organismal clock network upon jet lag[106]. These results suggest that the various peripheral organs react with a different pace to changes in environmental conditions compared to each other and to the SCN, leading to a transient state of misalignment of the body clocks. Conversely, an independent study from another group pointed at AVP receptors as key mediators of the gradual adaptation to jet lag[353]. Here, the authors demonstrated that mice lacking these receptors showed faster re-entrainment of locomotor rhythms as well as central and peripheral clock gene oscillations than their WT counterparts[353]. Therefore, additional experiments are needed to give further hints on the different response of single peripheral tissues to jet lag, which our current RE mouse fails to provide.

5.3 Communication between the SCN and the epidermal clock is sufficient to maintain a robust epidermal transcriptional output

In the present project, we show that a fraction of peripheral tissue circadian functions is autonomously controlled, implying that the remainder relies on clock:clock communication. Given the established role of the central clock, we wondered whether reconstitution of the SCN clock is sufficient for light memory and for restoring the other physiological functions. This question is of particular interest, given that we and others demonstrated that a functional SCN clock is dispensable for peripheral organs to achieve rhythmic oscillations of gene expression in LD, but not in constant conditions[198,218,319].

To investigate potential central:peripheral communication, we generated a double-reconstituted mouse, with a functional clock in both the SCN and the epidermis. This mouse allowed us to precisely unveil the contribution of the central clock to the peripheral transcriptome, via the rescue of the SCN clock outputs. Indeed, the results obtained from the LD and DD experiments performed on RERE mice were quite striking, as they demonstrated that: Firstly, communication between these two clocks is sufficient to achieve WT-like rhythmicity of the circadian clock machinery and a greater portion of the total transcriptional output under LD conditions; and secondly, communication between these two clocks is sufficient to preserve the oscillations of gene expression when external light stimulus is missing.

The phase and amplitude coherence of the core clock genes in the epidermis of RERE mice was greater than in RE mice, and this held true for both LD and DD experimental conditions. This phenomenon could be due to the SCN synchronising activity towards peripheral tissues. The SCN clock is a stable oscillator under constant conditions as SCN neurons are tightly connected through gap junctions and communicate with each other by neuropeptidergic paracrine signalling[354]. Therefore, it can provide the synchronising signals needed to maintain clock activity in DD, as well as phase and amplitude robustness to the transcriptional machineries in the brain and the periphery[355].

The SCN structure has long been known to coordinate the rhythmic release of circulating hormones, such as GCs from the adrenal gland via the HPA axis[78]. GCs receptors are nearly ubiquitous and, upon light stimulus-perception by the SCN, GCs fluctuations are able to synchronise peripheral organs with the external time[356,357].

Furthermore, Ishida *et al.* reported that environmental light signal is gated by the SCN, which conveys the light information to temporally regulate gene expression in the adrenal gland[356]. From here, light-induced rhythmic release of GCs shifts the peripheral cellular clocks according to the external light cycle[102]. In support of this, previous jet lag studies on adrenalectomised rats suggested that the adrenal clock is critical for circadian synchronisation[106]. Furthermore, in SCN clock-ablated mice, GCs rhythms persisted in LD photoperiod, albeit phase-advanced, but gradually dampened upon release in DD conditions[218]. Hence, one possible explanation to the WT-like transcriptional oscillations seen in RERE epidermis could indeed be lying in the rhythmic release of GCs by the adrenal gland of RERE mice. However, a functional adrenal clock was shown to be required for circadian GCs rhythms[357].

The SCN is further known to coordinate circadian behavioural activity[79]. Thus, we measured these parameters in SCN-RE mice, in order to uncover whether the clock restoration rescues these circadian activities, thus making them a possible source of transcriptional rescue. SCN-RE animals displayed a rhythmic locomotor activity when kept under LD photoperiod, with lower activity levels than WT mice, as was reported by McDearmon *et al.*[224]. However, activity rhythms were greatly shifted in conditions of constant darkness. In contrast, feeding and metabolic rhythms stayed circadian regardless of the light cycle, with the exception of energy expenditure that remained largely arrhythmic in both experimental conditions. Therefore, circadian locomotor and feeding behaviours could be the reason accounting for the transcriptional rhythms of the RERE epidermis. To further dissect and confirm the role of these SCN-clock outputs, time-restricted feeding, as well as forced activity experiments, would need to be performed to reveal the contribution of food/activity timing on tissue-specific rhythms. In this line, recent experiments of forced exercise led to robust peripheral clock entrainment[358].

Regarding the biological processes associated with the different gene groups across the various genotypes, we found that GO categories of cell cycle and DNA replication and repair are consistently present and circadian in the epidermis of the various genotypes, except in the full-body *Bmal1*-KO mice. Strikingly, SCN-RE epidermis displayed perfectly opposite phase as compared to all other genotypes, including WT, and this held true under both LD and DD experimental conditions. This surprising result points to competing phase-gating signals coming from the SCN and the local clockwork. Interestingly, this apparent competition between the local and peripheral clock shows similarities with studies comparing the hierarchy of different *Zeitgeber* stimuli in entraining peripheral tissue clocks[125–128]. However, these reports focused on

the role of feeding rhythms as entrainment cues for local clocks. Our finding suggests that the main homeostatic functions of the epidermis do not depend on the tissue-specific circadian machinery. Nevertheless, phase coherence strictly does. Therefore, regardless of the light schedule, the SCN clock alone sends synchronising signals to the epidermis, which conflict with the tissue-autonomous clock output. This finding adds an additional parallel pathway of peripheral clock entrainment mediated by the SCN clock. According to a more evolutionary perspective, the SCN could be seen as an ancestral clock, being it directly responsive to light stimulus. Thus, it could be that the SCN clock sends phase-setting signals to the epidermal clockwork that are rather detrimental for tissue homeostasis, and which are consequently contrasted by local phase settings. Conversely, it is also possible that the SCN sends synchronising signals at a specific time of the day, which are then interpreted by the local peripheral clock, even if this additional layer of coordination leads to opposite phase expression of the output. These theories are in line with the fact that the uncovered anti-phasic cell cycle genes are in phase with *Bmal1* expression. In contrast, another evolutionary explanation could be given by the hypothesis that the tissue/cell autonomous clock is the most evolutionarily basic of clocks, as it runs independently without the needs for any system-wide inputs. This autonomous clock is particularly useful in very basic organisms in which all clocks can be synchronised by light and drive the relevant cellular processes. However, in more complex organisms an additional level of control and synchronisation overlaid on top of this network of autonomous clocks is required, hereby resulting in the evolution of a central clock in the SCN. This central clock synchronises the peripheral clocks and provides additional circadian instructions, which are of varying relevance to different tissues. Hence, peripheral clocks may or may not integrate these signals, giving rise to the conflicting cell cycle results found in our SCN-RE model. Ongoing experiments with epidermis-restricted *Bmal1*-KO mice will reveal whether indeed the local clock machinery is solely responsible for setting the WT phase of the major homeostatic functions of the epidermis.

5.4 Tissue-autonomous clock entrainment is induced by light via the sympathetic nervous system

The mechanisms behind peripheral clock entrainment still require further studies to improve the current understanding in the field. The autonomic nervous system has been implicated in the circadian control of physiological functions of different peripheral tissues, such as kidney, liver, and hematopoietic stem cells[114–116]. Specifically, autonomic innervation plays a central role in conveying light signalling perceived by the SCN to the liver, in order to modulate the local circadian gene expression[116,117]. Furthermore, administration of epinephrine/norepinephrine stimulated core clock gene expression in murine liver, while lesioning the SCN led to an impairment of liver transcriptional rhythms and norepinephrine content[117]. Additionally, the phase of a food-unaffected peripheral oscillator, such as the submaxillary salivary gland, was seen to be misaligned with the external light cycle when sympathetic innervation to this organ was surgically removed in rats[118]. In this context, entrainment of the submandibular glands mediated by sympathetic innervation was reported to be attenuated in aged mice, and this was partly due to a downregulation of adrenergic receptor expression[119]. In the latter study, treatment with epinephrine, norepinephrine, or adrenergic receptor agonists potentiated the peripheral clock entrainment[119]. This response was likely mediated by an increase of Ca^{2+} intracellular levels, subsequent CREB phosphorylation, and induction of transcriptional oscillations, by binding to CRE elements in the promoters of *Per1* and *Per2*[87,359].

Since the skin is extensively innervated, it is plausible that the epidermis perceives neural synchronising inputs[259]. It has recently been reported that proliferation of hair follicle stem cells is stimulated by external light via sympathetic nervous system[235,327]. In both studies, sympathectomy experiments led to an impaired hair follicle cycling, as well as norepinephrine production[235,327]. Furthermore, Shwartz *et al.* demonstrated that knocking out the β2 adrenergic receptor specifically from hair follicle stem cells led to a similar phenotype as in sympathectomised mice, i.e. inhibition of cell proliferation and of hair follicle regeneration[235]. The same group elegantly showed that stress-induced norepinephrine release from the sympathetic nervous system activates melanocyte stem cell proliferation, differentiation, and subsequent depletion from the niche, thereby causing the phenomenon of hair greying[360].

In the present project, when the cutaneous sympathetic nervous system of WT and RE mice was chemically disrupted, the local clockwork was impaired in the RE but not in the WT epidermis under LD conditions. Therefore, the oscillations observed in the RE

epidermis in LD are dependent on light signals communicated through the sympathetic nervous system. In other words, in the absence of communication between clocks in different tissues, synchronisation of the circadian clockwork in the epidermal tissue, and potentially in other peripheral tissues, depends on the sympathetic nervous system. On the other hand, this outcome points to the existence of further mechanisms behind the light-driven epidermal transcriptional rhythmicity that we observe in WT animals. A possible entraining signal under a standard photoperiod could derive from rhythmic release of GCs. Light was reported to activate the adrenal gland, thereby inducing rhythmic gene expression and hormonal secretion[356]. Thus, adrenalectomy experiments are required to uncover whether the timing of hormonal production by the adrenal gland is responsible for the epidermal rhythms. Additionally, ongoing RNA-sequencing experiments involving mice lacking the β2 adrenergic receptor solely in the epidermis will unveil whether rhythmic sympathetic signalling is to account for the entrainment of the epidermal clockwork.

Conversely, when we placed sympathectomised WT mice under DD conditions, circadian oscillations of *Bmal1* and *Dbp* gene expression were lost. Hence, these results underlie the importance of cutaneous sympathetic innervation to provide a memory of light and keep the local clock machinery synchronised in the absence of external cues.

A further possibility could be that the epidermis itself senses the light signal and incorporates it to directly set the clockwork according to the time of the day. Despite the mechanisms behind such phenomenon have not been fully described, we cannot formally exclude that light might be directly detected by epidermal keratinocytes, in order to synchronise the local circadian machinery. Previous studies have reported UV-sensitive photopigments expression by human and murine keratinocytes, which enable the response to UV light[361,362]. This would not explain the oscillations observed in the livers of Liver-RE mice kept under LD photoperiod[319], but it could likely point to different mechanisms of entrainment for the various peripheral tissues. However, previous reports suggested that epidermal cells are not entrained by direct light, despite being constantly exposed to it[259]. Of note, according to our results, KO mice do not express transcriptional rhythms in the epidermis, while RE mice adjust their epidermal clockwork at the same pace of WT when exposed to a jet lag paradigm. These results, together with the evidence that RERE mice maintain robust epidermal oscillations of gene expression in DD, make it unlikely for the light to be directly perceived by the epidermis to mediate the local circadian machinery.

5.5 Tissue-intrinsic BMAL1 ensures physiological epidermal ageing but is insufficient to drive correct wound healing

A robust clock network is essential for overall organismal physiology and the data shown in this thesis further the current understanding of clock:clock communication and related circadian physiology. Previous studies from our laboratory have described a core set of tissue-specific homeostatic functions that remain imperturbable during ageing[183,184]. In the present project, we show that these physiological core functions are regulated by the tissue-autonomous clock.

Ageing influences the rhythmic physiology of tissue clocks, including epidermal stem cells[183,296]. During physiological ageing, the epidermal core clock machinery remains rhythmic but reprograms the epidermal circadian transcriptional output towards a stress-like state[183]. Conversely, *Bmal1*-KO mice display lower epidermal self-renewal, impaired hair growth and increased epidermal differentiation[196,217]. Remarkably, mice lacking a functional clock only in the epidermis experience advanced epidermal ageing[217], further implying a key role of the tissue-autonomous clock in the regulation of physiological ageing.

In our study, SCN-RE, RE[198] and Liver-RE[319] mice showed signs of premature ageing, as exemplified by their reduced life expectancy. Conversely, the severe premature epidermal ageing of *Bmal1*-KO mice was largely prevented by reconstituting the epidermal clock, leading us to the conclusion that the tissue-autonomous clock partly drives the physiological ageing process. However, a functional SCN clock alone did not further improve the early decline occurring in these mice, thereby underlying the importance of central:peripheral clock interactions in the context of physiological ageing. Nevertheless, communication between the central and epidermal clock did not drive a WT-like epidermal ageing, as shown by the histological characterisation and comparative transcriptional analyses. Thus, a robust organismal clock network is likely required for overall physiological ageing.

Interestingly, prior reports revealed that when *Bmal1* was conditionally knocked out in adulthood, fewer signs of systemic or tissue-specific premature ageing developed[363]. The exact BMAL1-driven mechanisms that regulate the ageing process are yet to be elucidated. One possible BMAL1-dependent pathway involved in the premature ageing phenotype of *Bmal1*$^{-/-}$ mice is the mTOR signalling. mTOR activity leads to the production of ROS and subsequent oxidative damage[364], similar to what was observed in *Bmal1*-deficient mice[196,200]. However, inhibition of the mTOR pathway in *Bmal1*-KO mice resulted in prolonged longevity, further strengthening the connection between

clockwork and metabolism[186]. In this line, it was shown that overexpression of SIRT1 in the brain protected WT mice from the ageing effects given by a functional decline of the circadian machinery[365]. Furthermore, caloric restriction regimens prevented the age-associated circadian reprogramming[183]. Therefore, future experiments of manipulation of diet or of metabolic pathways linked to the circadian clockwork could be used to expand our current knowledge about the impact of clock:clock communication on organismal and tissue physiological ageing.

It has been recently proposed that BMAL1 modulates epidermal healing through its negative influence on ROS production[288]. In agreement with this, *Bmal1*-KO mice experienced a delayed epidermal healing compared to the WT counterparts, accompanied by ROS accumulation[288]. In an independent study, lack of BMAL1 was further seen to impair wound closure[284]. These effects were proposed to be mediated by temporal gating of NONO (a partner of PER proteins) to the cell cycle machinery[284].

In our study, we show that the epidermal clock alone does not improve wound healing, contrary to the improvements obtained in the epidermal ageing phenotype. Thus, a tissue-autonomous clock is not sufficient to sustain physiological skin processes like wound healing. Conversely, an SCN functional clock accelerates the wound closure as compared to *Bmal1*-KO mice, but it does not improve the tissue-intrinsic histological parameters that are hallmarks of the healing process. In this context, no differences in the number of proliferating cells were observed when analysing the healing status of young and older mice, including WT mice. This contrasts with Silveira *et al.* study, which showed lower cell proliferation in *Bmal1*$^{-/-}$ mice than in the WT counterparts upon skin lesion[288]. Overall, no significant histological differences were observed in skin-lesioned young or older mice. These findings argue against previous reports where the circadian clock has been tightly implicated in the process of epithelium repair[288,366]. In contrast, a faster healing resolution took place in WT, as compared to *Bmal1*-KO mice, like previously described[284].

A possible factor to take into account is the timing of wound induction, which could elicit a different response in the various murine models used in the present project. In this context, previous reports demonstrated that a better healing outcome was achieved when lesions were induced at *Per2* peak and *Bmal1* trough[283]. Therefore, further assays will give a hint about the role of tissue-autonomous versus systemic BMAL1, as well as the role of central:peripheral clock communication on physiological processes, such as wound healing.

Altogether, the results presented in this PhD thesis pave the way for a better understanding of the mechanisms underlying circadian regulation of tissue functioning and the physiological consequences derived from clock desynchronisation, as regularly occurring in our modern lifestyle. Future work should focus on determining potential means of intervention on the circadian clock machinery, in order to preserve an overall robust organismal rhythmicity and delay the signs of ageing.

6. Conclusions

- Epidermal and liver clock machineries are entrained by light in the absence of functional clocks in other tissues.
- Tissue-autonomous clock suffices to sustain basic homeostatic functions.
- Tissue-specific BMAL1 regulates chromatin dynamics.
- Tissue-autonomous circadian oscillations are independent of rhythmic locomotor activity, feeding and related metabolic cycles.
- Non-epidermal BMAL1 is required for clock entrainment and physiological output in free-running conditions (i.e. in the absence of light).
- The tissue-autonomous clock adjusts to jet lag conditions independently of the presence of other body clocks.
- Communication between the SCN and the epidermal clock is sufficient to maintain a robust epidermal circadian transcriptional output.
- The SCN clock appears to send contrasting phase-setting signals to the epidermis as compared to local phase cues.
- A functional central clock is sufficient for behavioural rhythms.
- In the absence of non-epidermal clocks, epidermal clock entrainment may be mediated by the sympathetic nervous system in response to light.
- The tissue-autonomous clock does not sustain organismal physiological ageing.
- The epidermal clock prevents premature epidermal ageing.
- Organismal clock network interactions are required for physiological epidermal ageing and wound healing.

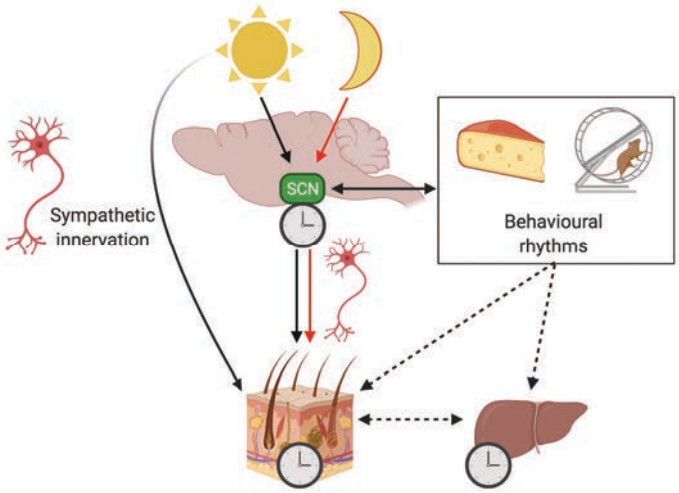

Figure 36. Working model for the daily synchronisation of peripheral tissues

External light signalling (sun symbol) is conveyed to peripheral tissue clocks, like the epidermis, in an SCN clock-dependent or -independent manner. In the latter case, the sympathetic nervous system might mediate the synchronisation of the epidermal clock in response to light. In the absence of light (moon symbol), communication between the SCN and the epidermal clock is required to attain transcriptional rhythmicity and physiological circadian output. This communication is likely mediated by sympathetic innervation. Additionally, *Zeitgebers* other than light, such as food timing and locomotor activity, can entrain the SCN clock, which in turn establishes behavioural rhythms under a standard light schedule. These rhythms might play a role in the circadian synchronisation of peripheral clocks (dashed arrows), though the circadian effects of the communication between peripheral clocks remains to be determined (bi-headed dashed arrow).

7. References

1. Takahashi, J. S. Transcriptional architecture of the mammalian circadian clock. *Nat Rev Genet* **18**, 164–179 (2016).

2. Hastings, M. H., Maywood, E. S. & Brancaccio, M. The Mammalian Circadian Timing System and the Suprachiasmatic Nucleus as Its Pacemaker. *Biology (Basel).* **8**, 1–22 (2019).

3. Dibner, C., Schibler, U. & Albrecht, U. The Mammalian Circadian Timing System: Organization and Coordination of Central and Peripheral Clocks. *Annu. Rev. Physiol.* **72**, 517–549 (2010).

4. Ibañez, C. Scientific Background: Discoveries of Molecular Mechanisms Controlling the Circadian Rhythm. *Nobel Media AB* (2014).

5. Pittendrigh, C. S. Circadian rhythms and the circadian organization of living systems. *Cold Spring Harb. Symp. Quant. Biol.* **25**, 159–184 (1960).

6. Konopka, R. J. & Benzer, S. Clock Mutants of Drosophila melanogaster. *PNAS* **68**, 2112–2116 (1971).

7. Bargiello, T. A. & Young, M. W. Molecular genetics of a biological clock in Drosophila. *PNAS* **81**, 2142–2146 (1984).

8. Bargiello, T. A., Jackson, F. R. & Young, M. W. Restoration of circadian behavioural rhythms by gene transfer in Drosophila. *Nature* **312**, 752–754 (1984).

9. Reddy, P. *et al.* Molecular analysis of the period locus in Drosophila melanogaster and identification of a transcript involved in biological rhythms. *Cell* **38**, 701–710 (1984).

10. Zehring, W. A. *et al.* P-element transformation with period locus DNA restores rhythmicity to mutant, arrhythmic drosophila melanogaster. *Cell* **39**, 369–376 (1984).

11. Siwicki, K. K., Eastman, C., Petersen, G., Rosbash, M. & Hall, J. C. Antibodies to the period gene product of drosophila reveal diverse tissue distribution and rhythmic changes in the visual system. *Neuron* **1**, 141–150 (1988).

12. Hardin, P. E., Hall, J. C. & Rosbash, M. Feedback of the Drosophila period gene product on circadian cycling of its messenger RNA levels. *Nature* **343**, 536–540 (1990).

13. Liu, X. *et al.* The period gene encodes a predominantly nuclear protein in adult Drosophila. *J. Neurosci.* **12**, 2735–2744 (1992).

14. Zeng, H., Hardin, P. E. & Rosbash, M. Constitutive overexpression of the Drosophila period protein inhibits period mRNA cycling. *EMBO J.* **13**, 3590–3598 (1994).

15. Myers, M. P., Wager-Smith, K., Wesley, C. S., Young, M. W. & Sehgal, A. Positional cloning and sequence analysis of the Drosophila clock gene, timeless. *Science* **270**, 805–808 (1995).

16. Sehgal, A. *et al.* Rhythmic expression of timeless: a basis for promoting circadian cycles in period gene autoregulation. *Science* **270**, 808–810 (1995).

17. Gekakis, N. *et al.* Isolation of timeless by PER protein interaction: defective interaction between timeless protein and long-period mutant PERL. *Science* **270**, 811–815 (1995).

18. Zylka, M. J., Shearman, L. P., Weaver, D. R. & Reppert, S. M. Three period homologs in mammals: differential light responses in the suprachiasmatic circadian clock and oscillating transcripts outside of brain. *Neuron* **20**, 1103–1110 (1998).

19. Thresher, R. J. *et al.* Role of mouse cryptochrome blue-light photoreceptor in circadian photoresponses. *Science* **282**, 1490–1494 (1998).

20. Vitaterna, M. H. *et al.* Mutagenesis and mapping of a mouse gene, Clock, essential for circadian behavior. *Science* **264**, 719–725 (1994).

21. King, D. *et al.* Positional Cloning of the Mouse Circadian Clock Gene. *Cell* **89**, 641–653 (1997).

22. Antoch, M. *et al.* Functional Identification of the Mouse Circadian Clock Gene by Transgenic BAC Rescue. *Cell* **89**, 655–667 (1997).

23. Gekakis, N. *et al.* Role of the CLOCK protein in the mammalian circadian mechanism. *Science* **280**, 1564–1569 (1998).

24. Allada, R., White, N., So, V., Hall, J. & Rosbash, M. A Mutant Drosophila Homolog of Mammalian Clock Disrupts Circadian Rhythms and Transcription of period and timeless. *Cell* **93**, 791–804 (1998).

25. Rutila, J. *et al.* CYCLE Is a Second bHLH-PAS Clock Protein Essential for Circadian Rhythmicity and Transcription of Drosophila period and timeless. *Cell* **93**, 805–814 (1998).

26. Brown, S., Kowalska, E. & Dallmann, R. (Re)inventing the Circadian Feedback Loop. *Dev. Cell* **22**, 477–487 (2012).

27. Ripperger, J. A. & Brown, S. A. *Transcriptional Regulation of Circadian Clocks*. *The Circadian Clock* (Springer, New York, 2010).

28. Reppert, S. M. & Weaver, D. R. Coordination of circadian clocks in mammals. *Nature* **418**, 935–941 (2002).

29. Partch, C. L., Green, C. B. & Takahashi, J. S. Molecular Architecture of the Mammalian Circadian Clock. *Trends Cell Biol.* **24**, 90–99 (2014).

30. Mohawk, J. A., Green, C. B. & Takahashi, J. S. Central and Peripheral Circadian Clocks in Mammals. *Annu. Rev. Neurosci.* **35**, 445–462 (2012).

31. Partch, C. L., Shields, K. F., Thompson, C. L., Selby, C. P. & Sancar, A. Posttranslational regulation of the mammalian circadian clock by cryptochrome and protein phosphatase 5. *PNAS* **103**, 10467–10472 (2006).

32. Lee, H. *et al.* The period of the circadian oscillator is primarily determined by the balance between casein kinase 1 and protein phosphatase 1. *PNAS* **108**, 16451–16456 (2011).

33. Narasimamurthy, R. *et al.* CK1 δ / e protein kinase primes the PER2 circadian phosphoswitch. *PNAS* **115**, 5986–5991 (2018).

34. Busino, L. *et al.* SCFFbxl3 controls the oscillation of the circadian clock by directing the degradation of cryptochrome proteins. *Science* **316**, 900–904 (2007).

35. Godinho, S. I. H. *et al.* The After-Hours Mutant Reveals a Role for Fbxl3 in Determining Mammalian Circadian Period. *Science* **316**, 897–900 (2007).

36. Siepka, S. M. *et al.* Circadian mutant Overtime reveals F-box protein FBXL3 regulation of cryptochrome and period gene expression. *Cell* **129**, 1011–1023 (2007).

37. Lee, Y. & Kim, E. K. AMP-activated protein kinase as a key molecular link between metabolism and clockwork. *Exp. Mol. Med.* **45**, e33 (2013).

38. Jee, H. U. *et al.* Activation of 5′-AMP-activated kinase with diabetes drug metformin induces casein kinase Iε (CKIε)-dependent degradation of clock protein mPer2. *J. Biol. Chem.* **282**, 20794–20798 (2007).

39. Relógio, A. *et al.* Tuning the mammalian circadian clock: Robust synergy of two loops. *PLoS Comput. Biol.* **7**, 1–18 (2011).

40. Canaple, L. *et al.* Reciprocal Regulation of Brain and Muscle Arnt-Like Protein 1 and Peroxisome Proliferator-Activated Receptor α Defines a Novel Positive Feedback Loop in the Rodent Liver Circadian Clock. *Mol. Endocrinol.* **20**, 1715–1727 (2006).

41. Yamajuku, D. *et al.* Cellular DBP and E4BP4 proteins are critical for determining the period length of the circadian oscillator. *FEBS Lett.* **585**, 2217–2222 (2011).

42. Honma, S. *et al.* Dec1 and Dec2 are regulators of the mammalian molecular clock. *Nature* **419**, 841–844 (2002).

43. Koike, N. *et al.* Transcriptional Architecture and Chromatin Landscape of the Core Circadian Clock in Mammals. *Science* **338**, 349–354 (2013).

44. Doi, M., Hirayama, J. & Sassone-Corsi, P. Circadian Regulator CLOCK Is a Histone Acetyltransferase. *Cell* **125**, 497–508 (2006).

45. Hirayama, J. *et al.* CLOCK-mediated acetylation of BMAL1 controls circadian function. *Nature* **450**, 1086–1090 (2007).

46. Etchegaray, J.-P., Lee, C., Wade, P. & Reppert, S. Rhythmic histone acetylation underlies transcription in the mammalian circadian clock. *Nature* **421**, 177–182 (2003).

47. Hosoda, H. *et al.* CBP/p300 is a cell type-specific modulator of CLOCK/BMAL1-mediated transcription. *Mol. Brain* **2**, 1–18 (2009).

48. Asher, G. *et al.* SIRT1 Regulates Circadian Clock Gene Expression through PER2 Deacetylation. *Cell* **134**, 317–328 (2008).

49. Nakahata, Y. *et al.* The NAD+-dependent deacetylase SIRT1 modulates CLOCK-mediated chromatin remodeling and circadian control. *Cell* **134**, 329–340 (2008).

50. Sassone-Corsi, P. Minireview: NAD+, a Circadian Metabolite with an Epigenetic Twist. *Endocrinology* **153**, 1–5 (2012).

51. Reddy, A. B. *et al.* Circadian orchestration of the hepatic proteome. *Curr. Biol.* **16**, 1107–1115 (2006).

52. Robles, M. S., Cox, J. & Mann, M. In-Vivo Quantitative Proteomics Reveals a Key Contribution of Post-Transcriptional Mechanisms to the Circadian Regulation of Liver Metabolism. *PLOS Genet.* **10**, e1004047 (2014).

53. Zhang, R., Lahens, N. F., Ballance, H. I., Hughes, M. E. & Hogenesch, J. B. A circadian gene expression atlas in mammals: Implications for biology and medicine. *PNAS* **111**, 16219–16224 (2014).

54. Mauvoisin, D. *et al.* Circadian clock-dependent and -independent rhythmic proteomes implement distinct diurnal functions in mouse liver. *PNAS* **111**, 167 LP – 172 (2014).

55. Storch, K. *et al.* Extensive and divergent circadian gene expression in liver and heart. *Nature* **417**, 0–6 (2002).

56. Panda, S. *et al.* Coordinated transcription of key pathways in the mouse by the circadian clock. *Cell* **109**, 307–320 (2002).

57. Akhtar, R. A. *et al.* Circadian cycling of the mouse liver transcriptome, as revealed by cDNA microarray, is driven by the suprachiasmatic nucleus. *Curr. Biol.* **12**, 540–550 (2002).

58. Wu, G. *et al.* Gene and Genome Parameters of Mammalian Liver Circadian Genes (LCGs). *PLoS One* **7**, (2012).

59. McCarthy, J. J. *et al.* Identification of the circadian transcriptome in adult mouse skeletal muscle. *Physiol. Genomics* **31**, 86–95 (2007).

60. Miller, B. H. *et al.* Circadian and CLOCK-controlled regulation of the mouse transcriptome and cell proliferation. *PNAS* **104**, 3342–3347 (2007).

61. Kojima, S., Shingle, D. L. & Green, C. B. Post-transcriptional control of circadian rhythms. *J. Cell Sci.* **124**, 311–320 (2011).

62. Staiger, D. & Köster, T. Spotlight on post-transcriptional control in the circadian system. *Cell. Mol. Life Sci.* **68**, 71–83 (2011).

63. Mauvoisin, D. Circadian rhythms and proteomics: It's all about posttranslational modifications! *WIREs Syst. Biol. Med.* **11**, e1450 (2019).

64. Brüning, F. *et al.* Sleep-wake cycles drive daily dynamics of synaptic phosphorylation. *Science* **366**, (2019).

65. Zhang, L., Weng, W. & Guo, J. Posttranscriptional mechanisms in controlling eukaryotic circadian rhythms. *FEBS Lett.* **585**, 1400–1405 (2011).

66. Duong, H. A., Robles, M. S., Knutti, D. & Weitz, C. J. A molecular mechanism for circadian clock negative feedback. *Science* **332**, 1436–1439 (2011).

67. Padmanabhan, K., Robles, M. S., Westerling, T. & Weitz, C. J. Feedback regulation of transcriptional termination by the mammalian circadian clock PERIOD complex. *Science* **337**, 599–602 (2012).

68. Lim, C. & Allada, R. Emerging roles for post-transcriptional regulation in circadian clocks. *Nat. Neurosci.* **16**, 1544–1550 (2013).

69. Kojima, S. & Green, C. B. Circadian genomics reveal a role for post-transcriptional regulation in mammals. *Biochemistry* **54**, 124–133 (2015).

70. Preußner, M. & Heyd, F. Post-transcriptional control of the mammalian circadian clock: implications for health and disease. *Pflugers Arch. Eur. J. Physiol.* **468**, 983–991 (2016).

71. Robles, M. S., Humphrey, S. J. & Mann, M. Phosphorylation Is a Central Mechanism for Circadian Control of Metabolism and Physiology. *Cell Metab.* **25**, 118–127 (2017).

72. Green, C. B. Circadian posttranscriptional regulatory mechanisms in mammals. *Cold*

Spring Harb. Perspect. Biol. **10**, 1–12 (2018).

73. Duffy, J. F. & Czeisler, C. A. Effect of light on human circadian physiology. *Sleep Med. Clin.* **4**, 165–177 (2009).

74. Bodenstein, C., Heiland, I. & Schuster, S. Temperature compensation and entrainment in circadian rhythms. *Phys. Biol.* **9**, (2012).

75. Aschoff, J. Freerunning and entrained circadian rhythms. in *Handbook of behavioral neurobiology. 4. Biological rhythms. Plenum Press, New York* (1981).

76. Honma, S. The mammalian circadian system: a hierarchical multi-oscillator structure for generating circadian rhythm. *J. Physiol. Sci.* **68**, 207–219 (2018).

77. Kyriacou, C. P. & Hastings, M. H. Circadian clocks: genes, sleep, and cognition. *Trends Cogn. Sci.* **14**, 259–267 (2010).

78. Moore, R. Y. & Eichler, V. B. Loss of a circadian adrenal corticosterone rhythm following suprachiasmatic lesions in the rat. *Brain Res.* **42**, 201–206 (1972).

79. Stephan, F. K. & Zucker, I. Circadian rhythms in drinking behavior and locomotor activity of rats are eliminated by hypothalamic lesions. *PNAS* **69**, 1583–6 (1972).

80. Sinturel, F. *et al.* Circadian hepatocyte clocks keep synchrony in the absence of a master pacemaker in the suprachiasmatic nucleus or other extrahepatic clocks. *Genes Dev.* 3–4 (2021).

81. Ralph, M. R., Foster, R. G., Davis, F. C. & Menaker, M. Transplanted suprachiasmatic nucleus determines circadian period. *Science* **247**, 975–978 (1990).

82. Weaver, D. R. The Suprachiasmatic Nucleus : A 25-Year Retrospective. *J Biol Rhythm.* **13**, 100–112 (1998).

83. Welsh, D. K., Yoo, S. H., Liu, A. C., Takahashi, J. S. & Kay, S. A. Bioluminescence imaging of individual fibroblasts reveals persistent, independently phased circadian rhythms of clock gene expression. *Curr. Biol.* 2289–2295 (2004).

84. Yoo, S. H. *et al.* PERIOD2::LUCIFERASE real-time reporting of circadian dynamics reveals persistent circadian oscillations in mouse peripheral tissues. *PNAS* **101**, 5339–5346 (2004).

85. Do, M. T. & Yau, K. W. Intrinsically photosensitive retinal ganglion cells. *Physiol. Rev.* 1547–1581 (2010).

86. Lucas, R. J., Lall, G. S., Allen, A. E. & Brown, T. M. Chapter 1 - How rod, cone, and melanopsin photoreceptors come together to enlighten the mammalian circadian clock. in *The Neurobiology of Circadian Timing* (eds. Kalsbeek, A., Merrow, M., Roenneberg, T. & Foster, R. G. B. T.) **199**, 1–18 (Elsevier, 2012).

87. Astiz, M., Heyde, I. & Oster, H. Mechanisms of Communication in the Mammalian Circadian Timing System. *Int J Mol Sci.* **20**, 343 (2019).

88. Brancaccio, M. *et al.* Cell-autonomous clock of astrocytes drives circadian behavior in mammals. *Science* **192**, 187–192 (2019).

89. Abe, H., Honma, S., Shinohara, K. & Honma, K. Substance P receptor regulates the photic induction of Fos-like protein in the suprachiasmatic nucleus of Syrian hamsters.

Brain Res. **708**, 135–142 (1996).

90. Aida, R. *et al.* Gastrin-releasing peptide mediates photic entrainable signals to dorsal subsets of suprachiasmatic nucleus via induction of Period gene in mice. *Mol. Pharmacol.* **61**, 26–34 (2002).

91. Meyer-Spasche, A. & Piggins, H. D. Vasoactive intestinal polypeptide phase-advances the rat suprachiasmatic nuclei circadian pacemaker in vitro via protein kinase A and mitogen-activated protein kinase. *Neurosci. Lett.* **358**, 91–94 (2004).

92. Patton, A. P. & Hastings, M. H. The suprachiasmatic nucleus. *Curr. Biol.* **28**, 816–822 (2018).

93. Kramer, A. *et al.* Regulation of Daily Locomotor Activity and Sleep by Hypothalamic EGF Receptor Signaling. *Science* **294**, 2511–2515 (2001).

94. Cheng, M. Y. *et al.* Prokineticin 2 transmits the behavioural circadian rhythm of the suprachiasmatic nucleus. *Nature* **417**, 405–410 (2002).

95. Buijs, R. M. *et al.* Organization of circadian functions: interaction with the body. *Prog. Brain Res.* **153**, 341–360 (2006).

96. Ripperger, J. A. & Schibler, U. Circadian regulation of gene expression in animals. *Curr. Opin. Cell Biol.* **13**, 357—362 (2001).

97. Pilorz, V., Astiz, M., Heinen, K. O., Rawashdeh, O. & Oster, H. The Concept of Coupling in the Mammalian Circadian Clock Network. *J. Mol. Biol.* (2020).

98. Oster, H. *et al.* The circadian rhythm of glucocorticoids is regulated by a gating mechanism residing in the adrenal cortical clock. *Cell Metab.* **4**, 163–173 (2006).

99. Spiga, F., Walker, J. J., Terry, J. R. & Lightman, S. L. HPA axis-rhythms. *Compr. Physiol.* **4**, 1273–1298 (2014).

100. Graber, A. L., Givens, J. R., Nicholson, W. E., Island, D. P. & Liddle, G. W. Persistence of Diurnal Rhythmicity in Plasma ACTH Concentrations in Cortisol-Deficient Patients. *J. Clin. Endocrinol. Metab.* **25**, 804–807 (1965).

101. Rees, L. H. *et al.* A Radioimmunoassay for Rat Plasma ACTH. *Endocrinology* **89**, 254–261 (1971).

102. Balsalobre, A. *et al.* Resetting of Circadian Time in Peripheral Tissues by Glucocorticoid Signaling. *Science* **289**, 2344–2347 (2000).

103. Yamamoto, T. *et al.* Acute Physical Stress Elevates Mouse Period1 mRNA Expression in Mouse Peripheral Tissues via a Glucocorticoid-responsive Element. *J. Biol. Chem.* **280**, 42036–42043 (2005).

104. Reddy, A. B. *et al.* Glucocorticoid signaling synchronizes the liver circadian transcriptome. *Hepatology* **45**, 1478–1488 (2007).

105. So, A. Y.-L., Bernal, T. U., Pillsbury, M. L., Yamamoto, K. R. & Feldman, B. J. Glucocorticoid regulation of the circadian clock modulates glucose homeostasis. *PNAS* **106**, 17582–17587 (2009).

106. Kiessling, S., Eichele, G. & Oster, H. Adrenal glucocorticoids have a key role in circadian resynchronization in a mouse model of jet lag. *J. Clin. Invest.* **120**, 2600–2609 (2010).

107. Cuesta, M., Cermakian, N. & Boivin, D. B. Glucocorticoids entrain molecular clock components in human peripheral cells. *FASEB J.* **29**, 1360–1370 (2015).

108. Zawilska, J. B., Skene, D. J. & Arendt, J. Physiology and pharmacology of melatonin in relation to biological rhythms. *Pharmacol. Reports* **61**, 383–410 (2009).

109. la Fleur, S. E., Kalsbeek, A., Wortel, J. & Buijs, R. M. Polysynaptic neural pathways between the hypothalamus, including the suprachiasmatic nucleus, and the liver. *Brain Res.* **871**, 50–56 (2000).

110. Bamshad, M., Aoki, V. T., Adkison, M. G., Warren, W. S. & Bartness, T. J. Central nervous system origins of the sympathetic nervous system outflow to white adipose tissue. *Am. J. Physiol.* **275**, R291–R299 (1998).

111. Gerendai, I., Tóth, I. E., Boldogköi, Z., Medveczky, I. & Halász, B. CNS structures presumably involved in vagal control of ovarian function. *J. Auton. Nerv. Syst.* **80**, 40–45 (2000).

112. Scheer, F. A. J. L., Ter Horst, G. J., van der Vliet, J. & Buijs, R. M. Physiological and anatomic evidence for regulation of the heart by suprachiasmatic nucleus in rats. *Am. J. Physiol. Circ. Physiol.* **280**, 1391–1399 (2001).

113. Buijs, R. M. *et al.* The suprachiasmatic nucleus balances sympathetic and parasympathetic output to peripheral organs through separate preautonomic neurons. *J. Comp. Neurol.* **464**, 36–48 (2003).

114. García-García, A. & Méndez-Ferrer, S. The Autonomic Nervous System Pulls the Strings to Coordinate Circadian HSC Functions. *Front. Immunol.* **11**, 1–8 (2020).

115. Becker, B. K., Zhang, D., Soliman, R. & Pollock, D. M. Autonomic Nerves and Circadian Control of Renal Function. *Auton. Neurosci.* **217**, 58–65 (2019).

116. Cailotto, C. *et al.* Effects of nocturnal light on (clock) gene expression in peripheral organs: A role for the autonomic innervation of the liver. *PLoS One* **4**, 1–12 (2009).

117. Terazono, H. *et al.* Adrenergic regulation of clock gene expression in mouse liver. *PNAS* **100**, 6795 LP – 6800 (2003).

118. Vujovic, N., Davidson, A. J. & Menaker, M. Sympathetic input modulates, but does not determine, phase of peripheral circadian oscillators. *Am. J. Physiol. Regul. Integr. Comp. Physiol.* **295**, R355-60 (2008).

119. Tahara, Y. *et al.* Age-related circadian disorganization caused by sympathetic dysfunction in peripheral clock regulation. *npj Aging Mech. Dis.* **3**, (2017).

120. Katayama, Y. *et al.* Signals from the sympathetic nervous system regulate hematopoietic stem cell egress from bone marrow. *Cell* **124**, 407–421 (2006).

121. Maryanovich, M., Takeishi, S. & Frenette, P. S. Neural regulation of bone and bone marrow. *Cold Spring Harb. Perspect. Med.* **8**, 1–23 (2018).

122. Maryanovich, M. *et al.* Adrenergic nerve degeneration in bone marrow drives aging of the hematopoietic stem cell niche. *Nat. Med.* **24**, 782–791 (2018).

123. Brown, S. A., Zumbrunn, G., Fleury-Olela, F., Preitner, N. & Schibler, U. Rhythms of mammalian body temperature can sustain peripheral circadian clocks. *Curr. Biol.* **12**,

1574–1583 (2002).

124. Reinke, H. *et al.* Differential display of DNA-binding proteins reveals heat-shock factor 1 as a circadian transcription factor. *Genes Dev.* **22**, 331–345 (2008).

125. Damiola, F., Minh, N. Le, Preitner, N., Fleury-olela, F. & Schibler, U. Restricted feeding uncouples circadian oscillators in peripheral tissues from the central pacemaker in the suprachiasmatic nucleus. *Genes Dev.* 2950–2961 (2000).

126. Stokkan, K. A., Yamazaki, S., Tei, H., Sakaki, Y. & Menaker, M. Entrainment of the circadian clock in the liver by feeding. *Science* **291**, 490–493 (2001).

127. Stephan, F. K., Swann, J. M. & Sisk, C. L. Entrainment of circadian rhythms by feeding schedules in rats with suprachiasmatic lesions. *Behav. Neural Biol.* **25**, 545–554 (1979).

128. Hara, R. *et al.* Restricted feeding entrains liver clock without participation of the suprachiasmatic nucleus. *Genes Cells* **6**, 269–278 (2001).

129. Liu, C., Li, S., Liu, T., Borjigin, J. & Lin, J. D. Transcriptional coactivator PGC-1alpha integrates the mammalian clock and energy metabolism. *Nature* **447**, 477–481 (2007).

130. Rodgers, J. T. *et al.* Nutrient control of glucose homeostasis through a complex of PGC-1alpha and SIRT1. *Nature* **434**, 113–118 (2005).

131. Heyde, I. & Oster, H. Differentiating external zeitgeber impact on peripheral circadian clock resetting. *Sci. Rep.* **9**, 1–13 (2019).

132. Ando, H. *et al.* Impairment of peripheral circadian clocks precedes metabolic abnormalities in ob/ob mice. *Endocrinology* **152**, 1347–1354 (2011).

133. Grosbellet, E., Gourmelen, S., Pévet, P., Criscuolo, F. & Challet, E. Leptin normalizes photic synchronization in male ob/ob mice, via indirect effects on the suprachiasmatic nucleus. *Endocrinology* **156**, 1080–1090 (2015).

134. Merkestein, M. *et al.* GHS-R1a signaling in the DMH and VMH contributes to food anticipatory activity. *Int. J. Obes.* **38**, 610–618 (2014).

135. Yamajuku, D. *et al.* Real-time monitoring in three-dimensional hepatocytes reveals that insulin acts as a synchronizer for liver clock. *Sci. Rep.* **2**, 439 (2012).

136. Sato, M., Murakami, M., Node, K., Matsumura, R. & Akashi, M. The role of the endocrine system in feeding-induced tissue-specific circadian entrainment. *Cell Rep.* **8**, 393–401 (2014).

137. Quagliarini, F. *et al.* Cistromic Reprogramming of the Diurnal Glucocorticoid Hormone Response by High-Fat Diet. *Mol. Cell* **76**, 531–545 (2019).

138. Lecocq, F. R., Mebane, D. & Madison, L. L. The Acute Effect of Hydrocortisone on Hepatic Glucose Output and Peripheral Glucose Utilization. *J. Clin. Invest.* **43**, 237–246 (1964).

139. Askew, E. W., Huston, R. L., Plopper, C. G. & Hecker, A. L. Adipose tissue cellularity and lipolysis. Response to exercise and cortisol treatment. *J. Clin. Invest.* **56**, 521–529 (1975).

140. López-Otín, C. & Kroemer, G. Hallmarks of Health. *Cell* **184**, 33–63 (2021).

141. Fu, L. & Lee, C. C. The circadian clock: Pacemaker and tumour suppressor. *Nat. Rev. Cancer* **3**, 350–361 (2003).

142. Lyall, L. M. *et al.* Association of disrupted circadian rhythmicity with mood disorders, subjective wellbeing, and cognitive function: a cross-sectional study of 91 105 participants from the UK Biobank. *The Lancet Psychiatry* **5**, 507–514 (2018).

143. Sahar, S. & Sassone-corsi, P. Metabolism and cancer : the circadian clock connection. **9**, (2009).

144. Marcheva, B. *et al.* Disruption of the clock components CLOCK and BMAL1 leads to hypoinsulinaemia and diabetes. *Nature* **466**, 627–631 (2010).

145. Zerón-Rugerio, M. F., Cambras, T. & Izquierdo-Pulido, M. Social Jet Lag Associates Negatively with the Adherence to the Mediterranean Diet and Body Mass Index among Young Adults. *Nutrients* **11**, (2019).

146. Strohmaier, S., Devore, E. E., Zhang, Y. & Schernhammer, E. S. A Review of Data of Findings on Night Shift Work and the Development of DM and CVD Events: a Synthesis of the Proposed Molecular Mechanisms. *Curr. Diab. Rep.* **18**, 132 (2018).

147. Shan, Z. *et al.* Rotating night shift work and adherence to unhealthy lifestyle in predicting risk of type 2 diabetes: results from two large US cohorts of female nurses. *BMJ* **363**, k4641 (2018).

148. Lieu, S. J., Curhan, G. C., Schernhammer, E. S. & Forman, J. P. Rotating night shift work and disparate hypertension risk in African-Americans. *J. Hypertens.* **30**, 61–66 (2012).

149. Wegrzyn, L. R. *et al.* Rotating Night-Shift Work and the Risk of Breast Cancer in the Nurses' Health Studies. *Am. J. Epidemiol.* **186**, 532–540 (2017).

150. Wang, X.-S. S., Armstrong, M., Cairns, B., Key, T. & X, T. Shift work and chronic disease: The epidemiological evidence. *Occup. Med. (Lond).* **61**, 78–89 (2011).

151. Orihara, K. & Saito, H. Controlling the peripheral clock might be a new treatment strategy in allergy and immunology. *The Journal of allergy and clinical immunology* **137**, 1236–1237 (2016).

152. Litinski, M., Scheer, F. A. & Shea, S. A. Influence of the Circadian System on Disease Severity. *Sleep Med. Clin.* **4**, 143–163 (2009).

153. Yamazaki, S. *et al.* Resetting Central and Peripheral Circadian Oscillators in Transgenic Rats. *Science* **288**, 682–685 (2000).

154. Davidson, A. J., Castanon-Cervantes, O., Leise, T. L., Molyneux, P. C. & Harrington, M. E. Visualizing jet lag in the mouse suprachiasmatic nucleus and peripheral circadian timing system. *Eur. J. Neurosci.* **29**, 171–180 (2009).

155. Tapp, W. N. & Natelson, B. H. Circadian rhythms and patterns of performance before and after simulated jet lag. *Am. J. Physiol.* **257**, (1989).

156. Waterhouse, J., Reilly, T., Atkinson, G. & Edwards, B. Jet lag: trends and coping strategies. *Lancet* **369**, 1117–1129 (2007).

157. Castanon-Cervantes, O. *et al.* Dysregulation of inflammatory responses by chronic

circadian disruption. *J. Immunol.* **185**, 5796–5805 (2010).

158. Grosbellet, E. *et al.* Circadian desynchronization triggers premature cellular aging in a diurnal rodent. *FASEB J.* **29**, 4794–4803 (2015).

159. Kettner, N. M. *et al.* Circadian Dysfunction Induces Leptin Resistance in Mice. *Cell Metab.* **22**, 448–459 (2015).

160. Gale, J. E. *et al.* Disruption of circadian rhythms accelerates development of diabetes through pancreatic beta-cell loss and dysfunction. *J. Biol. Rhythms* **26**, 423–433 (2011).

161. Papagiannakopoulos, T. *et al.* Circadian Rhythm Disruption Promotes Lung Tumorigenesis. *Cell Metab.* **24**, 324–331 (2016).

162. Kettner, N. M. *et al.* Circadian Homeostasis of Liver Metabolism Suppresses Hepatocarcinogenesis. *Cancer Cell* **30**, 909–924 (2016).

163. Davidson, A. J. *et al.* Chronic jet-lag increases mortality in aged mice. *Curr. Biol.* **16**, R914–R916 (2006).

164. Ortiz-Tudela, E., Mteyrek, A., Ballesta, A., Innominato, P. F. & Lévi, F. Cancer chronotherapeutics: experimental, theoretical, and clinical aspects. *Handb. Exp. Pharmacol.* 261–288 (2013).

165. Cortelli, P. Chronomedicine: A necessary concept to manage human diseases. *Sleep Med. Rev.* **21**, 1–2 (2015).

166. Duffy, J. F., Zitting, K.-M. & Chinoy, E. D. Aging and Circadian Rhythms. *Sleep Med. Clin.* **10**, 423–434 (2015).

167. Hood, S. & Amir, S. The aging clock: circadian rhythms and later life. *J. Clin. Invest.* **127**, 437–446 (2017).

168. Froy, O. Circadian Rhythms, Aging, and Life Span in Mammals. *Physiology* **26**, 225–235 (2011).

169. Viswanathan, N. & Davis, F. C. Suprachiasmatic nucleus grafts restore circadian function in aged hamsters. *Brain Res.* **686**, 10–16 (1995).

170. Cai, A., Scarbrough, K., Hinkle, D. A. & Wise, P. M. Fetal grafts containing suprachiasmatic nuclei restore the diurnal rhythm of CRH and POMC mRNA in aging rats. *Am. J. Physiol.* **273**, R1764-70 (1997).

171. Kolker, D. E. *et al.* Aging Alters Circadian and Light-Induced Expression of Clock Genes in Golden Hamsters. *J. Biol. Rhythms* **18**, 159–169 (2003).

172. Lupi, D., Semo, M. & Foster, R. G. Impact of age and retinal degeneration on the light input to circadian brain structures. *Neurobiol. Aging* **33**, 383–392 (2012).

173. Zhang, Y. *et al.* Effects of aging on lens transmittance and retinal input to the suprachiasmatic nucleus in golden hamsters. *Neurosci. Lett.* **258**, 167–170 (1998).

174. Semo, M. *et al.* Melanopsin retinal ganglion cells and the maintenance of circadian and pupillary responses to light in aged rodless/coneless (rd/rd cl) mice. *Eur. J. Neurosci.* **17**, 1793–1801 (2003).

175. Nygård, M., Hill, R. H., Wikström, M. A. & Kristensson, K. Age-related changes in

electrophysiological properties of the mouse suprachiasmatic nucleus in vitro. *Brain Res. Bull.* **65**, 149–154 (2005).

176. Nakamura, W., Yamazaki, S., Takasu, N. N., Mishima, K. & Block, G. D. Differential Response of Period 1 Expression within the Suprachiasmatic Nucleus. *J. Neurosci.* **25**, 5481 LP – 5487 (2005).

177. López-Otín, C., Blasco, M. A., Partridge, L., Serrano, M. & Kroemer, G. The hallmarks of aging. *Cell* **153**, 1194 (2013).

178. Kalló, I., Kalamatianos, T., Piggins, H. D. & Coen, C. W. Ageing and the diurnal expression of mRNAs for vasoactive intestinal peptide and for the VPAC2 and PAC1 receptors in the suprachiasmatic nucleus of male rats. *J. Neuroendocrinol.* **16**, 758–766 (2004).

179. Roozendaal, B., van Gool, W. A., Swaab, D. F., Hoogendijk, J. E. & Mirmiran, M. Changes in vasopressin cells of the rat suprachiasmatic nucleus with aging. *Brain Res.* **409**, 259–264 (1987).

180. Zhao, J., Warman, G. R. & Cheeseman, J. F. The functional changes of the circadian system organization in aging. *Ageing Res. Rev.* **52**, 64–71 (2019).

181. Benitah, S. A. & Welz, P. S. Circadian Regulation of Adult Stem Cell Homeostasis and Aging. *Cell Stem Cell* **26**, 817–831 (2020).

182. Welz, P.-S. & Benitah, S. A. Molecular Connections Between Circadian Clocks and Aging. *J. Mol. Biol.* **432**, 3661–3679 (2020).

183. Solanas, G. *et al.* Aged Stem Cells Reprogram Their Daily Rhythmic Functions to Adapt to Stress. *Cell* **170**, 678-692.e20 (2017).

184. Sato, S. *et al.* Circadian Reprogramming in the Liver Identifies Metabolic Pathways of Aging. *Cell* **170**, 664-677.e11 (2017).

185. Houtkooper, R. H., Pirinen, E. & Auwerx, J. Sirtuins as regulators of metabolism and healthspan. *Nat. Rev. Mol. Cell Biol.* **13**, 225–238 (2012).

186. Khapre, R. V. *et al.* BMAL1-dependent regulation of the mTOR signaling pathway delays aging. *Aging* **6**, 48–57 (2014).

187. Fontana, L., Partridge, L. & Longo, V. D. Extending healthy life span--from yeast to humans. *Science* **328**, 321–326 (2010).

188. Fernandez-Marcos, P. J. & Auwerx, J. Regulation of PGC-1α, a nodal regulator of mitochondrial biogenesis. *Am. J. Clin. Nutr.* **93**, 884S–90 (2011).

189. Xie, J., Zhang, X. & Zhang, L. Negative regulation of inflammation by SIRT1. *Pharmacol. Res.* **67**, 60–67 (2013).

190. Salminen, A., Kaarniranta, K. & Kauppinen, A. Inflammaging: disturbed interplay between autophagy and inflammasomes. *Aging* **4**, 166–175 (2012).

191. Massudi, H. *et al.* Age-Associated Changes In Oxidative Stress and NAD+ Metabolism In Human Tissue. *PLoS One* **7**, e42357 (2012).

192. Yoshino, J., Mills, K. F., Yoon, M. J. & Imai, S. Nicotinamide Mononucleotide, a Key NAD+ Intermediate, Treats the Pathophysiology of Diet- and Age-Induced Diabetes in

Mice. *Cell Metab.* **14**, 528–536 (2011).

193. Trammell, S. A. J. *et al.* Nicotinamide Riboside Opposes Type 2 Diabetes and Neuropathy in Mice. *Sci. Rep.* **6**, 26933 (2016).

194. Zhang, H. *et al.* NAD+ repletion improves mitochondrial and stem cell function and enhances life span in mice. *Science* **352**, 1436 LP – 1443 (2016).

195. Vaur, P. *et al.* Nicotinamide riboside, a form of vitamin B(3), protects against excitotoxicity-induced axonal degeneration. *FASEB J.* **31**, 5440–5452 (2017).

196. Kondratov, R. V, Kondratova, A. A., Gorbacheva, V. Y., Vykhovanets, O. V & Antoch, M. P. Early aging and age-related pathologies in mice deficient in BMAL1, the core component of the circadian clock. *Genes Dev.* 1868–1873 (2006).

197. Dubrovsky, Y. V., Samsa, W. E. & Kondratov, R. V. Deficiency of circadian protein CLOCK reduces lifespan and increases age-related cataract development in mice. *Aging (Albany NY)* **2**, 936–944 (2010).

198. Welz, P.-S. *et al.* BMAL1-Driven Tissue Clocks Respond Independently to Light to Maintain Homeostasis. *Cell* **177**, 1436–1447 (2019).

199. Kohsaka, A. *et al.* The circadian clock maintains cardiac function by regulating mitochondrial metabolism in mice. *PLoS One* **9**, e112811 (2014).

200. Jacobi, D. *et al.* Hepatic Bmal1 regulates rhythmic mitochondrial dynamics and promotes metabolic fitness. *Cell Metab.* **22**, 709–720 (2015).

201. Kondratov, R. V., Vykhovanets, O., Kondratova, A. A. & Antoch, M. P. Antioxidant N-acetyl-L-cysteine ameliorates symptoms of premature aging associated with the deficiency of the circadian protein BMAL1. *Aging* **1**, 979–987 (2009).

202. van der Horst, G. T. *et al.* Mammalian Cry1 and Cry2 are essential for maintenance of circadian rhythms. *Nature* **398**, 627–630 (1999).

203. Vitaterna, M. H. *et al.* Differential regulation of mammalian Period genes and circadian rhythmicity by cryptochromes 1 and 2. *PNAS* **96**, 12114 LP – 12119 (1999).

204. Fu, L., Patel, M. S., Bradley, A., Wagner, E. F. & Karsenty, G. The Molecular Clock Mediates Leptin-Regulated Bone Formation. *Cell* **122**, 803–815 (2005).

205. Chao-Yung, W. *et al.* Increased Vascular Senescence and Impaired Endothelial Progenitor Cell Function Mediated by Mutation of Circadian Gene Per2. *Circulation* **118**, 2166–2173 (2008).

206. Yang, S. *et al.* The role of mPer2 clock gene in glucocorticoid and feeding rhythms. *Endocrinology* **150**, 2153–2160 (2009).

207. Carvas, J. M. *et al.* Period2 gene mutant mice show compromised insulin-mediated endothelial nitric oxide release and altered glucose homeostasis. *Front. Physiol.* **3**, 337 (2012).

208. Destici, E. *et al.* Altered Phase-Relationship between Peripheral Oscillators and Environmental Time in Cry1 or Cry2 Deficient Mouse Models for Early and Late Chronotypes. *PLoS One* **8**, e83602 (2013).

209. King, D. P. *et al.* The mouse Clock mutation behaves as an antimorph and maps within

the W19H deletion, distal of Kit. *Genetics* **146**, 1049–1060 (1997).

210. Turek, F. W. *et al.* Obesity and Metabolic Syndrome in Circadian Clock Mutant Mice. *Science* **308**, 1043 LP – 1045 (2005).

211. Debruyne, J. P. *et al.* A clock shock: mouse CLOCK is not required for circadian oscillator function. *Neuron* **50**, 465–477 (2006).

212. DeBruyne, J. P., Weaver, D. R. & Reppert, S. M. CLOCK and NPAS2 have overlapping roles in the suprachiasmatic circadian clock. *Nat. Neurosci.* **10**, 543–545 (2007).

213. Bunger, M. K. *et al.* Mop3 is an essential component of the master circadian pacemaker in mammals. *Cell* **103**, 1009–1017 (2000).

214. Bunger, M. K. *et al.* Progressive arthropathy in mice with a targeted disruption of the Mop3/Bmal-1 locus. *Genesis* **41**, 122–132 (2005).

215. J., W. E. *et al.* Genetic Components of the Circadian Clock Regulate Thrombogenesis In Vivo. *Circulation* **117**, 2087–2095 (2008).

216. Lamia, K. A., Storch, K.-F. & Weitz, C. J. Physiological significance of a peripheral tissue circadian clock. *PNAS* **105**, 15172 LP – 15177 (2008).

217. Janich, P. *et al.* The circadian molecular clock creates epidermal stem cell heterogeneity. *Nature* **480**, 209–214 (2011).

218. Husse, J., Leliavski, A., Tsang, A. H., Oster, H. & Eichele, G. The light-dark cycle controls peripheral rhythmicity in mice with a genetically ablated suprachiasmatic nucleus clock. *FASEB J.* **28**, 4950–4960 (2014).

219. Guo, H., Brewer, J. M., Lehman, M. N. & Bittman, E. L. Suprachiasmatic Regulation of Circadian Rhythms of Gene Expression in Hamster Peripheral Organs: Effects of Transplanting the Pacemaker. *J. Neurosci.* **26**, 6406 LP – 6412 (2006).

220. Guo, H., Brewer, J. M., Champhekar, A., Harris, R. B. S. & Bittman, E. L. Differential control of peripheral circadian rhythms by suprachiasmatic-dependent neural signals. *PNAS* **102**, 3111–3116 (2005).

221. Sakamoto, K. *et al.* Multitissue circadian expression of rat period homolog (rPer2) mRNA is governed by the mammalian circadian clock, the suprachiasmatic nucleus in the brain. *J. Biol. Chem.* **273**, 27039–27042 (1998).

222. Stephan, F. K. & Zucker, I. Circadian rhythms in drinking behavior and locomotor activity of rats are eliminated by hypothalamic lesions. *PNAS* **69**, 1583–1586 (1972).

223. Husse, J., Eichele, G. & Oster, H. Synchronization of the mammalian circadian timing system: Light can control peripheral clocks independently of the SCN clock. *BioEssays* **37**, 1119–1128 (2015).

224. McDearmon, E. L. *et al.* Dissecting the functions of the mammalian clock protein BMAL1 by tissue-specific rescue in mice. *Science* **314**, 1304–1308 (2006).

225. Watt, F. M. Mammalian skin cell biology: At the interface between laboratory and clinic. *Science* **346**, (2014).

226. Solanas, G. & Benitah, S. A. Regenerating the skin: A task for the heterogeneous stem cell pool and surrounding niche. *Nat. Rev. Mol. Cell Biol.* **14**, 737–748 (2013).

227. Plikus, M. V. *et al.* The circadian clock in skin: Implications for adult stem cells, tissue regeneration, cancer, aging, and immunity. *J. Biol. Rhythms* **30**, 163–182 (2015).

228. Rognoni, E. & Watt, F. M. Skin Cell Heterogeneity in Development, Wound Healing, and Cancer. *Trends Cell Biol.* **28**, 709–722 (2018).

229. Rabbani, P. *et al.* Coordinated activation of Wnt in epithelial and melanocyte stem cells initiates pigmented hair regeneration. *Cell* **145**, 941–955 (2011).

230. Woo, S.-H., Stumpfova, M., Jensen, U. B., Lumpkin, E. A. & Owens, D. M. Identification of epidermal progenitors for the Merkel cell lineage. *Development* **137**, 3965–3971 (2010).

231. Romani, N., Clausen, B. E. & Stoitzner, P. Langerhans cells and more: langerin-expressing dendritic cell subsets in the skin. *Immunol. Rev.* **234**, 120–141 (2010).

232. Wegner, J. *et al.* Laminin α5 in the keratinocyte basement membrane is required for epidermal–dermal intercommunication. *Matrix Biol.* **56**, 24–41 (2016).

233. Kretzschmar, K. & Watt, F. M. Markers of Epidermal Stem Cell Subpopulations in Adult Mammalian Skin. 1–14 (2014).

234. Fujiwara, H. *et al.* The basement membrane of hair follicle stem cells is a muscle cell niche. *Cell* **144**, 577–589 (2011).

235. Shwartz, Y. *et al.* Cell Types Promoting Goosebumps Form a Niche to Regulate Hair Follicle Stem Cells. *Cell* **182**, 578-593.e19 (2020).

236. Fuchs, E. & Green, H. The expression of keratin genes in epidermis and cultured epidermal cells. *Cell* **15**, 887–897 (1978).

237. Fuchs, E. & Green, H. Changes in keratin gene expression during terminal differentiation of the keratinocyte. *Cell* **19**, 1033–1042 (1980).

238. Coulombe, P. A., Hutton, M. E., Vassar, R. & Fuchs, E. A function for keratins and a common thread among different types of epidermolysis bullosa simplex diseases. *J. Cell Biol.* **115**, 1661–1674 (1991).

239. Vassar, R., Coulombe, P. A., Degenstein, L., Albers, K. & Fuchs, E. Mutant keratin expression in transgenic mice causes marked abnormalities resembling a human genetic skin disease. *Cell* **64**, 365–380 (1991).

240. Cheng, J. *et al.* The genetic basis of epidermolytic hyperkeratosis: A disorder of differentiation-specific epidermal keratin genes. *Cell* **70**, 811–819 (1992).

241. Proksch, E., Brandner, J. M. & Jensen, J.-M. The skin: an indispensable barrier. *Exp. Dermatol.* **17**, 1063–1072 (2008).

242. Ishitsuka, Y. & Roop, D. R. Loricrin: Past, Present, and Future. *Int. J. Mol. Sci.* **21**, 2271 (2020).

243. Steinert, P. M., Cantieri, J. S., Teller, D. C., Lonsdale-Eccles, J. D. & Dale, B. A. Characterization of a class of cationic proteins that specifically interact with intermediate filaments. *PNAS* **78**, 4097–4101 (1981).

244. Blanpain, C. & Fuchs, E. Epidermal homeostasis: a balancing act of stem cells in the skin. *Nat. Rev. Mol. Cell Biol.* **10**, 207–217 (2009).

245. Festa, E. *et al.* Adipocyte lineage cells contribute to the skin stem cell niche to drive hair cycling. *Cell* **146**, 761–771 (2011).

246. Greco, V. *et al.* A two-step mechanism for stem cell activation during hair regeneration. *Cell Stem Cell* **4**, 155–169 (2009).

247. Plikus, M. V *et al.* Cyclic dermal BMP signalling regulates stem cell activation during hair regeneration. *Nature* **451**, 340–344 (2008).

248. Lowry, W. E. *et al.* Defining the impact of beta-catenin/Tcf transactivation on epithelial stem cells. *Genes Dev.* **19**, 1596–1611 (2005).

249. Kobielak, K., Stokes, N., de la Cruz, J., Polak, L. & Fuchs, E. Loss of a quiescent niche but not follicle stem cells in the absence of bone morphogenetic protein signaling. *PNAS* **104**, 10063 LP – 10068 (2007).

250. Nishimura, E. K. *et al.* Key Roles for Transforming Growth Factor β in Melanocyte Stem Cell Maintenance. *Cell Stem Cell* **6**, 130–140 (2010).

251. Collins, C. A., Kretzschmar, K. & Watt, F. M. Reprogramming adult dermis to a neonatal state through epidermal activation of β-catenin. *Development* **138**, 5189 LP – 5199 (2011).

252. Plikus, M. V & Chuong, C.-M. Complex hair cycle domain patterns and regenerative hair waves in living rodents. *J. Invest. Dermatol.* **128**, 1071–1080 (2008).

253. Sherratt, M. J. *et al.* Circadian rhythms in skin and other elastic tissues. *Matrix Biol.* **84**, 97–110 (2019).

254. Geyfman, M. & Andersen, B. How the skin can tell time. *J. Invest. Dermatol.* **129**, 1063–1066 (2009).

255. Bullough, W. S. & Hammond, J. Mitotic activity in the adult male mouse, Mus musculus L. The diurnal cycles and their relation to waking and sleeping. *Proc. R. Soc. London. Ser. B - Biol. Sci.* **135**, 212–233 (1948).

256. Zanello, S. B., Jackson, D. M. & Holick, M. F. Expression of the Circadian Clock Genes clock and period1 in Human Skin. *J. Invest. Dermatol.* **115**, 757–760 (2000).

257. Bjarnason, G. A. *et al.* Circadian expression of clock genes in human oral mucosa and skin: association with specific cell-cycle phases. *Am. J. Pathol.* **158**, 1793–1801 (2001).

258. Oishi, K. *et al.* Differential expressions of mPer1 and mPer2 mRNAs under a skeleton photoperiod and a complete light-dark cycle. *Brain Res. Mol. Brain Res.* **109**, 11–17 (2002).

259. Tanioka, M. *et al.* Molecular Clocks in Mouse Skin. *J. Invest. Dermatol.* **129**, 1225–1231 (2009).

260. Lin, K. K. *et al.* Circadian clock genes contribute to the regulation of hair follicle cycling. *PLoS Genet.* **5**, e1000573 (2009).

261. Matsuo, T. *et al.* Control mechanism of the circadian clock for timing of cell division in vivo. *Science* **302**, 255–259 (2003).

262. Sasaki, T. *et al.* Phosphorylation regulates SIRT1 function. *PLoS One* **3**, e4020 (2008).

263. Khapre, R. V., Samsa, W. E. & Kondratov, R. V. Circadian regulation of cell cycle: Molecular connections between aging and the circadian clock. *Ann. Med.* **42**, 404–415 (2010).

264. Solanas, G. & Benitah, S. A. Regenerating the skin : a task for the heterogeneous stem cell pool and surrounding niche. *Nat. Publ. Gr.* **14**, 737–748 (2013).

265. Gréchez-Cassiau, A., Rayet, B., Guillaumond, F., Teboul, M. & Delaunay, F. The circadian clock component BMAL1 is a critical regulator of p21 WAF1/CIP1 expression and hepatocyte proliferation. *J. Biol. Chem.* **283**, 4535–4542 (2008).

266. Gaddameedhi, S., Selby, C. P., Kaufmann, W. K., Smart, R. C. & Sancar, A. Control of skin cancer by the circadian rhythm. *PNAS* **108**, 18790–18795 (2011).

267. Ikehata, H. & Ono, T. The mechanisms of UV mutagenesis. *J. Radiat. Res.* **52**, 115–125 (2011).

268. Geyfman, M. *et al.* Brain and muscle Arnt-like protein-1 (BMAL1) controls circadian cell proliferation and susceptibility to UVB-induced DNA damage in the epidermis. *PNAS* **109**, (2012).

269. Plikus, M. V. *et al.* Local circadian clock gates cell cycle progression of transient amplifying cells during regenerative hair cycling. *PNAS* **110**, (2013).

270. Flo, A., Calpena, A. C., Díez-Noguera, A., Del Pozo, A. & Cambras, T. Daily Variation of UV-induced Erythema and the Action of Solar Filters. *Photochem. Photobiol.* **93**, 632–635 (2017).

271. Shaw, T. J. & Martin, P. Wound repair: A showcase for cell plasticity and migration. *Curr. Opin. Cell Biol.* **42**, 29–37 (2016).

272. Sun, B. K., Siprashvili, Z. & Khavari, P. A. Advances in skin grafting and treatment of cutaneous wounds. *Science* **346**, 941–945 (2014).

273. Gurtner, G. C., Werner, S., Barrandon, Y. & Longaker, M. T. Wound repair and regeneration. *Nature* **453**, 314–321 (2008).

274. Park, S. *et al.* Tissue-scale coordination of cellular behaviour promotes epidermal wound repair in live mice. *Nat. Cell Biol.* **19**, 155–163 (2017).

275. Aragona, M. *et al.* Defining stem cell dynamics and migration during wound healing in mouse skin epidermis. *Nat. Commun.* **8**, 14684 (2017).

276. Ito, M. *et al.* Stem cells in the hair follicle bulge contribute to wound repair but not to homeostasis of the epidermis. *Nat. Med.* **11**, 1351–1354 (2005).

277. Levy, V., Lindon, C., Zheng, Y., Harfe, B. D. & Morgan, B. A. Epidermal stem cells arise from the hair follicle after wounding. *FASEB J.* **21**, 1358–1366 (2007).

278. Jaks, V., Kasper, M. & Toftgård, R. The hair follicle-a stem cell zoo. *Exp. Cell Res.* **316**, 1422–1428 (2010).

279. Page, M. E., Lombard, P., Ng, F., Göttgens, B. & Jensen, K. B. The epidermis comprises autonomous compartments maintained by distinct stem cell populations. *Cell Stem Cell* **13**, 471–482 (2013).

280. Gonzales, K. A. U. & Fuchs, E. Skin and Its Regenerative Powers: An Alliance between

Stem Cells and Their Niche. *Dev. Cell* **43**, 387–401 (2017).

281. Ge, Y. *et al.* Stem Cell Lineage Infidelity Drives Wound Repair and Cancer. *Cell* **169**, 636-650.e14 (2017).

282. Sada, A. *et al.* Defining the cellular lineage hierarchy in the interfollicular epidermis of adult skin. *Nat. Cell Biol.* **18**, 619–631 (2016).

283. Hoyle, N. P. *et al.* Circadian actin dynamics drive rhythmic fibroblast mobilization during wound healing. *Sci. Transl. Med.* **9**, 1–11 (2017).

284. Kowalska, E. *et al.* NONO couples the circadian clock to the cell cycle. *PNAS* **110**, 1592–1599 (2013).

285. Brown, S. A. *et al.* PERIOD1-associated proteins modulate the negative limb of the mammalian circadian oscillator. *Science* **308**, 693–696 (2005).

286. Kowalska, E. *et al.* Distinct roles of DBHS family members in the circadian transcriptional feedback loop. *Mol. Cell. Biol.* **32**, 4585–4594 (2012).

287. Maier, B. & Kramer, A. A NONO-gate times the cell cycle. *PNAS* **110**, 1565–1566 (2013).

288. Silveira, E. J. D. *et al.* BMAL1 modulates epidermal healing in a process involving the antioxidative defense mechanism. *Int. J. Mol. Sci.* **21**, 1–11 (2020).

289. Jones, P. H. & Watt, F. M. Separation of human epidermal stem cells from transit amplifying cells on the basis of differences in integrin function and expression. *Cell* **73**, 713–724 (1993).

290. Legg, J., Jensen, U. B., Broad, S., Leigh, I. & Watt, F. M. Role of melanoma chondroitin sulphate proteoglycan in patterning stem cells in human interfollicular epidermis. *Development* **130**, 6049–6063 (2003).

291. Giangreco, A., Goldie, S. J., Failla, V., Saintigny, G. & Watt, F. M. Human skin aging is associated with reduced expression of the stem cell markers β1 integrin and MCSP. *Journal of Investigative Dermatology* **130**, 604–608 (2010).

292. Barrandon, Y. & Green, H. Three clonal types of keratinocyte with different capacities for multiplication. *PNAS* **84**, 2302–2306 (1987).

293. Stern, M. M. & Bickenbach, J. R. Epidermal stem cells are resistant to cellular aging. *Aging Cell* **6**, 439–452 (2007).

294. Giangreco, A., Qin, M., Pintar, J. E. & Watt, F. M. Epidermal stem cells are retained in vivo throughout skin aging. *Aging Cell* **7**, 250–259 (2008).

295. Doles, J., Storer, M., Cozzuto, L., Roma, G. & Keyes, W. M. Age-associated inflammation inhibits epidermal stem cell function. *Genes Dev.* **26**, 2144–2153 (2012).

296. Janich, P. *et al.* Human epidermal stem cell function is regulated by circadian oscillations. *Cell Stem Cell* **13**, 745–753 (2013).

297. Vasioukhin, V., Degenstein, L., Wise, B. & Fuchs, E. The magical touch: genome targeting in epidermal stem cells induced by tamoxifen application to mouse skin. *PNAS* **96**, 8551–8556 (1999).

298. Husse, J., Zhou, X., Shostak, A., Oster, H. & Eichele, G. Synaptotagmin10-Cre, a driver to disrupt clock genes in the SCN. *J. Biol. Rhythms* **26**, 379–389 (2011).

299. Kellendonk, C., Opherk, C., Anlag, K., Schütz, G. & Tronche, F. Hepatocyte-specific expression of Cre recombinase. *Genesis* **26**, 151–153 (2000).

300. Jensen, K. B., Driskell, R. R. & Watt, F. M. Assaying proliferation and differentiation capacity of stem cells using disaggregated adult mouse epidermis. *Nat. Protoc.* **5**, 898–911 (2010).

301. Lipp, H.-P. *et al.* Automated behavioral analysis of mice using INTELLICAGE: Inter-laboratory comparisons and validation with exploratory behavior and spatial learning. *Proc. Meas. Behav.* 69 (2005).

302. Buenrostro, J., Wu, B., Chang, H. & Greenleaf, W. ATAC-seq: A Method for Assaying Chromatin Accessibility Genome-Wide. *Curr Protoc Mol Biol.* **109**, 1–10 (2016).

303. Luna, L. G. *Manual of histologic staining methods of the Armed Forces Institute of Pathology*. (McGraw-Hill, New York, 1968).

304. Schindelin, J. *et al.* Fiji: an open-source platform for biological-image analysis. *Nat. Methods* **9**, 676–682 (2012).

305. Bankhead, P. *et al.* QuPath: Open source software for digital pathology image analysis. *Sci. Rep.* **7**, 16878 (2017).

306. Bolger, A. M., Lohse, M. & Usadel, B. Trimmomatic: a flexible trimmer for Illumina sequence data. *Bioinformatics* **30**, 2114–2120 (2014).

307. Langmead, B. & Salzberg, S. L. Fast gapped-read alignment with Bowtie 2. *Nat. Methods* **9**, 357–359 (2012).

308. Stark, R. & Brown, G. DiffBind: differential binding analysis of ChIP-Seq peak datatle. 1–29 (2011).

309. Heinz, S. *et al.* Simple Combinations of Lineage-Determining Transcription Factors Prime cis-Regulatory Elements Required for Macrophage and B Cell Identities. *Mol. Cell* **38**, 576–589 (2010).

310. Kim, D. *et al.* TopHat2: accurate alignment of transcriptomes in the presence of insertions, deletions and gene fusions. *Genome Biol.* **14**, R36 (2013).

311. Liao, Y., Smyth, G. K. & Shi, W. featureCounts: an efficient general purpose program for assigning sequence reads to genomic features. *Bioinformatics* **30**, 923–930 (2014).

312. Hughes, M. E., Hogenesch, J. B. & Kornacker, K. JTK_CYCLE: an efficient non-parametric algorithm for detecting rhythmic components in genome-scale datasets. **4**, 1687–1697 (2011).

313. Love, M. I., Huber, W. & Anders, S. Moderated estimation of fold change and dispersion for RNA-seq data with DESeq2. *Genome Biol.* **15**, 550 (2014).

314. Wold, H. Estimation of principal components and related models by iterative least squares. in *Multivariate analysis* 391–420 (NewYork: Academic Press, 1966).

315. Nguyen, D. V & Rocke, D. M. Tumor classification by partial least squares using microarray gene expression data. *Bioinformatics* **18**, 39–50 (2002).

316. Barker, M. & Rayens, W. Partial least squares for discrimination. *J. Chemom.* **17**, 166–173 (2003).

317. Lê Cao, K.-A., Boitard, S. & Besse, P. Sparse PLS discriminant analysis: biologically relevant feature selection and graphical displays for multiclass problems. *BMC Bioinformatics* **12**, 253 (2011).

318. Tibshirani, R. Regression Shrinkage and Selection Via the Lasso. *J. R. Stat. Soc. Ser. B* **58**, 267–288 (1996).

319. Koronowski, K. B. *et al.* Defining the Independence of the Liver Circadian Clock. *Cell* **177**, 1448–1462 (2019).

320. Dang, F. *et al.* Insulin post-transcriptionally modulates Bmal1 protein to affect the hepatic circadian clock. *Nat. Commun.* **7**, 1–12 (2016).

321. Lipton, J. O. *et al.* The Circadian Protein BMAL1 Regulates Translation in Response to S6K1-Mediated Phosphorylation. *Cell* **161**, 1138–1151 (2015).

322. Ezagouri, S. & Asher, G. Circadian control of mitochondrial dynamics and functions. *Curr. Opin. Physiol.* **5**, 25–29 (2018).

323. Peek, C. B. *et al.* Circadian Clock NAD+ Cycle Drives Mitochondrial Oxidative Metabolism in Mice. *Science* **342**, 1243417 (2013).

324. Hans, F. & Dimitrov, S. Histone H3 phosphorylation and cell division. *Oncogene* **20**, 3021–3027 (2001).

325. Menet, J. S., Pescatore, S. & Rosbash, M. CLOCK:BMAL1 is a pioneer-like transcription factor. *Genes Dev.* **28**, 8–13 (2014).

326. Masri, S., Cervantes, M. & Sassone-Corsi, P. The circadian clock and cell cycle: Interconnected biological circuits. *Curr Opin Cell Biol* **25**, 730–734 (2013).

327. Fan, S. M.-Y. *et al.* External light activates hair follicle stem cells through eyes via an ipRGC–SCN–sympathetic neural pathway. *PNAS* **115**, E6880–E6889 (2018).

328. Kostrzewa, R. M. & Jacobowitz, D. M. Pharmacological actions of 6-hydroxydopamine. *Phamacological Rev.* **26**, (1974).

329. Harrison, D. E. & Archer, J. R. Biomarkers of aging: Tissue markers. Future research needs, strategies, directions and priorities. *Exp. Gerontol.* **23**, 309–321 (1988).

330. Tyner, S. D. *et al.* p53 mutant mice that display early ageing-associated phenotypes. *Nature* **415**, 45–53 (2002).

331. Wang, A. S. & Dreesen, O. Biomarkers of Cellular Senescence and Skin Aging. *Front. Genet.* **9**, 247 (2018).

332. Ge, Y. *et al.* The aging skin microenvironment dictates stem cell behavior. *PNAS* **117**, 5339 LP – 5350 (2020).

333. Joost, S. *et al.* Single-Cell Transcriptomics Reveals that Differentiation and Spatial Signatures Shape Epidermal and Hair Follicle Heterogeneity. *Cell Syst.* **3**, 221-237.e9 (2016).

334. Guo, S. & DiPietro, L. A. Factors affecting wound healing. *J. Dent. Res.* **89**, 219–229

(2010).

335. Gosain, A. & DiPietro, L. A. Aging and Wound Healing. *World J. Surg.* **28**, 321–326 (2004).

336. Lee, P. *et al.* Dynamic expression of epidermal caspase 8 simulates a wound healing response. *Nature* **458**, 519–523 (2009).

337. Wounds UK. Management of hyperkeratosis of the lower limb: Consensus recommendations. *Wounds UK* (2015).

338. Welsh, D. K., Takahashi, J. S. & Kay, S. A. Suprachiasmatic nucleus: Cell autonomy and network properties. *Annu. Rev. Physiol.* **72**, 551–577 (2010).

339. Pando, M. P., Morse, D., Cermakian, N. & Sassone-Corsi, P. Phenotypic rescue of a peripheral clock genetic defect via SCN hierarchical dominance. *Cell* **110**, 107–117 (2002).

340. Nagoshi, E. *et al.* Circadian Gene Expression in Individual Fibroblasts: Cell-Autonomous and Self-Sustained Oscillators Pass Time to Daughter Cells. *Cell* **119**, 693–705 (2004).

341. Masri, S. *et al.* Lung Adenocarcinoma Distally Rewires Hepatic Circadian Homeostasis. *Cell* **165**, 896–909 (2016).

342. Storch, K.-F. *et al.* Intrinsic circadian clock of the mammalian retina: importance for retinal processing of visual information. *Cell* **130**, 730–741 (2007).

343. Tso, C. F. *et al.* Astrocytes Regulate Daily Rhythms in the Suprachiasmatic Nucleus and Behavior. *Curr. Biol.* **27**, 1055–1061 (2017).

344. Yamamoto, T. *et al.* Transcriptional oscillation of canonical clock genes in mouse peripheral tissues. *BMC Mol. Biol.* **5**, 18 (2004).

345. Yamazaki, S. *et al.* Ontogeny of circadian organization in the rat. *J. Biol. Rhythms* **24**, 55–63 (2009).

346. Al-Nuaimi, Y. *et al.* A meeting of two chronobiological systems: circadian proteins Period1 and BMAL1 modulate the human hair cycle clock. *J. Invest. Dermatol.* **134**, 610–619 (2014).

347. Dyar, K. A. *et al.* Atlas of Circadian Metabolism Reveals System-wide Coordination and Communication between Clocks. *Cell* **174**, 1571-1585.e11 (2018).

348. Tahara, Y. *et al.* In vivo monitoring of peripheral circadian clocks in the mouse. *Curr. Biol.* **22**, 1029–1034 (2012).

349. Crosio, C., Cermakian, N., Allis, C. D. & Sassone-Corsi, P. Light induces chromatin modification in cells of the mammalian circadian clock. *Nat. Neurosci.* **3**, 1241–1247 (2000).

350. Granda, T. G. *et al.* Circadian regulation of cell cycle and apoptosis proteins in mouse bone marrow and tumor. *FASEB J.* **19**, 304–306 (2005).

351. Izumo, M. *et al.* Differential effects of light and feeding on circadian organization of peripheral clocks in a forebrain Bmal1 mutant. *Elife* **3**, 1–27 (2014).

352. Saini, C. *et al.* Real-time recording of circadian liver gene expression in freely moving

mice reveals the phase-setting behavior of hepatocyte clocks. *Genes Dev.* **27**, 1526–1536 (2013).

353. Yamaguchi, Y. *et al.* Mice genetically deficient in vasopressin V1a and V1b receptors are resistant to jet lag. *Science* **342**, 85–90 (2013).

354. Maywood, E. S., Chesham, J. E., O'Brien, J. A. & Hastings, M. H. A diversity of paracrine signals sustains molecular circadian cycling in suprachiasmatic nucleus circuits. *PNAS* **108**, 14306 LP – 14311 (2011).

355. Albrecht, U. Timing to perfection: the biology of central and peripheral circadian clocks. *Neuron* **74**, 246–260 (2012).

356. Ishida, A. *et al.* Light activates the adrenal gland: Timing of gene expression and glucocorticoid release. *Cell Metab.* **2**, 297–307 (2005).

357. Son, G. H. *et al.* Adrenal peripheral clock controls the autonomous circadian rhythm of glucocorticoid by causing rhythmic steroid production. *PNAS* **105**, 20970–20975 (2008).

358. Sasaki, H. *et al.* Forced rather than voluntary exercise entrains peripheral clocks via a corticosterone/noradrenaline increase in PER2::LUC mice. *Sci. Rep.* **6**, 1–15 (2016).

359. Travnickova-Bendova, Z., Cermakian, N., Reppert, S. M. & Sassone-Corsi, P. Bimodal regulation of mPeriod promoters by CREB-dependent signaling and CLOCK/BMAL1 activity. *PNAS* **99**, 7728–7733 (2002).

360. Zhang, B. *et al.* Hyperactivation of sympathetic nerves drives depletion of melanocyte stem cells. *Nature* **577**, 676–681 (2020).

361. Kojima, D. *et al.* UV-Sensitive Photoreceptor Protein OPN5 in Humans and Mice. *PLoS One* **6**, e26388 (2011).

362. Kim, H.-J. *et al.* Violet Light Down-Regulates the Expression of Specific Differentiation Markers through Rhodopsin in Normal Human Epidermal Keratinocytes. *PLoS One* **8**, e73678 (2013).

363. Yang, G. *et al.* Timing of expression of the core clock gene Bmal1 influences its effects on aging and survival. *Sci. Transl. Med.* **8**, 324ra16 (2016).

364. Iglesias-Bartolome, R. *et al.* mTOR inhibition prevents epithelial stem cell senescence and protects from radiation-induced mucositis. *Cell Stem Cell* **11**, 401–414 (2012).

365. Chang, H.-C. & Guarente, L. SIRT1 mediates central circadian control in the SCN by a mechanism that decays with aging. *Cell* **153**, 1448–1460 (2013).

366. Xue, Y. *et al.* Modulation of Circadian Rhythms Affects Corneal Epithelium Renewal and Repair in Mice. *Invest. Ophthalmol. Vis. Sci.* **58**, 1865–1874 (2017).